

University of Montana

## ScholarWorks at University of Montana

---

Graduate Student Theses, Dissertations, &  
Professional Papers

Graduate School

---

2001

### Distributed in situ gas measurements for the analysis and modeling of biogeochemical changes in the Clark Fork River

Jason Charles Reynolds  
*The University of Montana*

Follow this and additional works at: <https://scholarworks.umt.edu/etd>

**Let us know how access to this document benefits you.**

---

#### Recommended Citation

Reynolds, Jason Charles, "Distributed in situ gas measurements for the analysis and modeling of biogeochemical changes in the Clark Fork River" (2001). *Graduate Student Theses, Dissertations, & Professional Papers*. 6584.  
<https://scholarworks.umt.edu/etd/6584>

This Thesis is brought to you for free and open access by the Graduate School at ScholarWorks at University of Montana. It has been accepted for inclusion in Graduate Student Theses, Dissertations, & Professional Papers by an authorized administrator of ScholarWorks at University of Montana. For more information, please contact [scholarworks@mso.umt.edu](mailto:scholarworks@mso.umt.edu).



**Maureen and Mike  
MANSFIELD LIBRARY**

The University of

**Montana**

---

Permission is granted by the author to reproduce this material in its entirety, provided that this material is used for scholarly purposes and is properly cited in published works and reports.

**\*\*Please check "Yes" or "No" and provide signature\*\***

Yes, I grant permission

\_\_\_\_\_

No, I do not grant permission

\_\_\_\_\_

Author's Signature: \_\_\_\_\_

*Jason C. Reynolds*

Date: \_\_\_\_\_

*6/08/01*

Any copying for commercial purposes or financial gain may be undertaken only with the author's explicit consent.

---



DISTRIBUTED *IN SITU* GAS MEASUREMENTS FOR THE  
ANALYSIS AND MODELING OF BIOGEOCHEMICAL  
CHANGES IN THE CLARK FORK RIVER

by

Jason Charles Reynolds

B.S. Chemistry, The University of Montana 1995

presented in partial fulfillment of the requirements

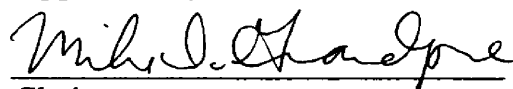
for the degree of

Master of Science

The University of Montana

2001

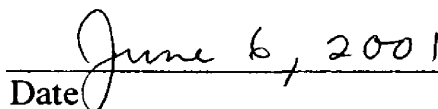
Approved by:



Chairperson



Dean, Graduate School



Date

UMI Number: EP37385

All rights reserved

INFORMATION TO ALL USERS

The quality of this reproduction is dependent upon the quality of the copy submitted.

In the unlikely event that the author did not send a complete manuscript and there are missing pages, these will be noted. Also, if material had to be removed, a note will indicate the deletion.



UMI EP37385

Published by ProQuest LLC (2013). Copyright in the Dissertation held by the Author.

Microform Edition © ProQuest LLC.

All rights reserved. This work is protected against unauthorized copying under Title 17, United States Code



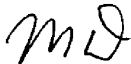
ProQuest LLC.  
789 East Eisenhower Parkway  
P.O. Box 1346  
Ann Arbor, MI 48106 - 1346

## Abstract

Reynolds, Jason C., M.S., April 2001

Chemistry

Distributed *In Situ* Gas Measurements for the Analysis and Modeling of Biogeochemical Changes in the Clark Fork River (118 pp.)

Director: Michael D. DeGrandpre 

*In situ* time-series measurements of the partial pressure of carbon dioxide ( $p\text{CO}_2$ ) and dissolved oxygen (DO) were obtained in the Clark Fork River, Montana during September and December 1999. New instrumentation for measuring  $p\text{CO}_2$  was employed for the first time in a riverine environment. Instrument arrays were deployed at up and downstream locations with the purpose of evaluating sources of biogeochemical variability over a discrete stretch of impounded river. The present work focuses on strategies for distributing *in situ* instrumentation as well as the subsequent modeling of physical and biogeochemical processes. Instrument locations should be selected to minimize complicating factors, such as surface or groundwater input. In these locales net community metabolism and air-water gas transfer presumably dominate gas variability. Total rates of change originating from these processes can be determined directly from the difference of up and downstream data and water travel time. Analyses of September and December river data reveal that community metabolism is predominantly responsible for diel variability in  $\text{CO}_2$  and DO. Surface gas transfer was often masked by community metabolism, though modeling suggests that it is significant. This work demonstrates that riverine monitoring using distributed *in situ* sensors is an effective approach for quantifying the processes that control biogenic gases in lotic systems.

## Acknowledgements

When I decided to shift my focus from climbing mountains (for a while) and embark upon a different path of learning in graduate school, I didn't know what to expect. As it turned out, I was given the opportunity to acquire and develop a blend of skills that would help me with research and ultimately, in refining my scientific persona. I have many people to thank for this opportunity, but I am indebted to the chemistry department as a whole for the wealth of knowledge and experience it offered along the way. Each person, whether staff or student, had something to offer that would be useful at some juncture should I choose to listen.

The third floor analytical lab is where I spent most of my hours, and I thank my advisor Michael DeGrandpre for accepting me into his unique research group. Among other things, he has shown me the need for critical examination of both data and scientific writings. I am now particularly aware of the challenges that lie ahead in the field of environmental research. Working in the lab allowed me to get to know Jeff Carr and Matt Baehr, whose presence was indispensable in achieving my objectives. I will never forget their willingness to provide friendship and support. I also offer special thanks to Cory Beatty for his brand of assistance and companionship throughout every day.

I thank Charlie B's for supporting some of Missoula's most creative and interesting characters, many of which are my closest friends. To them I offer thanks for reminding me to relax.

I appreciate the time and energy that my committee members have provided as their final evaluation will ultimately bring this chapter to an end; thank you Dr. Richard J. Field and Dr. Johnnie Moore. I include an additional note of thanks to Dr. Garon Smith, who is one of the more interesting scientists I have encountered, as well as being an influential environmental chemist.

To my mother and father, I am indebted beyond words, but nonetheless I thank them for always accepting me, regardless of whichever path I choose. They are an unwavering source of support, whether it involves advice or financial assistance. Without them, life would have not offered me the opportunities that I have consistently enjoyed. In countless ways, my accomplishments reflect their continued presence throughout the years.

Lastly, I offer my appreciation to my love Ursula who has provided support during this experience. She has remained through many moments of stress, forever maintaining a voice of good sense. Through it all, we have consistently emerged stronger. I hope that I can provide similar support in her upcoming trials.

# Table of Contents

	page
<b>Title Page</b> .....	<b>i</b>
<b>Abstract</b> .....	<b>ii</b>
<b>Acknowledgements</b> .....	<b>iii</b>
<b>Table of Contents</b> .....	<b>iv</b>
<b>List of Tables</b> .....	<b>vii</b>
<b>List of Figures</b> .....	<b>viii</b>
<b>Chapter 1: Introduction</b> .....	<b>1</b>
1.1 Overview and Rationale .....	1
1.2 DO and $p\text{CO}_2$ in Lotic Systems .....	3
1.2.1 Overview .....	3
1.2.2 Net community metabolism .....	4
1.2.2a Photosynthesis and respiration .....	4
1.2.2b Mass balance .....	4
1.2.2c Direct measurements .....	6
1.2.3 Surface gas exchange .....	7
1.2.3a Gas transfer .....	7
1.2.3b Methods .....	7
1.2.4 Other processes affecting DO and $p\text{CO}_2$ .....	8
1.2.4a Heating and cooling .....	8
1.2.4b Groundwater input .....	9
1.2.4c Calcite precipitation and dissolution .....	9
1.2.4d Photo-oxidation of organic matter .....	10
1.2.5 Summary .....	10
1.3 Principal Objectives .....	11
<b>Chapter 2: Methods</b> .....	<b>13</b>
2.1 Field Site Description .....	13
2.2 Analytical Methods .....	15
2.2.1 $p\text{CO}_2$ .....	15
2.2.2 Dissolved Oxygen .....	16
2.2.3 Chlorophyll- <i>a</i> .....	17
2.2.4 pH .....	18
2.2.5 Alkalinity .....	19
2.2.6 Meteorology .....	21
2.2.7 Hydrology .....	21
<b>Chapter 3: Data Analysis and Modeling</b> .....	<b>22</b>
3.1 Mass Balance Method .....	22
3.1.1 $\text{CO}_2$ and DO equations .....	22
3.1.2 Mass balance and $K_L$ .....	23
3.2 Photosynthesis .....	27
3.2.1 Rate model .....	27
3.2.2 Irradiance .....	28
3.2.3 Biomass .....	29



3.2.4	Photosynthetic quotient .....	30
3.3	Respiration.....	31
3.3.1	Rate model .....	31
3.3.2	Respiration quotient .....	32
3.4	$p\text{CO}_2$ and DO models.....	32
<b>Chapter 4: Results</b>	.....	<b>35</b>
4.1	Travel times .....	35
4.2	September Biogeochemical Data.....	36
4.2.1	$p\text{CO}_2$ .....	36
4.2.2	Dissolved oxygen.....	39
4.2.3	Alkalinity .....	39
4.2.4	pH.....	40
4.2.5	Atmospheric $p\text{CO}_2$ .....	42
4.3	December Biogeochemical Data .....	45
4.3.1	$p\text{CO}_2$ .....	45
4.3.2	Dissolved oxygen.....	45
4.3.3	Alkalinity .....	49
4.3.4	pH.....	49
4.4	<i>In situ</i> Chlorophyll- <i>a</i> .....	52
4.5	Impoundment Effects.....	53
4.6	Study Conditions .....	57
4.6.1	September .....	57
4.6.2	December.....	57
4.7	Depth, Discharge, and Conductivity.....	60
4.7.1	September .....	60
4.7.2	December.....	62
<b>Chapter 5: Modeling and Discussion</b>	.....	<b>64</b>
5.1	Modeling parameters.....	64
5.1.1	Overview .....	64
5.1.2	Biomass .....	64
5.1.3	Photosynthetic efficiency and photoinhibition .....	65
5.1.4	Photosynthetic potential .....	66
5.1.5	Regression Analysis .....	67
5.1.5a	September .....	67
5.1.5b	December.....	68
5.1.5c	Regression error analysis.....	68
5.1.6	Equation estimates of $K_C$ and $K_O$ .....	69
5.1.7	PQ and RQ.....	71
5.1.8	Respiration.....	72
5.1.9	Gas transfer velocities .....	73
5.2	Model Results .....	74
5.2.1	September .....	74
5.2.2	December.....	78
5.2.3	Calcite cycling .....	81
5.2.4	Evaluating travel error.....	83
5.2.5	Longitudinal dispersion.....	84

5.3	Model evaluation summary .....	85
<b>Chapter 6: Conclusions</b>	.....	<b>86</b>
<b>Appendix 1</b>	.....	<b>94</b>
<b>Appendix 2</b>	.....	<b>109</b>

## List of Tables

	page
<b>Table 2.1:</b> <i>In situ</i> instrumentation and deployment location.....	15
<b>Table 3.1:</b> Coefficients for empirical Schmidt number dependence for CO <sub>2</sub> and O <sub>2</sub> .....	26
<b>Table 3.2:</b> Thermodynamic constants and equations for CO <sub>2</sub> system.....	34
<b>Table 4.1:</b> Discrete measurements of alkalinity and pH, and calculated <i>p</i> CO <sub>2</sub> for September 1999 deployment .....	43
<b>Table 4.2:</b> Discrete measurements of alkalinity and pH, and calculated <i>p</i> CO <sub>2</sub> for December 1999 deployment .....	51
<b>Table 5.1:</b> Summary of important modeling parameters .....	65
<b>Table 5.2:</b> Results of multiple regression analyses .....	72

## List of Figures

	page
<b>Figure 1:</b> Map of Clark Fork River study reach.....	14
<b>Figure 2:</b> Representative Gran plot for alkalinity determination.....	20
<b>Figure 3:</b> <i>In situ</i> $p\text{CO}_2$ , $\Delta p\text{CO}_2$ , and PAR time-series during September 1999.....	37
<b>Figure 4:</b> <i>In situ</i> DO, $\Delta\text{DO}$ , and PAR time-series during September 1999.....	38
<b>Figure 5:</b> Discrete alkalinity measurements during September 1999 .....	40
<b>Figure 6:</b> Spectrophotometric pH measurements during September 1999.....	42
<b>Figure 7:</b> Atmospheric $p\text{CO}_2$ , temperature, and wind speed times-series during September and October 2000.....	44
<b>Figure 8:</b> <i>In situ</i> $p\text{CO}_2$ , $\Delta p\text{CO}_2$ , and PAR time-series during December 1999 .....	47
<b>Figure 9:</b> <i>In situ</i> DO, $\Delta\text{DO}$ , and PAR time-series during December 1999 .....	48
<b>Figure 10:</b> Discrete alkalinity measurements during December 1999 .....	49
<b>Figure 11:</b> Spectrophotometric pH measurements during December 1999 .....	50
<b>Figure 12:</b> <i>In situ</i> chlorophyll- <i>a</i> measurements during September and December 1999 .....	53
<b>Figure 13:</b> Expanded time-series of up and downstream <i>in situ</i> $p\text{CO}_2$ and DO measurements during September 1999 illustrating reservoir residence effect .....	56
<b>Figure 14:</b> <i>In situ</i> temperature, $\Delta T$ , and PAR time-series during September 1999 .....	58
<b>Figure 15:</b> <i>In situ</i> temperature, $\Delta T$ , and PAR time-series during December 1999 .....	59
<b>Figure 16:</b> Specific conductance, discharge, and depth time-series during September 1999.....	61

<b>Figure 17:</b> Specific conductance, discharge, and depth time-series during December 1999 .....	63
<b>Figure 18:</b> Representative plots for PQ and RQ estimation .....	70
<b>Figure 19:</b> Modeled and <i>in situ</i> $p\text{CO}_2$ and DO during September 1999.....	74
<b>Figure 20:</b> Modeled contributions to $\Delta\text{DIC}$ and $\Delta\text{DO}$ from photosynthesis, respiration, and surface gas transfer during September 1999.....	77
<b>Figure 21:</b> Modeled $K_C$ and $K_O$ time-series during September 1999.....	78
<b>Figure 22:</b> Modeled and <i>in situ</i> $p\text{CO}_2$ and DO during December 1999 .....	80
<b>Figure 23:</b> Modeled contributions to $\Delta\text{DIC}$ and $\Delta\text{DO}$ from photosynthesis, respiration, and surface gas transfer during December 1999.....	81
<b>Figure 24:</b> Modeled $\text{CaCO}_3$ saturation ration .....	83

# Chapter 1

## Introduction

### 1.1 Overview and Rationale

The dissolved gases oxygen and carbon dioxide regulate many biological and geochemical processes in riverine environments. They are termed *biogenic gases* because the utilization of each gas during metabolism is vital for all aquatic life. Dissolved O<sub>2</sub> (DO) also controls redox conditions, and hence chemical oxidation states and speciation. Similarly, dissolved CO<sub>2</sub>, which is customarily represented as the partial pressure of CO<sub>2</sub> ( $p\text{CO}_2$ ), is involved in many geochemical processes, such as trace metal solubility, largely due to its effect on pH. For these reasons, understanding the processes that control these gases is of great importance.

The study of biogenic gases in rivers is not new and much is known [e.g. *Owens et al.*, 1964; *Simonsen and Harremoës*, 1992; *Melching and Flores*, 1999], but few studies have adequately characterized short-term variability. Evaluations of short-term variability are often limited in duration or are undersampled, compromising interpretations and modeling. For example, *Greb and Graczyk* (1995) found that undersampling causes significant uncertainty in conclusions based upon changes in DO. Discrete sample analysis, which is a standard method used in riverine gas studies [e.g. *Odum*, 1956; *Wright and Mills*, 1967], is subject to contamination and other artifacts. The utilization of continuous-automated sensors in lotic, i.e. flowing, systems has revealed dynamic short-term variability in biogenic gas concentrations [e.g. *Kelly et al.*, 1974b; *Thyssen and Kelly*, 1985; *Neal et al.*, 1998]. Much of this variability originates

from biological processes (see Section 1.2). Consequently, low-frequency measurements are inadequate for characterizing productive riverine systems.

Autonomous DO and  $p\text{CO}_2$  sensors have been employed together for extended periods ( $\geq 1$  week) in lake studies [*Carignan*, 1998; *Baehr*, 2000], but river studies seldom measure *in situ*  $p\text{CO}_2$ . Although simultaneous river DO and  $p\text{CO}_2$  data have been obtained [*Thyssen* and *Kelly*, 1985; *Gausch et al.*, 1998], to my knowledge no one has autonomously monitored both *in situ*. Limited availability of *in situ*  $\text{CO}_2$  sensors is a principal reason for the lack of  $p\text{CO}_2$  data. Direct measurements of river  $p\text{CO}_2$  have been limited to bulky infrared gas analyzers [e.g. *Park*, 1969] that are not suitable for remote or submersed deployments. Changes in  $p\text{CO}_2$  can also be determined from measurements of other carbonate parameters. Any two measured parameters of  $p\text{CO}_2$ , pH, alkalinity, and total dissolved inorganic carbon (DIC) are used to calculate the remaining two from equations of carbonate equilibria [*Stumm* and *Morgan*, 1996]. The carbonate system is often characterized using pH measurements [*Wright* and *Mills*, 1967; *Simonsen* and *Harremoës*, 1992; *Thyssen* and *Kelly*, 1985; *Neal et al.*, 1998; *Ballester et al.*, 1999], which can lead to significant errors due to potentiometric pH uncertainty. A typical pH error of  $\pm 0.1$  pH units for instance, can lead to  $\sim 100$   $\mu\text{atm}$  error in calculated  $p\text{CO}_2$ . Another method of  $p\text{CO}_2$  determination is headspace analysis, which utilizes the equilibration of  $\text{CO}_2$  in a very small air-filled space above a discrete freshwater sample. Once equilibrated via surface gas exchange,  $p\text{CO}_2$  is determined from infrared gas analysis and Henry's Law [*Kling et al.*, 1991; *Dawson et al.*, 1995; *Raymond et al.*, 1997]. This method has proven useful, but it does not provide high frequency measurements.

DO and  $p\text{CO}_2$  data are often used to develop models and/or estimate biological and physical rates. A more detailed background of the controlling processes and the methods used to evaluate the contributions from each are presented in Section 1.2. Efforts by researchers to model stream productivity and gas exchange are numerous [e.g. *Simonsen and Harremoës, 1978; Gulliver and Stefan, 1984; Marzolf et al., 1994*], but there is little documentation of simultaneous modeling of DO and  $p\text{CO}_2$  in a riverine system. The use of a new autonomous  $p\text{CO}_2$  sensor in this study allows for the first continuous look at simultaneous *in situ* riverine DO and  $p\text{CO}_2$  data. The ability to measure both DO and  $p\text{CO}_2$  *in situ* allows the evaluation of combined modeling of both gases in detail never before accomplished. The utilization of the gas data also enables comparison and internal verification because river  $p\text{CO}_2$  and DO are interrelated through metabolism. Therefore, the fundamental objective of this study was to improve upon past riverine  $\text{CO}_2$  and DO research.

## **1.2 DO and $p\text{CO}_2$ in Lotic Systems**

### **1.2.1 Overview**

Net community metabolism, or the net balance of photosynthesis and respiration, is the dominant influence on DO and  $p\text{CO}_2$  in most riverine systems [*Odum, 1956*]. Photosynthesis consumes  $\text{CO}_2$  and produces DO during daylight periods, while respiration of organic matter occurs both day and night but typically dominates only during dark periods. The diel biological cycle results in pronounced inverse relationships between DO and  $p\text{CO}_2$  [*Thyssen and Kelly, 1985*].



Riverine air-water gas transfer rates have been studied extensively because DO reaeration is critical to aquatic health in waters with high biological oxygen demand [Owens *et al.*, 1964; Melching and Flores, 1999]. If the gas transfer rate is known, it can be used to estimate recovery times during periods of DO depletion. Accurate knowledge of reaeration rate is especially important in streams and rivers receiving large inputs of municipal or industrial wastes. Similarly, CO<sub>2</sub> gas transfer can be very important with respect to river biological and geochemical processes. Photosynthesis can significantly lower *p*CO<sub>2</sub> during daylight hours [Kelly *et al.*, 1974a]. Surface gas exchange and community respiration act to replenish aqueous CO<sub>2</sub> during the night, controlling pH and subsequently, river geochemistry [Brick and Moore, 1996].

Other riverine processes that can significantly affect DO and *p*CO<sub>2</sub> include heating and cooling, groundwater inputs, photo-oxidation of organic matter, and calcite dissolution and precipitation. Ideally, in studies focused upon metabolism and/or gas transfer, these processes are constrained or negligible.

### 1.2.2 Net community metabolism

**1.2.2a Photosynthesis and respiration:** Net community metabolism is the net balance of photosynthesis and respiration. Community describes all flora and fauna present in the river reach. Biota exist in the river water column, on substratum, and in benthic regions. Periphyton, or microflora inhabiting cobble, etc., often comprise the majority of the biomass [Bott *et al.*, 1978; Boston and Hill, 1991; Bowker *et al.*, 1996]. Consequently, much research has focused on these organisms.

**1.2.2b Mass balance:** The upstream-downstream technique, hereafter referred to as the *Odum method*, is a principle method for determining the changes in gas

concentrations between two river locations [Odum, 1956]. The gas flux can be utilized in the estimation of metabolic and physical rates. In theory, this can be accomplished using a steady-state assumption and one monitoring station, or two monitoring stations separated by a practical distance. To determine gas flux, the twin-station method requires accurate knowledge of travel time between monitoring stations. Utilizing the changes in biogenic gas concentrations (usually DO) over a stretch of flowing water, gas transfer velocities and biological processes can be estimated from mass balance. In fact, this technique is valuable for any parameter measured at two locations in a flowing system, providing the factors controlling variability are known. The single-station method can lead to erroneous results, since anomalous sources of variability upstream (e.g. impoundments) can be misinterpreted. The success of the Odum method is largely dependent upon the validity of various simplifications. For example, assumptions are often made regarding flow hydraulics, mixing, residence time, groundwater interactions, and biology. To minimize sources of variability, and uncertainty in metabolic and physical rates, experimental streams or channels are often selected for study [Parkhill and Gulliver, 1998].

Photosynthetic and respiratory rates have been determined in streams using DO monitoring with both chamber [Bott *et al.*, 1978] and Odum methods [Odum, 1956; Kelly *et al.*, 1974b; Hornberger *et al.*, 1976; Thyssen and Kelly, 1985; Marzolf *et al.*, 1994; Parkhill and Gulliver, 1998]. In a comparison of five different methods conducted on a benthic algae-dominated third-order stream, Bott *et al.* (1978) determined net community respiration and production. The three chamber methods examined utilize changes in DO or calculated DIC in a closed system, but only one method involves *in situ* measurements.

Although the *in situ* chamber technique better represents stream biology, water flow was restricted by the closed system. A problem associated with the closed chamber method is the shift from a lotic to a static system. The other two techniques maintain a flowing system, but involve incubated substrate removed from the natural environment. A significant feature of any lotic system is the continual replenishment of nutrients; metabolic studies employing a closed system inherently eliminate this factor.

**1.2.2c Direct measurements:** Metabolic rates of periphyton are often determined through isolated studies of algal assemblages in troughs or on tiles placed in a lotic system [*Jasper and Bothwell, 1986; Boston and Hill, 1991; Wellnitz and Rinne, 1999*]. These studies use periphyton grown in natural lotic systems and transfer them to laboratory incubation chambers for rate estimation. A principal motivation for this approach is to resolve photosynthetic rate under controlled light and nutrient conditions. Wellnitz and Rinne (1999) used measurements of O<sub>2</sub> to determine net photosynthesis, while other studies utilize C<sup>14</sup>-labeled CO<sub>2</sub> or biomass measurements (chlorophyll-*a*) to quantify growth directly. These studies are classically referred to as “light- and dark-bottle” techniques because net metabolism is determined from incubations in lighted enclosures, while incubations in dark chambers yield net respiration rates [*Wetzel, 1983*]. The difference in rates between the two incubations is net production. The assumption is often made that respiration during daylight is equal to dark net respiration, essentially discounting photorespiration. Additional problems with the light- and dark-bottle techniques include nutrient depletion, biomass samples unrepresentative of whole stream life, and the loss of natural conditions (e.g. turbulence).

### 1.2.3 Surface gas exchange

**1.2.3a Gas transfer:** Surface gas exchange is driven by the concentration gradient between the water and atmosphere and turbulence at the air-water interface. For example, when DO exceeds atmospheric saturation, O<sub>2</sub> outgases into the atmosphere in an effort to attain equilibrium. Likewise, CO<sub>2</sub> outgases when aqueous  $p\text{CO}_2$  is supersaturated, and ingases when it is below atmospheric  $p\text{CO}_2$ .  $K_L$ , or the liquid gas transfer velocity, is a measure of how rapidly a gas diffuses across the air-water boundary. Each gas has a different  $K_L$ , primarily because of differences in diffusivity, though temperature-dependent empirical models predict that they are interrelated (see Section 3.1.2). Field and laboratory investigations have quantified  $K_L$  under a wide variety of natural and simulated conditions because of the importance of DO reaeration. These studies show that  $K_L$  can be dependent upon wind speed [*Clark et al.*, 1994 ; *Chu and Jirka*, 1998], macroroughness of the streambed [*Moog and Jirka*, 1998a], and bubble entrainment [*Gulliver et al.*, 1997]. Hydrological agitation also increases gas transfer, and in a study on a carbonate rich stream, calcite precipitation was observed in cascades due to CO<sub>2</sub> outgasing [*Hoffer-French and Herman*, 1989]. The increased calcite (CaCO<sub>3</sub>) precipitation was caused by CO<sub>2</sub> outgasing, which drives the equilibrium of dissolved CaCO<sub>3</sub> towards formation of solid CaCO<sub>3</sub> (see Section 1.2.4c).

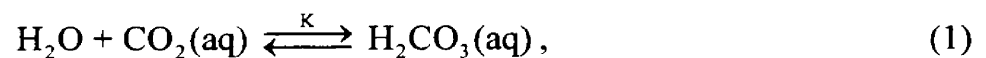
**1.2.3b Methods:** Volatile and nonvolatile tracers are often utilized to determine gas transfer velocity. Tracer techniques work on the assumption that tracer gas transfer rates can be used as proxies for O<sub>2</sub> and CO<sub>2</sub> transfer velocities. Both deliberate (e.g. SF<sub>6</sub>, <sup>3</sup>He) and natural (e.g. <sup>222</sup>Rn) tracers have been used [*Elsinger and Moore*, 1983; *Wanninkhof et al.*, 1990; *Genereux and Hemond*, 1992; *Marzolf et al.*, 1994]. Tracers are

also used with the “helmet” method, where gas flux is measured over time in an inverted dome on top of the water’s surface [*Hartman and Hammond, 1984*]. The helmet method perturbs the turbulent action of surface water and may not represent undisturbed systems. Although tracer gas studies are expected to provide the most accurate values of  $K_L$ , they are often difficult and time-consuming. Equation estimates based upon stream characteristics are often used for this reason.

Owens et al. (1964) summarized many equations for gas exchange determined from stream data. Reviews can also be found in Moog and Jirka (1998b) and Melching and Flores (1999). These predictive equations are often based upon lotic morphology and inaccuracies can arise between studies due to widely differing environments. Uncertainty in  $K_L$  is one of the most frequently cited concerns regarding river modeling.

#### 1.2.4 Other processes affecting DO and $pCO_2$

**1.2.4a Heating and cooling:** Temperature changes caused by weather variation and solar heating have many effects on biogenic gas concentrations. For example, solubilities for both DO and  $CO_2$  are temperature-dependent. A decrease in temperature will increase the solubility of both gases, however  $pCO_2$  is more complex. In contrast to DO, when  $CO_2$  dissolves in water, the aqueous  $CO_2$  ( $CO_2(aq)$ ) does not all remain as  $CO_2$ . Further reaction with water, as shown in Equation 1:

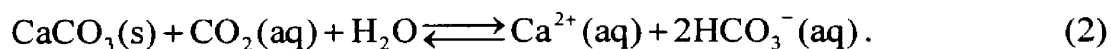


results in the formation of carbonic acid. Subsequent acid dissociation results in the dissolved species  $HCO_3^-$  and/or  $CO_3^{2-}$ . Concentrations of the carbonate species are dependent upon temperature. In contrast,  $O_2(aq)$  doesn’t change with variation in temperature. Metabolic and gas transfer processes are also influenced by temperature

changes, and empirical models have been generated to estimate the effect (see Section 3.3).

**1.2.4b Groundwater input:** The input of groundwater can have a significant effect upon the chemical composition of rivers. Microbial respiration in soil releases large amounts of CO<sub>2</sub> into groundwater. Since there is often no contact with the atmosphere, groundwater can become highly supersaturated in CO<sub>2</sub>. This tends to increase alkalinity in the groundwater through the dissolution of CaCO<sub>3</sub> and other minerals. High-alkaline groundwater affects the acid-base condition, and hence pH, of the surface water it reaches. Local geochemistry is also affected by gas exchange as groundwater *p*CO<sub>2</sub> equilibrates with the atmosphere upon mixing with surface waters [Hoffer-French and Herman, 1989]. Conversely, groundwater can be depleted in DO due to biological consumption. Relative to the river-groundwater gradient of *p*CO<sub>2</sub>, however, DO differences are often not as significant [Stumm and Morgan, 1996]. Groundwater inputs need to be quantified to accurately determine rates of other processes such as gas exchange and biological metabolism.

**1.2.4c Calcite precipitation and dissolution:** Calcite (CaCO<sub>3</sub>) precipitation and dissolution occur in natural waters via the following reaction:



This reaction may proceed through a number of different pathways. For example, groundwater rich in Ca<sup>2+</sup>, HCO<sub>3</sub><sup>-</sup> and CO<sub>3</sub><sup>2-</sup> may enter the river and lose CO<sub>2</sub> to outgasing, driving Equation 2 to the left, forming CaCO<sub>3</sub> and releasing more CO<sub>2</sub> [Hoffer-French and Herman, 1989; Dawson *et al.*, 1995; Cicerone *et al.*, 1999]. Temperature changes, evaporation, and biological processes also affect the

precipitation/dissolution cycle of  $\text{CaCO}_3$  [Stumm and Morgan, 1996]. The saturation ratio ( $\Omega$ ) is one gauge of whether the thermodynamic conditions in an aqueous system favor  $\text{CaCO}_3$  precipitation:

$$\Omega = \frac{\{\text{Ca}^{2+}\}\{\text{CO}_3^{2-}\}}{K_{s0}} \quad (3)$$

where  $\{\text{Ca}^{2+}\}$  and  $\{\text{CO}_3^{2-}\}$  are the activities of  $\text{Ca}^{2+}$  and  $\text{CO}_3^{2-}$ , respectively, and  $K_{s0}$  is the solubility product of  $\text{CaCO}_3$  [Cicerone et al., 1999]. If  $\Omega > 1$ , the reaction can proceed forming  $\text{CaCO}_3$ , while conditions support dissolution if  $\Omega < 1$ .  $\text{CaCO}_3$  precipitation and dissolution are strongly affected by the kinetics (nucleation and crystal growth) of the aqueous system and therefore,  $\Omega$  simply indicates the potential for reaction [Stumm and Morgan, 1996; Cicerone et al., 1999]. For example, Hoffer-French and Herman (1989) report that in an outgassing karst stream, most precipitation did not occur until  $\Omega \geq 5$ .

**1.2.4d Photo-oxidation of organic matter:** Photo-oxidation of colored dissolved organic matter (CDOM) is another abiotic process that can impact riverine  $\text{CO}_2$  and DO. Granelli et al. (1996) report that photodegradation is more significant with increasing CDOM. Additionally, they propose that photo-oxidation of CDOM to DIC is important in freshwater with long residence times (e.g. lakes). Rivers with high flow rates and turbulent mixing probably do not experience significant short-term production of DIC from photolysis.

### 1.2.5 Summary

A comprehensive determination of every variable is often too expensive, time-consuming, or impossible, even in the simplest lotic systems. To determine metabolic

and gas transfer rates, simplifications often need to be made. The assumption that photosynthesis, respiration, and surface gas exchange are the dominant processes is justified, providing other sources of variability are minimal. Although laboratory studies provide constrained and reproducible conditions, it is uncertain how accurately they represent gas transfer in natural flowing waters. Many previous studies focus on small streams and it is not known how they compare to larger streams and rivers. More research is needed on large rivers to refine current understanding of the major processes controlling DO and  $p\text{CO}_2$ .

### 1.3 Principal Objectives

The work included herein was motivated principally by interest in riverine  $\text{CO}_2$  gas exchange and specifically, the evaluation of new  $p\text{CO}_2$  instrumentation in supplementing present understanding of riverine biogeochemical cycles. We hoped to improve upon past river research by monitoring both  $p\text{CO}_2$  and DO at distributed locations. Comparison of  $p\text{CO}_2$  and DO data can show the importance of *in situ* biological processes. The dense temporal coverage obtained from the autonomous sensors allows a more detailed examination of the processes that control gas variability than previously possible. Another principal objective was the development and evaluation of a riverine biogeochemical gas model. The known biological relationships between  $\text{CO}_2$  and  $\text{O}_2$  can link the gas models developed from *in situ* data. Models assist researchers in the examination of biological, physical, and geochemical components of variability. They forecast variability during a wide variety of conditions without the need for sampling procedures. Therefore, the development of models is essential in interpreting gas data, since the contributions to variability can be individually analyzed. Increased success in



river gas modeling will increase our understanding of the specific processes controlling variability.

## Chapter 2

### Methods

#### 2.1 Field Site Description

The river reach studied in both September and December 1999 is located along the Clark Fork River in the Upper Columbia River Basin (Figure 1). Great interest in the geochemistry of this high-order river has been generated as a result of persistent mine tailings pollution [Brick and Moore, 1996; Lambing *et al.*, 1994]. The river is alkaline ( $\text{pH} > 8$ ) due to significant upstream groundwater input. The portion of the Clark Fork River examined in this study is greater in elevation than the local aquifer, so groundwater accrual is assumed to be negligible [Gestring, 1994]. Marshall Creek, a small drainage, empties into the river about 5 km above the downstream location, but its effect on the water chemistry was also assumed insignificant as its discharge was very small. Likewise, other surface inputs were also assumed negligible. The surface water of the reach ranges between rapid to slow moving, with little whitewater or wave breaking. The riverbed is comprised largely of cobble. Periphyton dominates the biomass over the study reach. Diatoms and filamentous green algae (e.g. *Claudophora*) are the dominant species, although some blue green algae species (e.g. *Nostoc*) are also important [Vicki Watson, pers. comm.].

In September 1999, two sensor arrays were deployed in the river separated by 8.69 km (Figure 1). The upstream sensors were deployed approximately 1 km downstream from the Milltown Dam. A second deployment was made in December and upstream

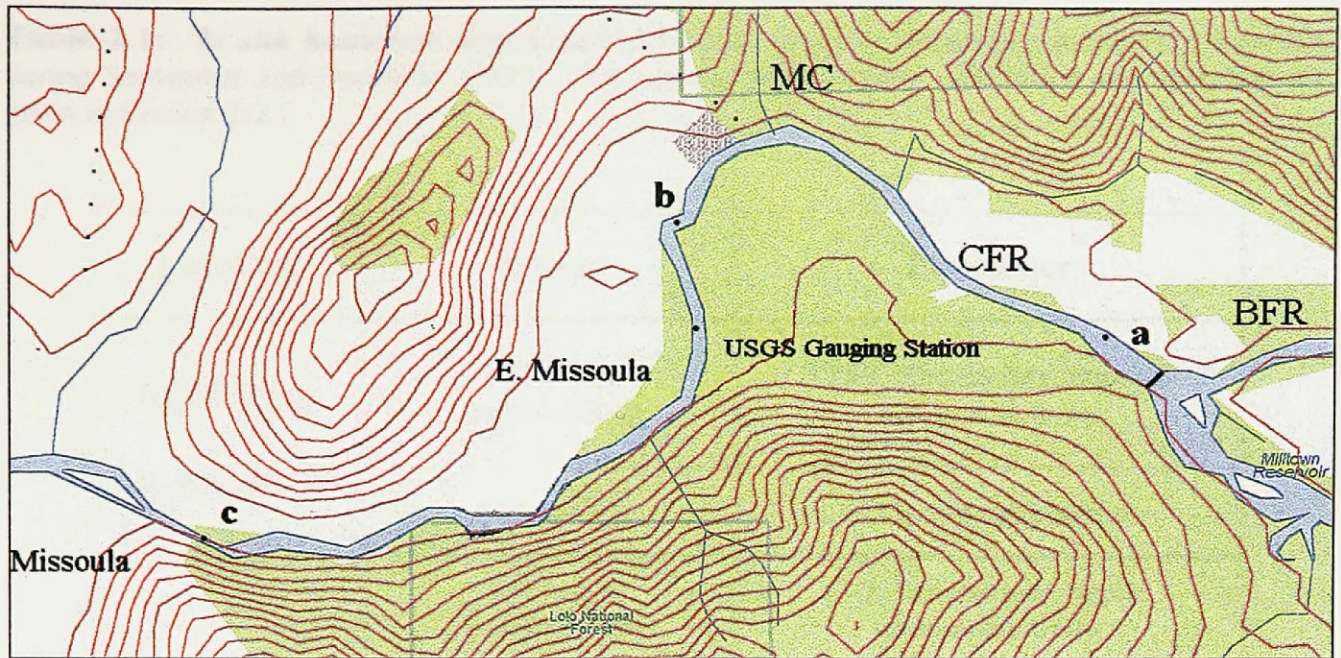


**Figure 1:** The Clark Fork River from the Milltown Dam to Missoula, Montana. The dam (represented by a black line) is situated at the confluence of the Blackfoot (BFR) and Clark Fork Rivers (CFR). During the September deployment, up and downstream sensor arrays were located at **a** and **c**, respectively. In December, the upstream monitoring station was moved to **b**, while the downstream station remained at **c**. MC represents Marshall Creek, the small drainage mentioned in the text. Transportation routes (i.e. roads, highways) are omitted for clarity.

sensors were located 3.80 km from the dam. The downstream location remained the same for a total travel distance of 5.04 km. The average slopes of the river for the September and December study reaches, determined from topographic maps, are 0.0014 and 0.0017  $\text{m m}^{-1}$ , respectively. Table 2.1 lists the location, types of sensors, and parameters measured during both study periods.

**Table 2.1:** *In situ* instrumentation deployed at both up and downstream monitoring locations during September and December 1999. Descriptions of instrument calibration and operation are given in Section 2.2.

Location	Sensor	Parameter
<b>Upstream</b> (a, b in Fig.1)	YSI Sonde (model 6000)	DO, temperature, depth, and conductivity
	SAMI-CO <sub>2</sub>	<i>p</i> CO <sub>2</sub> and temperature
<b>Downstream</b> (c in Fig. 1)	YSI Sonde (model 6000)	DO, temperature, depth, and conductivity
	SAMI-CO <sub>2</sub>	<i>p</i> CO <sub>2</sub> and temperature
	Chelsea Instruments Ltd, Minitrack II	Chlorophyll- <i>a</i> fluorescence
	LiCOR (model LI-192SA)	PAR

## 2.2 Analytical Methods

### 2.2.1 *p*CO<sub>2</sub>

River *p*CO<sub>2</sub> was recorded every 15 minutes using Submersible Autonomous Moored Instruments for CO<sub>2</sub> (SAMI-CO<sub>2</sub>) at both up and downstream locations. This is the first investigation using a SAMI-CO<sub>2</sub> in a riverine environment. DeGrandpre et al. (1995,1999) provide a thorough description of the performance and operational principles of the SAMI-CO<sub>2</sub>, so only a brief overview of the calibration procedure is given here.

The SAMI-CO<sub>2</sub> instruments were calibrated prior to deployment using a LiCOR infrared gas analyzer (model LI-6251) and CO<sub>2</sub> gas standards. The SAMI-CO<sub>2</sub> in-lab

accuracy is estimated at  $\pm 3 \mu\text{atm}$  at  $360 \mu\text{atm}$ , based upon  $\text{CO}_2$  standards used during calibration. Unless otherwise noted, reported errors represent one standard deviation. Precision is estimated at better than  $\pm 1 \mu\text{atm}$  (@  $200\text{-}600 \mu\text{atm}$ ) [DeGrandpre *et al.*, 1999], except where noted in December (see Section 4.3.1). Instrument response is less sensitive at higher  $p\text{CO}_2$ , which results in increased uncertainty. To validate the accuracy of the *in situ* response, discrete samples were obtained daily at both sites and analyzed for pH and total alkalinity. The  $p\text{CO}_2$  was calculated from these parameters at the *in situ* temperature using carbonate equilibria equations and freshwater equilibrium constants in a model (CO2SYS v1.05) [Lewis and Wallace, 1998]. In December, an additional check on drift and reproducibility was obtained by placing the  $\text{CO}_2$  sensors in the river at the same location after the 13-d deployment. Data quality is discussed in Section 4.3.

Following a review of the  $p\text{CO}_2$  data, it was determined that direct measurements of atmospheric  $p\text{CO}_2$  would have been valuable. As a result, during September 2000 atmospheric  $p\text{CO}_2$  and temperature were continuously monitored during a wide range of conditions to determine the likely range of variability. This was accomplished using a meteorological station containing a LiCOR infrared  $\text{CO}_2$  gas analyzer (model LI-6251) and Tattletale (Onset Computer Corp.) data logger. Measurements were recorded every half-hour for three weeks. The autonomous station was located on the riverbank across from the downstream monitoring location (c in Figure 1).

### 2.2.2 Dissolved Oxygen

DO measurements were made every 15 minutes using YSI DO sondes (Yellow Springs Instruments, model 6000). Each sonde included a temperature probe with reported accuracy and resolution of  $\pm 0.15$  and  $\pm 0.01$   $^\circ\text{C}$ , respectively. The sondes also

included conductivity and depth sensors. The depth and conductivity sensors have reported accuracies of  $\pm 0.018$  m and  $\pm 0.001$  mS  $\text{cm}^{-1}$ , respectively. Prior to deployment, DO probes were calibrated in water-saturated air corrected for local barometric pressure. The depth sensors rely upon changes in hydrostatic pressure and were zeroed in ambient air, while the conductivity probes were calibrated in a freshwater standard provided by YSI. In December, once the sondes were recovered from the river they were placed in deionized water in a refrigerator ( $\sim 4$  °C) for two days. DO data were compared to triplicate Winkler titration analyses performed on the refrigerated water [Wetzel and Likens, 1991]. Following both deployments, DO sensors were allowed to equilibrate in water-saturated air to establish if any drift had occurred. A discussion of DO data quality can be found in Sections 4.2.2 and 4.3.2. Saturation concentrations of DO were determined from temperature and barometric pressure using an empirically-determined relationship given by (Wetzel and Likens, 1991):

$$\text{DO}_{\text{sat}} = P \cdot \text{Exp}(7.117 - 1.31403 \cdot \ln(T + 45.93)) \quad (4)$$

where P is local barometric pressure (atm) and T is temperature (°C).

### 2.2.3 Chlorophyll-*a*

Suspended chlorophyll-*a* concentrations were determined during both deployments using an *in situ* fluorometer (Chelsea Instruments, Minitrack II) as a part of the downstream sensor array. Chlorophyll-*a* pigment fluoresces when excited by the 470 nm light and emits at a wavelength of 685 nm. Chlorophyll-*a* concentrations are determined from a linear calibration equation and measurements of *in situ* fluorescence. Matt Baehr performed instrument calibration, and accuracy is based upon discrete freshwater lake samples analyzed using a bench top fluorometer (Shimadzu, Model RF-1501).

Measurements of chlorophyll-*a* extracted in acetone were used. Concentrations determined from the laboratory and *in situ* measurements agreed within  $1.2 \pm 1.0 \mu\text{g L}^{-1}$  ( $n = 6$ ).

#### 2.2.4 pH

Discrete water samples were obtained once or twice daily at both monitoring sites. Samples were analyzed for pH using a spectrophotometric method developed for ocean water [Byrne and Breland, 1989] and adapted for freshwater [Carr, 2000; French *et al.*, 2001]. During collection, freshwater samples were spiked with 100- $\mu\text{L}$  aliquots of mercuric chloride ( $\text{HgCl}_2$ ) to suppress further metabolism. Two or three samples were taken at each site in clean 500-mL glass bottles. Bottles were completely filled following three rinses of freshwater to minimize the headspace in each bottle. Although exchange of carbon dioxide with the atmosphere will not affect alkalinity, it will alter the pH of freshwater. For this reason, spectrophotometric analyses of pH were performed prior to alkalinity determination. Bottles of freshwater were kept on ice until they reached the laboratory ( $\sim 30$  min). Samples were then placed in a laboratory refrigerator ( $\sim 4$  °C) and stored until analysis. Freshwater sample was added to a 10-cm thermostated cell and absorbances at 439, 577, and 724 nm were recorded at 20 °C using a Lambda 11 UV-Vis spectrophotometer (Perkin Elmer). After addition of the sulfonephthalein-indicator cresol red, absorbances were once again measured. The measurement sequence was then repeated for a total of three replicates. The pH was calculated using [Byrne and Breland, 1989]:

$$\text{pH} = \text{pK}_a' + \log \frac{R - e_1}{e_2 - R \cdot e_3} \quad (5)$$

where R equals the ratio of absorbances at 577 and 439 nm, and  $e_1$ ,  $e_2$ , and  $e_3$  are the molar absorptivity ratios for cresol red equaling 0.000, 2.740, and 0.105, respectively [Carr, 2000]. The pH accuracy is dependent upon the accuracy of cresol red's  $pK_a$ . In Equation 5,  $pK_a'$  is defined as the apparent  $pK_a$ , which includes the ion activity coefficients for cresol red. Calculations of pH in this study utilized a  $pK_a'$  of 8.3495 at 20 °C. The probable error in pH is  $<\pm 0.01$  pH units, but more investigation into the  $pK_a'$  is required for verification [French *et al.*, 2001]. Measurements of pH during September had an average standard deviation of  $\pm 0.0064$  between 28 sets of three replicates. In December, replicate measurements of pH yielded an average standard deviation of  $\pm 0.0041$  (n = 29 sets).

### 2.2.5 Alkalinity

Freshwater alkalinity (ALK) is often defined by:

$$ALK = [HCO_3^-] + [2CO_3^{2-}] + [OH^-] - [H^+], \quad (6)$$

though any other source of acid or base must be included to be fully accurate. In freshwater however, carbonate alkalinity (CA) is typically the principal component of alkalinity.

Total alkalinity was determined by potentiometric titration and Gran plot analysis [Edmond, 1970]. The titration pH was monitored using a ROSS combination electrode (ATI ORION, model 8102) and an accumet pH/ion meter (Fischer Scientific, model 25). The nearly full titration cell was sealed with a large rubber stopper to minimize errors from gas exchange, while solution temperature was monitored using a  $\pm 0.1$  °C temperature probe. HCl standard ( $\sim 0.1$  N) was added to  $\sim 180$  mL of preweighed freshwater sample using an automatic titrator (Denver Instruments, model 85). HCl



(Aldrich) was standardized before each study using titration of dried primary standard-grade sodium carbonate ( $\text{Na}_2\text{CO}_3$ ) and bromocresol green indicator [Harris, 1995]. Alkalinity is determined from the plot of F1, the Gran function, versus the volume of acid standard added ( $V_{\text{HCl}}$ ). F1 is given by:

$$F1 = (V_i + V_{\text{HCl}}) \cdot [\text{HCl}]^1 \cdot [\text{H}^+] \quad (7)$$

where  $V_i$  is the initial volume of freshwater sample and  $[\text{H}^+]$  is determined from the electrode measurements. The equivalence point was determined using 10-15 points beyond the apparent equivalence point. A representative Gran plot is shown in Figure 2, and illustrates the linear increase in F1 beyond the equivalence point. This method yielded an average precision of  $\pm 6 \mu\text{eq kg}^{-1}$  for freshwater analyses ( $n = 28$ ) and an accuracy of  $\pm 3 \mu\text{eq kg}^{-1}$  when using standards ( $n = 11$ ). Gran alkalinity was assumed to equal total alkalinity, though any unknown sources of weak acid (e.g. dissolved

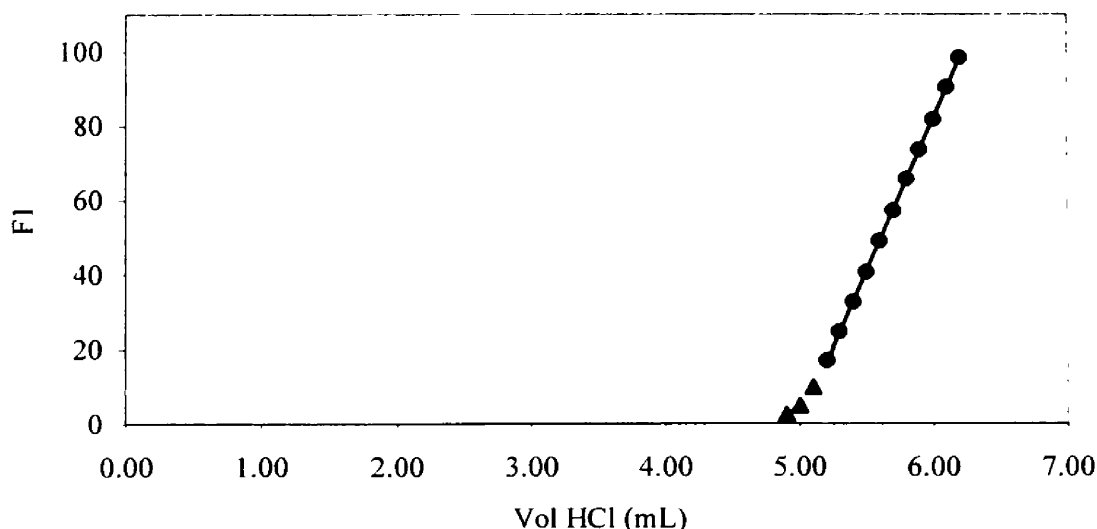


**Figure 2:** Typical Gran plot of F1 vs. volume of HCl added, with circles representing the points on the titration curve used for alkalinity determination. The triangles are points near the bicarbonate equivalence point where the data are not linear. The line has an  $R^2 = 1.0000$ , a characteristic value for the Gran plots used for analysis in this study.

organic or humic acids) could result in an over or underestimation of carbonate alkalinity [Hemond, 1990; Hongve, 1990]. Anions of weak acids can act as buffering agents during Gran titration and be misinterpreted as carbonate alkalinity. Conversely, weak acids can act to neutralize carbonate alkalinity. Under certain conditions, iron and aluminum hydroxides can also have a significant effect on alkalinity determination [Hemond, 1990; Hongve, 1990].

### **2.2.6 Meteorology**

Local meteorological data were obtained from the NOAA National Climatic Data Center in Missoula, Montana. The site is located at Johnson-Bell Field, ~11 km west of the downstream monitoring station. Meteorological time-series included hourly wind, barometric pressure, precipitation, air temperature, and cloud cover. The downstream sensor array was also equipped with a photosynthetically-active radiation (PAR) sensor (LiCOR, model LI-192SA) to determine *in situ* irradiance.

### **2.2.7 Hydrology**

Discharge data (every 15 min.) were obtained from the USGS gauging station 12340500, located ~6.3 km downstream from the Milltown Dam.

## Chapter 3

### Data Analysis and Modeling

#### 3.1 Mass Balance Method

##### 3.1.1 CO<sub>2</sub> and DO equations

Changes in DIC (defined in Table 3.2), rather than just  $p\text{CO}_2$ , must be considered in the analysis of the carbonate system because of the distribution of CO<sub>2</sub> throughout its dissolved species. Rates of change of CO<sub>2</sub> in a river with negligible longitudinal dispersion, or mixing (discussed in Section 5.2.5), are described by:

$$H \frac{d\text{DIC}}{dt} = K_c S (p\text{CO}_{2s} - p\text{CO}_{2w}) - P + R + A - C \quad (8)$$

where  $H$  is river depth,  $\frac{d\text{DIC}}{dt}$  is the rate of change of DIC,  $S$  is CO<sub>2</sub> solubility, and  $K_c$  is the gas transfer velocity of CO<sub>2</sub>. Local atmospheric CO<sub>2</sub> partial pressure ( $p\text{CO}_{2s}$ ) needs to be measured because of its dependence on local CO<sub>2</sub> sinks and sources (e.g. biomass, anthropogenic sources). Additional effects on  $p\text{CO}_{2w}$  include photosynthesis ( $P$ ), respiration ( $R$ ), groundwater accrual ( $A$ ), and calcite formation ( $C$ ). In the particular Clark Fork River reach studied however, effects from groundwater and calcite cycling were initially assumed negligible. A similar mass balance can be written for O<sub>2</sub>:

$$H \frac{d\text{O}_2}{dt} = K_o (\text{O}_{2s} - \text{O}_{2w}) + P - R + A \quad (9)$$

where  $\text{O}_{2s}$  and  $\text{O}_{2w}$  are the saturation and bulk water concentrations, respectively, and  $K_o$  is the gas transfer velocity of O<sub>2</sub>. In contrast to CO<sub>2</sub>, O<sub>2</sub> comprises more of the atmosphere (>20%) and saturation concentrations of O<sub>2</sub> ( $\text{O}_{2s}$ ) can be estimated using

reliable equations based upon atmospheric pressure (Equation 4).  $P$  and  $R$  represent photosynthetic production and respiratory consumption of  $O_2$ , respectively. In comparison to the  $CO_2$  system, differences in groundwater  $O_2$  are much less important as discussed earlier.

Equations 8 and 9 can be solved by finite approximation by fixing  $dt$  as a time step of the total residence time between the two river locations ( $\Delta t$ ). The total measured changes in DIC and DO can likewise be divided into increments approximating  $dDIC$  and  $dO_2$ . The theoretical mass balances are used to model downstream gas concentrations using semi-empirical expressions for metabolism and gas transfer (see Section 3.1.2). Accurate travel time is essential for estimating rates or downstream concentrations of DO and  $pCO_2$ . This parameter is often measured using conservative salt [Marzolf *et al.*, 1994] or dye tracers [Wright and Mills, 1967; Kelly *et al.*, 1974b]. If nighttime data is used, the flux due to photosynthesis can be omitted from the equations. Community dark respiration is then estimated using DO (or  $pCO_2$ ) time-series and a  $K_L$  ( $K_O$  or  $K_C$ ) estimated from equations dependent on river hydraulic conditions [Simonsen and Harremoës, 1978] or conservative gas tracers [Wanninkhof *et al.*, 1990; Marzolf *et al.*, 1994]. If daytime respiration is simplified as nighttime respiration, daytime photosynthetic gas flux is determined by excluding contributions from respiration and gas transfer.

### 3.1.2 Gas Exchange Flux

In this study, estimates of  $K_O$  and  $K_C$  (20 °C) were obtained directly from river gas data (5.1.5) and predictive equation approximations. Tsivoglou and Wallace (1972) derived Equation 10 based upon the energy dissipation in a flowing system:

$$\frac{K_o}{H} = K_2 = c \cdot \left( \frac{S \cdot L}{T_h} \right) \quad (10)$$

where  $S$  is the slope of the reach ( $m \ m^{-1}$ ),  $L$  is its length ( $m$ ),  $T_h$  is the residence time, and  $c$  is a constant equal to 0.177 and 0.154 for  $O_2$  and  $CO_2$ , respectively.  $K_2$  ( $d^{-1}$ ) is the reaeration coefficient for  $O_2$  converted to  $K_o$  ( $cm \ h^{-1}$ ) using depth [Moog and Jirka, 1998b]. Past gas exchange research often reported reaeration coefficients in terms of  $K_2$  [e.g. Owens *et al.*, 1964; Thyssen and Kelly, 1985; Simonsen and Harremoës, 1992], however more recent studies take flow depth into consideration and focus upon the liquid gas transfer velocity, or  $K_L$ . Except where noted, in this work  $K_L$  is used exclusively. Melching and Flores (1999) provide a semiempirical equation determined from 65 gas exchange studies using tracer gases in lotic systems with flows similar to the Clark Fork River. This equation differs from Equation 10 because it is based upon lotic morphology and is given by:

$$\frac{K_o}{H} = K_2 = 142 \cdot (VS)^{0.333} D^{-0.66} W^{-0.243} \quad (11)$$

where  $V$  is flow velocity ( $m \ s^{-1}$ ), and  $D$  and  $W$  represent mean river depth ( $m$ ) and width ( $m$ ), respectively.

$CO_2$  gas transfer velocity and nighttime community respiration at 20 °C, or  $K_{C(20)}$  and  $R_{20}$ , can also be determined mathematically using multiple linear regression on nighttime data [Thyssen and Kelly, 1985]. Using Equation 8, and applying a finite approximation, two independent variables are derived:

$$x1_t = \theta_K^{(T_m - 20)} S(pCO_{2sat} - pCO_{2m}) \quad (12)$$

$$x2_t = \theta_R^{(T_m - 20)} \quad (13)$$

where  $\theta_K$  and  $\theta_R$  are modified Arrhenius constants fixed at 1.0241<sup>1</sup> and 1.045 (see Section 3.3), respectively. These constants adjust for temperature effects on surface gas transfer and respiration, respectively. In the equations,  $pCO_{2m}$  and  $T_m$  represent the mean  $pCO_2$  and temperature measured at up and downstream locations. The means are used instead of upstream measurements on the assumption that they better approximate the *in situ* processes. For instance, the  $pCO_2$  gradient between the water and atmosphere changes appreciably as the water flows downstream. Change in DIC, calculated from  $pCO_2$  and discrete measurements of alkalinity, becomes the independent variables' response. Assuming respiration and gas transfer are only dependent upon temperature (i.e.  $K_{C(20)}$  and  $R_{20}$  are constant),

$$\frac{[DIC]_t - [DIC]_{t+\Delta t}}{\Delta t} = \frac{K_C}{H} x1_t + R_{20} x2_t \quad (14)$$

is used to solve for  $K_{C(20)}$  and  $R_{20}$  using time-series' of  $pCO_2$ , atmospheric partial pressures of  $CO_2$ , and temperature. A similar set of equations can be derived for  $O_2$  and  $K_{O(20)}$  and  $R_{20}$  are determined using time-series' of DO concentration, temperature, and DO saturation. Multiple regressions were performed using Microsoft EXCEL Analyze-it software. A discussion of the technique's accuracy and results is given in Section 5.1.5.

In all subsequent modeling,  $K_O$  and  $K_C$  are adjusted for temperature using a proportional relationship to the dimensionless Schmidt number ( $S_c$ ),  $K_L \propto S_c^{-1/2}$  yielding the equation:

---

<sup>1</sup> The modified Arrhenius relationship (Equation 13) and the Schmidt number dependence (Equation 16) agree within  $\pm 0.3$  when  $\theta_K = 1.0241$ . This value of  $\theta_K$  is taken from Thyssen and Kelly (1985), though it is widely used by other researchers [Daniil and Gulliver, 1988]. In this study, multiple regression analyses utilize the modified Arrhenius equation for simplification; otherwise the Schmidt number relationship is preferred.

$$K_{L(T)} = K_{L(20^{\circ}\text{C})} \left( \frac{S_c(T)}{S_c(20^{\circ}\text{C})} \right)^{-1/2} \quad (15)$$

where  $S_c$  is defined as the kinematic viscosity of freshwater divided by the diffusivity of the gas. Freshwater Schmidt numbers are determined using  $S_c = A - Bt + Ct^2 - Dt^3$  (t in degrees Celsius) where A, B, C, and D are given in Table 3.1 [Wanninkhof, 1992]. The Schmidt numbers for  $\text{CO}_2$  and  $\text{O}_2$  at 20 °C are equal to 600 and 530, respectively.

$K_L$  is related to wind speed, but mathematical relationships dependent on wind are often developed using ocean data [Wanninkhof, 1992]. In the ocean, wind is the primary source of turbulence driving surface gas transfer. Wind was not used to predict  $K_L$  in this study however, because turbulence is intrinsic in a riverine system and not simply dependent upon wind.

Surface gas transfer of  $\text{CO}_2$  is also driven by chemical reactions in surface waters.  $\text{CO}_2$  reacts with  $\text{OH}^-$  and water in the surface boundary layer, which increases the difference in  $p\text{CO}_2$  between the surface and water boundary layers [Wanninkhof, 1992]. The greater difference causes increased  $\text{CO}_2$  gas exchange, however chemical enhancement of  $\text{CO}_2$  gas exchange is assumed insignificant in the river's pH range.

**Table 3.1:** Coefficients for least squares third-order polynomial fits of Schmidt number versus temperature for freshwater (0 - 30°C).  $S_c$  (dimensionless) at 20°C is also given for  $\text{CO}_2$  and  $\text{O}_2$ . [Wanninkhof, 1992].

Gas	$S_c$ (20 °C)	A	B	C	D
$\text{CO}_2$	600	1911.1	118.11	3.4527	0.041320
$\text{O}_2$	530	1800.6	120.10	3.7818	0.047608

## 3.2 Photosynthesis

### 3.2.1 Rate model

Photosynthetic rates are dependent upon nutrient availability, biomass, and light. Models derived from field studies do a reasonable job of predicting observed rates [Hornberger *et al.*, 1976; Platt *et al.*, 1980; Jasper and Bothwell, 1986]. Equations used to model net photosynthesis are similar, the major distinction being their parameterizations. A commonly used relationship utilizing chlorophyll-*a* concentration and a hyperbolic tangent function of light intensity was first introduced by Jasby and Platt (1976). This model, derived from marine data, was further modified by Platt *et al.* (1980) to include a photoinhibition parameter. The modified model has been used to predict lotic periphyton photosynthesis [Jasper and Bothwell, 1986]. Photosynthetic rates normalized to chlorophyll-*a*,  $P^B$  (mg C (mg Chl-*a*)<sup>-1</sup> h<sup>-1</sup>) are predicted using [Jasper and Bothwell, 1986]:

$$P^B = P_s^B (1 - e^{-a}) e^{-b} \quad (16)$$

where  $a = \alpha I / P_s^B$  and  $b = \beta I / P_s^B$ . The parameters  $\alpha$  and  $\beta$  regulate photosynthetic efficiency and photoinhibition effects, respectively, while  $I$  symbolizes solar irradiance. The initial slope of the photosynthesis-irradiance (P-I) curve, or  $\alpha$ , was estimated from rate of change-irradiance curves normalized to chlorophyll-*a* during the earliest part of the day when photosynthesis was assumed to be the dominant process (see Section 5.1.3).  $\beta$  characterizes the effects of photoinhibition on photosynthetic rate and is discussed further in Section 5.1.3.  $P_s^B$  (mg C (mg Chl-*a*)<sup>-1</sup> h<sup>-1</sup>) represents the maximal rate of photosynthesis without photoinhibition. By setting  $\beta = 0$ , the photosynthesis relationship



becomes equivalent to earlier models that did not include photoinhibition. Typical values of  $P_s^B$  in lotic systems fall between 0.11-5.49 mg C (mg Chl-*a*)<sup>-1</sup> h<sup>-1</sup> [Jones and Adams, 1982; Jasper and Bothwell, 1986; Boston and Hill, 1991; Wellnitz and Rinne, 1999], so we selected a  $P_s^B$  that fell within this range. Although periphyton is the dominant life form along the study reach and the focus for developing the model, photosynthesis determined through modeling actually represents community net photosynthesis, including contributions from all lotic autotrophic and heterotrophic flora and fauna.

### 3.2.2 Irradiance

PAR irradiance, or  $I$  ( $\mu\text{E m}^{-2} \text{s}^{-1}$ ) in Equation 16, had to be estimated in September due to saturation of the PAR sensor output during midday over the deployment period. This shortcoming was corrected prior to the winter deployment allowing *in situ* measurements of PAR to be used for December modeling. PAR, defined as irradiance in the range of 400-700 nm, is the primary portion of the spectrum used in plant photosynthesis. It is estimated as 46% of the total solar surface irradiance. The model relies on the solar angle, dependent on geographic position, date, and local time, to determine the maximum irradiance. A complete description is given in Baehr (2000). Local NOAA cloud cover time-series' and sensor depth (1 m) are used to model the amount of irradiance reaching the sensor location. Hourly cloud cover data, described using 6 different meteorological terms, were converted to transmissivity and interpolated. Total solar irradiance was then adjusted for transmissivity to model the effects of clouds. A difficulty with PAR modeling is the determination of an appropriate extinction coefficient ( $\eta$ ) for the water. In the aqueous environment,  $\eta$  is the measure of irradiance absorbed by the water and varies with wavelength and depth. An average  $\eta$  for

September was estimated using PAR measurements early in the day, prior to circuit saturation. PAR modeling for one cloudy day in December resulted in overestimation of the maximum *in situ* PAR by  $<20 \mu\text{E m}^{-2} \text{s}^{-1}$  (~13 %). The difference is likely caused by an underestimation of  $\eta$ , although seasonal changes in water composition (e.g. dissolved organic matter) are expected to alter  $\eta$ .

### 3.2.3 Biomass

*In situ* measurements of suspended chlorophyll-*a* were made during both deployments. However, as in many lotic systems, the majority of algae inhabit the substrata. Speciation and biomass analyses were not performed; so suspended chlorophyll-*a* is used as a proxy for attached biomass. The resulting chlorophyll-*a* concentrations are used in Equation 16 for modeling periphyton photosynthetic rates. Bowker et al. (1996) tested the hypothesis that suspended algae originate from periphyton. They report that greater than 80% of the lotic organisms inventoried were found both in suspended and attached communities. The study also indicates that the physical action of the flow was not the primary factor dislodging the biota. They suggest that biological processes are a significant source of suspended periphyton. The relationship utilized to determine periphytic biomass from chlorophyll-*a* measurements is given by:

$$\ln x = 4.392 + 0.315 \ln y \quad (17)$$

where  $y$  = suspended algal biomass ( $\text{mg m}^{-3}$ ) and  $x$  = periphytic biomass ( $\text{mg m}^{-2}$ ) [Bowker et al., 1996]<sup>2</sup>. The mean suspended chlorophyll-*a* for each deployment period

---

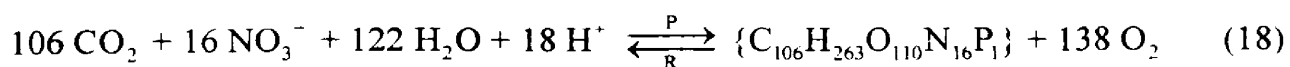
<sup>2</sup>Bowker et al. (1996) report suspended algal and periphytic biomasses as "standing crops", however, due to confusion regarding the term's definition, biomass is used instead. Evaluation of their sampling technique indicates that biomass is an accurate description of the sampled quantities.

was chosen for use in modeling to maintain simplicity and, in part, as a result of unforeseen complications (see Section 4.4). Once the periphytic biomass is estimated (per unit area), the concentration of chlorophyll-*a* is determined using the average area of the reach and USGS discharge data.

Possible sources of error using this method include differences between the Clark Fork River and the Welsh river where Equation 17 was determined. The surface area used to calculate total chlorophyll-*a*, estimated from river length and width, is also possibly much larger due to the greater surface area of cobble. This would result in increased chlorophyll-*a* concentrations and subsequently, greater photosynthesis estimates. However, this source of error is offset, in part, by the photosynthetic model, which is based upon the assumption that the chlorophyll-*a* originates from suspended phytoplankton. Comparisons between suspended and attached periphyton suggest that periphytic suspensions have greater photosynthetic rates than attached communities [Jasper and Bothwell, 1986]. It is not known if the suspended chlorophyll-*a* determined from field measurements arises from living or dead organisms, so an assumption was made that its contribution to community production was negligible.

### 3.2.4 Photosynthetic quotient

Conversion of photosynthetic rates between  $p\text{CO}_2$  and DO models is often accomplished assuming a widely accepted aquatic photosynthetic quotient (PQ) of 1.2 [Kirk, 1994], where PQ equals the molar ratio of  $\text{O}_2$  produced to  $\text{CO}_2$  consumed. The PQ is expected to agree closely with Redfield stoichiometry (Equation 18), which predicts a  $\text{PQ} = 1.3$  [Stumm and Morgan, 1996]. The Redfield equation:



provides a simplification for a plethora of complex metabolic process involving a large range of aquatic organisms [*Stumm and Morgan, 1996*]. The stoichiometry of reaction between the nutrients will vary to some degree for each locale, but the simplification is quite valuable nonetheless. The PQ used in our model however, was estimated from plots of daytime  $\Delta DO$  vs.  $-\Delta DIC$ , where both fluxes were adjusted for gas transfer effects (see Section 5.1.7).

### 3.3 Respiration

#### 3.3.1 Rate model

Community respiration (R) can be modeled using the modified Arrhenius relationship:

$$R = R_{20} \theta^{(T-20)} \quad (19)$$

where  $R_{20}$  is the respiratory rate at 20 °C, T is *in situ* temperature (°C), and  $\theta$  is the Arrhenius coefficient. In other studies,  $\theta$  was estimated as 1.07 [*Erlandsen and Thyssen, 1983*] and 1.045 [*Parkhill and Gulliver, 1999*]. In this study a value of 1.045 was chosen. Estimates of  $R_{20}$  were found using a multiple regression technique discussed in Section 5.1.5. Photorespiration, or the increase in respiratory rate due to light, is known to occur in many plants including algae, but is not adequately quantified because of the difficulty determining its contribution to daily net metabolism [*Wetzel, 1983*]. Recent efforts to model photorespiration have shown increased agreement with field data when compared to Equation 19 [*Parkhill and Gulliver, 1999*]. They use the equation:

$$R = (R_{20} + \beta_R I_t) \cdot \theta^{(T-20)}, \quad (20)$$

where  $\beta_R$  is termed the photorespiration constant and  $I_t$  is the mean irradiance for the previous  $t$  hours. Respiratory contributions were modeled using both equations; a discussion of the results can be found in Section 5.1.8.

### 3.3.2 Respiration quotient

Net community respiratory rates are typically converted between  $p\text{CO}_2$  and DO models using a respiration quotient (RQ) of 0.85, where RQ is the molar ratio of  $\text{CO}_2$  produced to  $\text{O}_2$  consumed [Wetzel, 1983]. Redfield stoichiometry predicts a  $\text{RQ} = 0.77$  for comparison. In modeling respiration effects on  $p\text{CO}_2$  and DO, an RQ was also estimated from plots of nighttime  $\Delta\text{O}_2$  vs.  $-\Delta\text{DIC}$  (see Section 5.1.7).

## 3.4 $p\text{CO}_2$ and DO models

The modeling programs, RIVERCO2.BAS and RIVERDO.BAS, given in Appendices 1 and 2, solve Equations 8 and 9 iteratively using upstream field measurements as initial values. Community respiration is modeled using Equation 20. Photosynthetic rates are determined using Equation 16 in a commercial spreadsheet application and input into the model as an array. Likewise, upstream *in situ* gas measurements, atmospheric  $p\text{CO}_2$ , PAR, temperature, and alkalinity are stored as individual files for input into the model. Temperature input from up and downstream *in situ* measurements is linearly interpolated as the water travels downstream. The  $p\text{CO}_2$  model uses temperature in calculations of DIC,  $p\text{CO}_2$ ,  $K_C$ , and respiratory rates. In the DO model, temperature is used to calculate saturation concentration and adjust  $K_O$  and respiratory rates. In the  $\text{CO}_2$  model, upstream alkalinity and  $p\text{CO}_2$  are used to calculate the upstream DIC. Alkalinities, determined from discrete sample analyses, are linearly

interpolated between available data. Metabolic effects on alkalinity are estimated using Redfield stoichiometry, which results in an 18/106-mol increase in alkalinity for each mol of CO<sub>2</sub> consumed (Equation 18). Other information such as  $K_L$ , respiration ( $R_{20}$ ), travel time, number of iterations, and filenames are input directly by the user. This format allows flexibility for evaluating sensitivity to parameter changes.

Carbonate equilibria in the model are solved using the Newton-Raphson method. Table 3.2 provides a summary of the equations and constants used in these calculations. Total travel time is divided into time steps ( $dt$ ) using the number of iterations chosen by the user ( $dt = \text{travel time} / \# \text{ steps}$ ). Beginning with the initial upstream DIC, flux due to metabolism is imposed and the new DIC is used in conjunction with the new alkalinity to determine a new  $p\text{CO}_2$ . The new  $p\text{CO}_2$  is then used to calculate the  $\Delta\text{DIC}$  resulting from gas transfer. This new DIC is used to calculate  $p\text{CO}_2$  and begin the process at the next time step. The whole process is continued until the total residence time has been reached. A similar structure without equilibrium calculations is used in modeling changes in DO.

The model allows for iterations  $\leq 100$ , though 20 and 10 were convenient for September and December, respectively. This resulted in a time step,  $dt = 13 \text{ min}$ . As mentioned, the models assume negligible longitudinal dispersion and similarly, water in the reach is assumed well mixed, both vertically and laterally.

**Table 3.2:** Thermodynamic constants and mass balance equations defining the aqueous carbonate system for use in calculations and modeling.

<b>Carbonate System</b>	
<b>Equilibrium Constants</b>	<b>Source</b>
$K_0 = \frac{[\text{H}_2\text{CO}_3^*]}{p\text{CO}_2}$	Weiss (1974)
$K_w = [\text{H}^+][\text{OH}^-]$	Millero (1979)
$K_1 = \frac{[\text{HCO}_3^-][\text{H}^+]}{[\text{H}_2\text{CO}_3^*]}$	Millero (1979)
$K_2 = \frac{[\text{CO}_3^{2-}][\text{H}^+]}{[\text{HCO}_3^-]}$	Millero (1979)
$K_{sp} = [\text{Ca}^{2+}][\text{CO}_3^{2-}]$	Stumm and Morgan (1996)
<b>Mass Balance Equations</b>	
$[\text{H}_2\text{CO}_3^*] = [\text{CO}_2(\text{aq})] + [\text{H}_2\text{CO}_3]$	
$\text{DIC} = [\text{H}_2\text{CO}_3^*] + [\text{HCO}_3^-] + [\text{CO}_3^{2-}]$	
$\text{ALK} = [\text{HCO}_3^-] + 2[\text{CO}_3^{2-}] + [\text{OH}^-] - [\text{H}^+]$	
$\text{CA} = [\text{HCO}_3^-] + 2[\text{CO}_3^{2-}]$	

## Chapter 4

### Results

#### 4.1 Travel times

A conservative tracer was not used during either September or December, so travel time between up and downstream locations was determined via an alternative method. Short-lived increases in discharge during each study period resulted in obvious conductivity spikes (presented later) at both monitoring stations (Figures 16a and 17a). These isolated surges, caused by changes in Milltown Dam discharge, were validated through comparison between USGS gauging station and YSI depth sensor data. Spikes in conductivity that coincided with distinctive discharge events were used to estimate travel time. This approach resulted in travel times of 4.25 and 2.5 h in September and December, respectively. Travel time error is estimated to be  $\pm 0.5$  h, based upon conductivity data and the sensor measurement intervals. Travel time estimates were also calculated using flow velocity and stream parameters. The average discharge divided by the vertical area of the river (width  $\cdot$  depth) results in an estimate of average velocity. The reach's distance is divided by the velocity, which results in travel times of 3.69 and 1.93 h for September and December, respectively. Calculated travel times closely agree to within the uncertainty of those determined from *in situ* conductivity measurements. Based upon these calculations, travel time increases  $\sim 6$  min for every  $1 \text{ m}^3 \text{ s}^{-1}$  decrease in discharge. However, travel times determined from conductivity spikes are used for calculations and modeling.



## 4.2 September Biogeochemical Data

### 4.2.1 $p\text{CO}_2$

The September  $p\text{CO}_2$  time-series are shown in Figure 3a. Autonomous  $p\text{CO}_2$  measurements were compared with  $p\text{CO}_2$ 's calculated from discrete sample measurements of pH and alkalinity (Figure 3a). A summary of these data is given in Table 4.1. Discrete samples deviate  $\pm 42.6 \mu\text{atm}$  from *in situ* measurements ( $n = 28$ ). Instrument biofouling was minimal on upstream instruments, however the downstream sensor array had significant growth. Slower moving water at the downstream sensor array was probably a major factor, as periphyton were given a better opportunity to proliferate. Calculated and measured  $p\text{CO}_2$  does not agree better, in part due to biofouling of the downstream instrument towards the end of the deployment period, but pH uncertainty is also a factor. During this time, downstream field measurements of  $p\text{CO}_2$  are also consistently lower than calculated values (Table 4.1).

*In situ*  $p\text{CO}_2$  time-series' reveal a considerable range of variability during September, ranging from  $118 \mu\text{atm}$  during the day and  $604 \mu\text{atm}$  at night (Figure 3a). Although up and downstream data are difficult to interpret, the difference plot shown in Figure 3b reveals a clear diel  $\Delta p\text{CO}_2$ . The inverse correlation of the  $\Delta p\text{CO}_2$  plot with PAR (Figure 3c) suggests that the trend is dominated by community metabolism. Net community photosynthesis appears to be primarily responsible for decreases in  $p\text{CO}_2$  during the day and net respiration causes the subsequent increase at night.

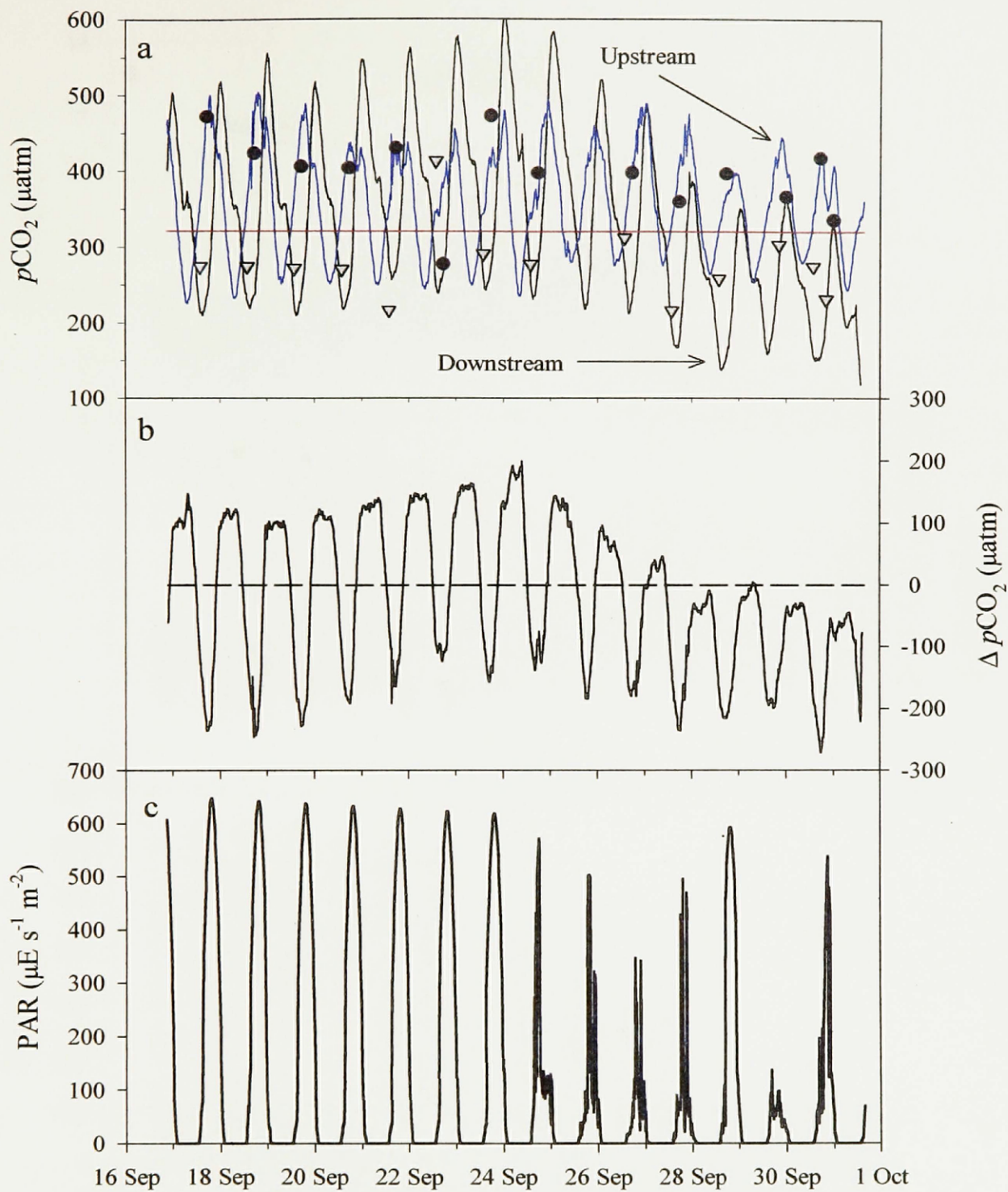


**Figure 3:** Measured  $p\text{CO}_2$  in the Clark Fork River during September 1999 (GMT). Up and downstream data are represented in plot a by blue and black curves, respectively. The red curve represents an estimate of local atmospheric saturation. Calculated up and downstream  $p\text{CO}_2$  are black circles and gray triangles, respectively. Downstream data is shifted back 4.25 h to account for travel time, so that up and downstream measurements represent the same water. Note the reduced complexity of the  $\Delta p\text{CO}_2$  curve (b) and its negative correlation with PAR (c), signifying the importance of net community metabolism.

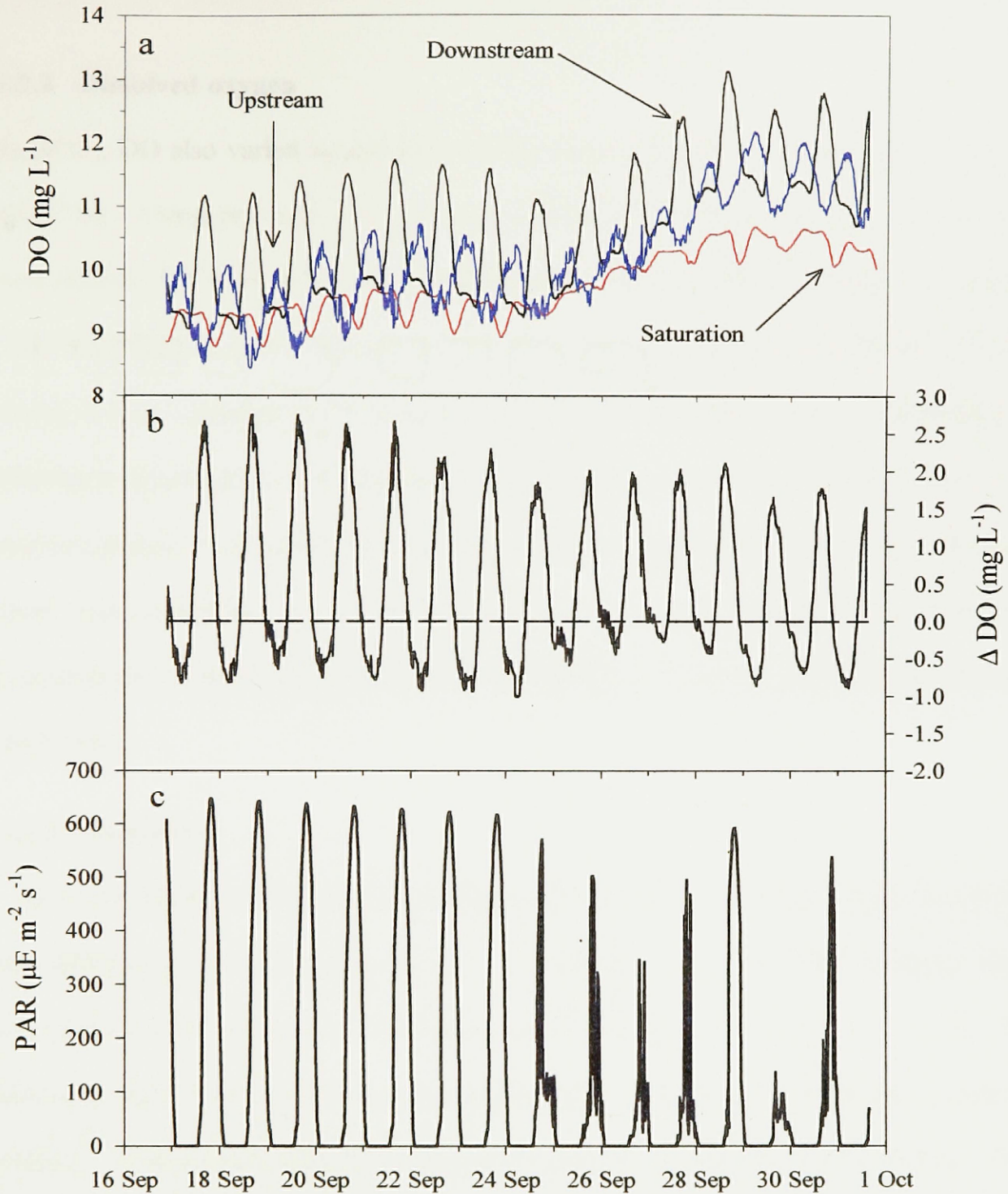


**Figure 4:** September *in situ* DO measurements in the Clark Fork River 1999 (GMT). In plot a, up and downstream data are represented by blue and black curves, respectively. The red curve in plot a represents downstream DO saturation. Downstream data is shifted back 4.25 h for travel time. Note the reservoir effect on the upstream DO cycle. The change in DO from up to downstream (b) is correlated with PAR (c), indicating that metabolism is the dominant process at work.

### 4.2.2 Dissolved oxygen

Like  $p\text{CO}_2$ , DO also varied significantly in September, ranging from 8.43 to 13.12 mg L<sup>-1</sup> (Figure 4a). Using pre- and post-deployment data, it was determined that the upstream sensor drifted ~6% during the deployment period. A linear drift was assumed, as claimed by the manufacturer, and a linearly interpolated correction factor was applied. The diel increase in  $\Delta\text{DO}$  coincides with increases in PAR and a decrease in  $p\text{CO}_2$ , supporting that community metabolism is the principal factor controlling variability (Figures 3 and 4). A consistent pattern in the  $\Delta\text{DO}$  plot is observed throughout the first half of the deployment period, when conditions were similar (Figure 4b). Up and downstream minimum DO concentrations correlate with saturation concentration (Figure 4a), and hence temperature (Figure 14a).

### 4.2.3 Alkalinity

River alkalinities were generally higher upstream than downstream, with an absolute mean difference of 18 ( $\pm 11$ )  $\mu\text{eq kg}^{-1}$  ( $n = 14$ ) (Figure 5). Upstream alkalinity varied from 2704 to 2777  $\mu\text{eq kg}^{-1}$  with a mean concentration of 2731  $\mu\text{eq kg}^{-1}$  ( $n = 14$ ). The addition of  $\text{Hg}^{2+}$  to suppress biological consumption of  $\text{CO}_2$  had no discernible effect on alkalinity. Comparisons between spiked and unperturbed samples yielded results within the error of measurement technique (i.e.  $\pm 6$   $\mu\text{eq kg}^{-1}$ ). Concentrations downstream ranged from 2688 to 2767  $\mu\text{eq kg}^{-1}$  with a mean of 2714  $\mu\text{eq kg}^{-1}$  ( $n = 14$ ). A plot of both up and downstream concentrations is given in Figure 5. Tables 4.1 and 4.2 summarize the measurements of alkalinity and pH used for  $p\text{CO}_2$  calculation. On September 21, up and downstream alkalinities increased sharply and remained high, apparently caused by a

discharge spike. Both conductivity and discharge plots support this interpretation (Figure 16). Photosynthesis increases alkalinity through the consumption of ions (e.g.  $\text{NO}_3^-$ ,  $\text{HPO}_4^{2-}$ , and  $\text{H}^+$ ) (e.g. Equation 18).

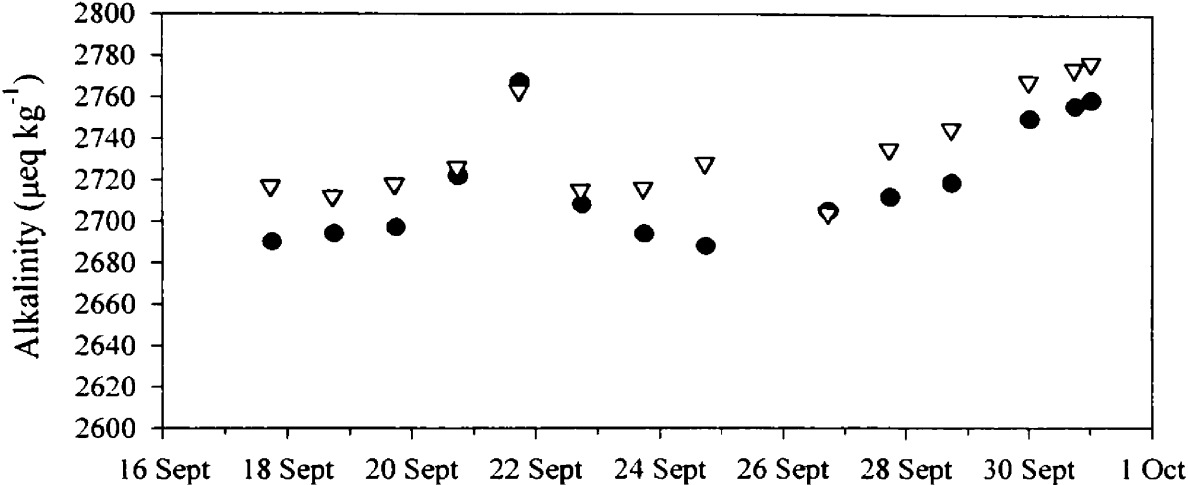


**Figure 5:** Up (gray triangles) and downstream alkalinity (black circles) data in the Clark Fork River during September 1999 (GMT). Error bars representing one standard deviation are included but not visible on this scale.

Since discrete sampling was performed during the day, alkalinity is expected to increase downstream as a result of photosynthesis. However, lower downstream alkalinities suggest a source of  $\text{CO}_2$  over the reach if the trend is consistent between available data. Sampling at both sites was performed within 0.5 h, much less than the travel time. The differences in alkalinity between up and downstream measurements do not necessarily represent processes occurring over the reach because of effects from the impoundment (Section 4.5). The long-term trend over the study period is one of increasing alkalinity.

**4.2.4 pH**

Discrete spectrophotometric pH measurements were performed as described in Section 2.2.4. It was discovered that the addition of  $\text{Hg}^{2+}$  to inhibit metabolism

significantly altered sample pH. The addition of  $\text{Hg}^{2+}$  affects sample pH through two mechanisms: 1) Freshwater is hydrolyzed by  $\text{Hg}^{2+}$  to form  $\text{Hg}(\text{OH})_2$ , and 2) complexation with the sulfur-moiety in cresol red perturbs the indicator's response to pH. The effect of pH perturbation by  $\text{Hg}^{2+}$  was not discovered until the December study. A mean pH offset of 0.196 ( $\pm 0.031$ ) pH units ( $n = 4$ ) was applied to September pH data to correct for  $\text{Hg}^{2+}$  perturbation. This offset was determined by comparing discrete sample pH to pH's calculated from *in situ*  $p\text{CO}_2$  and alkalinity.

During September, discrete sample analyses indicate that downstream pH was higher than upstream on all but one day (Table 4.1). The mean absolute difference between up and downstream pH was 0.180 ( $\pm 0.053$ ) pH units. Although the pH trend appears to contradict associated alkalinity measurements, the seeming inconsistency can be explained by examining the  $p\text{CO}_2$  data. The river is supersaturated with respect to dissolved  $\text{CaCO}_3$  and subsequently, well buffered. Alkalinity is expected to be relatively constant, so  $p\text{CO}_2$  is probably the dominant factor controlling pH. As a consequence of the unsynchronized up and downstream diel patterns (discussed in Section 4.5),  $p\text{CO}_2$  is greater upstream during sampling times, which results in a lower pH (Table 4.1). No long-term trends in pH data are apparent (Figure 6).

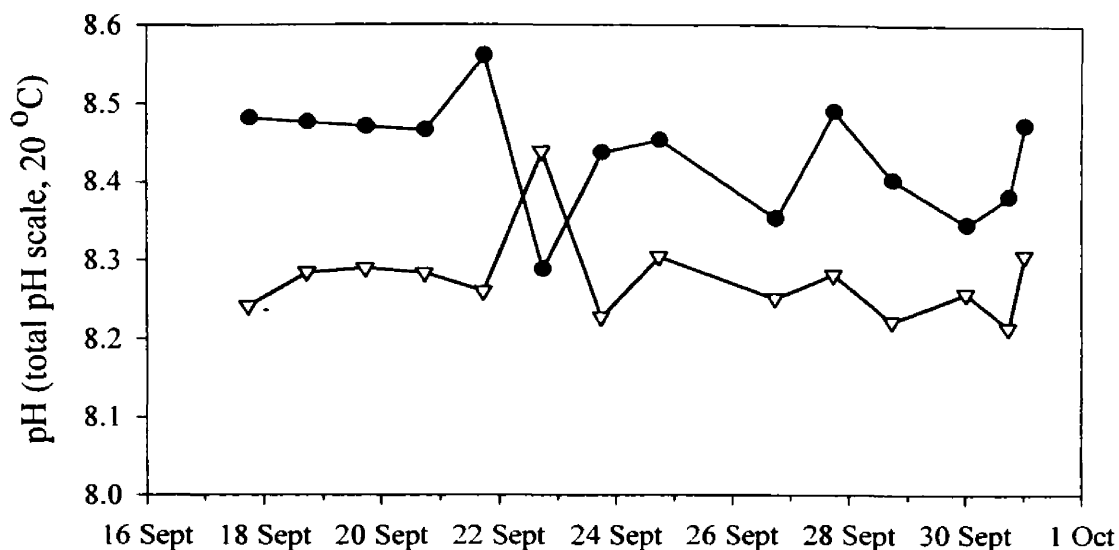


**Figure 6:** September spectrophotometric pH measurements, where up and downstream data are represented by triangles and circles, respectively. Lines are presented for clarity only.

#### 4.2.5 Atmospheric $p\text{CO}_2$

In September and October 2000, atmospheric  $p\text{CO}_2$  was monitored in order to learn more about local atmospheric  $p\text{CO}_2$  variability. Oceanographers often utilize  $360 \mu\text{atm}$  for a mean  $p\text{CO}_2$  at sea level. When this is corrected to  $0.89 \text{ atm}$ , the typical local barometric pressure, the resulting  $p\text{CO}_2$  is  $320 \mu\text{atm}$ . Post-deployment calibrations revealed that the  $\text{CO}_2$  system drifted, resulting in atmospheric  $p\text{CO}_2$  accuracy of  $\pm 7 \mu\text{atm}$ . Over the course of  $\sim 3$  weeks,  $p\text{CO}_2$  experienced diurnal fluctuations with a minimum and maximum of  $311$  and  $411 \mu\text{atm}$ , respectively (Figure 7a). The mean  $p\text{CO}_2$  during this period was  $333 \mu\text{atm}$  ( $n = 884$ ). A clear pattern of increasing  $p\text{CO}_2$  is observed after dark, returning to a baseline of  $\sim 320 \mu\text{atm}$  during the day. Given the inverse correlation with the photoperiod, nightly increases in local atmospheric  $p\text{CO}_2$  must be significantly influenced by local respiration. Atmospheric  $p\text{CO}_2$  remains closer to  $320 \mu\text{atm}$  when local wind speeds, measured at the NOAA meteorological station, are clearly higher and

sustained (Figure 7c). The correlation with wind indicates that local sources of atmospheric  $p\text{CO}_2$  are less important during periods of high winds. Photosynthesis also appears to be an important sink for  $\text{CO}_2$ , since the  $p\text{CO}_2$  also decreases daily during periods of low wind.

**Table 4.1:** Discrete alkalinity and spectrophotometric measurements in the Clark Fork River during **September 1999**. Samples marked with an (x) in the  $\text{Hg}^{2+}$  column were spiked to deter further metabolic  $\text{CO}_2$  consumption or production. Perturbed sample pH is offset using methods described in Section 4.2.4. Calculated and measured  $p\text{CO}_2$ 's are given for comparison.

Location	Date 1999 GMT	Year Day GMT	$\text{Hg}^{2+}$	pH	ALK $\mu\text{mol kg}^{-1}$	SAMI $p\text{CO}_2$ $\mu\text{atm}$	Calculated $p\text{CO}_2$ $\mu\text{atm}$	$\Delta$ $\mu\text{atm}$
Upstream	9/17	259.7326	x	8.4378	2717	467	472	5
	9/18	260.7319	x	8.4811	2712	472	423	-49
	9/19	261.7292	x	8.4866	2718	464	405	-59
	9/20	262.7319	x	8.4804	2726	428	404	-24
	9/21	263.7319	x	8.4573	2763	426	430	6
	9/22	264.7257	x	8.6353	2715	379	278	-101
	9/23	265.7340	x	8.4242	2716	414	473	59
	9/24	266.7319	x	8.5013	2728	366	398	32
	9/26	268.7250	x	8.4479	2704	400	398	-2
	9/27	269.7257	x	8.4785	2735	410	360	-50
	9/28	270.7271	x	8.4185	2745	371	397	26
	9/30	272.0042	x	8.4554	2768	406	367	-39
	9/30	272.7299	x	8.4112	2774	425	418	-7
9/31	273.0063	x	8.5039	2777	405	336	-69	
Downstream	9/17	259.7632	x	8.4821	2690	260	274	12
	9/18	260.7535	x	8.4765	2694	261	274	13
	9/19	261.7507	x	8.4711	2697	284	272	-12
	9/20	262.7507	x	8.4667	2722	277	270	-7
	9/21	263.7514	x	8.5612	2767	337	216	-121
	9/22	264.7465	x	8.2897	2708	311	414	103
	9/23	265.7500	x	8.4386	2694	329	291	-38
	9/24	266.7479	x	8.4542	2688	323	277	-46
	9/26	268.7403	x	8.3542	2705	312	312	0
	9/27	269.7417	x	8.4908	2712	250	216	-34
	9/28	270.7417	x	8.4036	2719	200	259	59
	9/30	272.0201	x	8.3472	2750	228	303	75
	9/30	272.7465	x	8.3836	2756	190	275	85
9/31	273.0174	x	8.4744	2759	169	232	63	



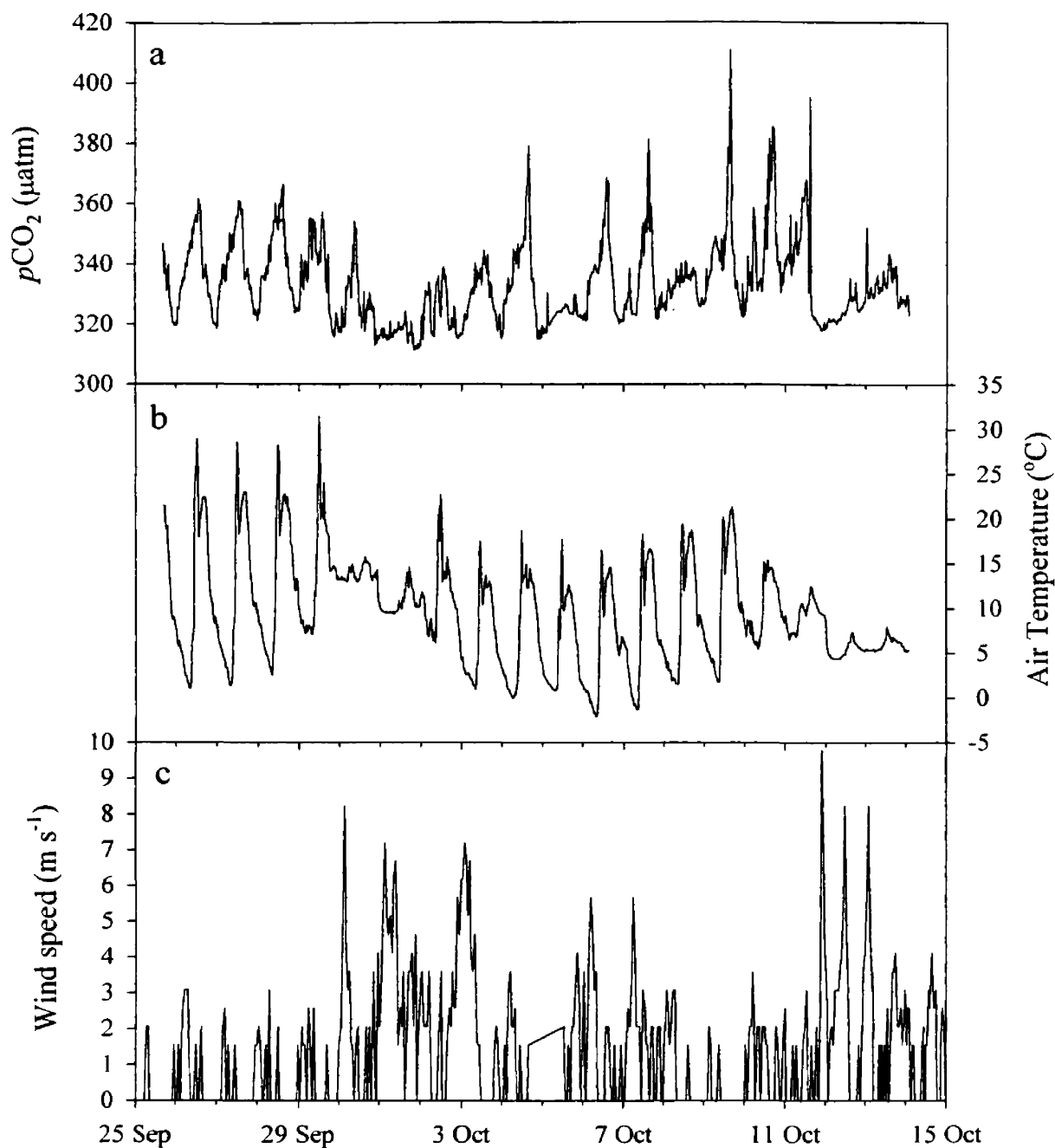


**Figure 7:** Atmospheric  $p\text{CO}_2$  (a), air temperature (b), and wind speed (c) during September and October 2000 (GMT). Note nighttime  $p\text{CO}_2$  remains near 320  $\mu\text{atm}$  during periods of high winds (e.g. October 12 and 15). The temperature spike observed every morning in plot b is probably a result of sunshine striking the sensor for a short period.

## 4.3 December Biogeochemical Data

### 4.3.1 $p\text{CO}_2$

During December 1999, mean absolute differences between calculated  $p\text{CO}_2$  and *in situ* levels are  $\pm 15.4 \mu\text{atm}$  ( $n = 27$ ). Both pH data from unperturbed samples (i.e. no  $\text{Hg}^{2+}$ ) and spiked samples were used for calculation of  $p\text{CO}_2$  (Table 4.2). Once corrected for the perturbation, the spiked sample  $p\text{CO}_2$  calculations agree closely with unperturbed sample calculations (Figure 8). Near the end of the 13-d deployment, when both SAMI- $\text{CO}_2$  sensors were located together at the downstream site, data reveal differences up to  $20 \mu\text{atm}$  during short periods when the  $p\text{CO}_2$  was changing rapidly (i.e. during the day). This effect was much less at night ( $\pm 5 \mu\text{atm}$ ) when the rate of change of  $p\text{CO}_2$  was not as rapid. A poorly functioning pump in the downstream instrument likely played a role in these offsets. Reduced flushing in the cell increased instrument response time.

Diel trends in  $p\text{CO}_2$  are dramatically smaller in magnitude than in September, but again suggest that net community photosynthesis was significant (Figure 8a). Reduced PAR (Figure 8c), lower temperatures, and a shorter transit time between sites were all contributing factors. Changes in  $p\text{CO}_2$  are very small during the night, suggesting that respiration was not as important as in the autumn deployment (Figure 8b).

### 4.3.2 Dissolved oxygen

DO concentrations ranged from  $11.87$  to  $14.16 \text{ mg L}^{-1}$  in December (Figure 9a). Pre- and post-deployment calibrations and Winkler titration data indicate that the downstream DO sensor drifted  $\sim 15\%$ . A linear drift correction was also applied to the downstream data in this instance. As a consequence, DO field measurements are considerably more

reliable towards the end of the study period when Winkler data were available. DO accuracy late in the study period is estimated at  $\pm 0.2 \text{ mg L}^{-1}$  from comparisons between corrected DO data and Winkler titrations. These analyses yielded a standard deviation of  $0.05 \text{ mg DO L}^{-1}$  ( $n = 3$ ). During the night when respiration is expected to control DO flux,  $p\text{CO}_2$  data reveal  $< 20 \text{ } \mu\text{atm}$  changes over the study reach (Figure 9b). Since respiration caused large nightly changes in  $p\text{CO}_2$  during September, this is strong evidence that respiration did not dominate DO flux. Consequently, surface gas exchange would be significant. This conclusion is supported by strong agreement between downstream field DO measurements and saturation at dusk (Figure 9a). As available PAR diminishes, respiration and gas transfer drive DO towards saturation. During the night, gas transfer maintains DO near saturation.

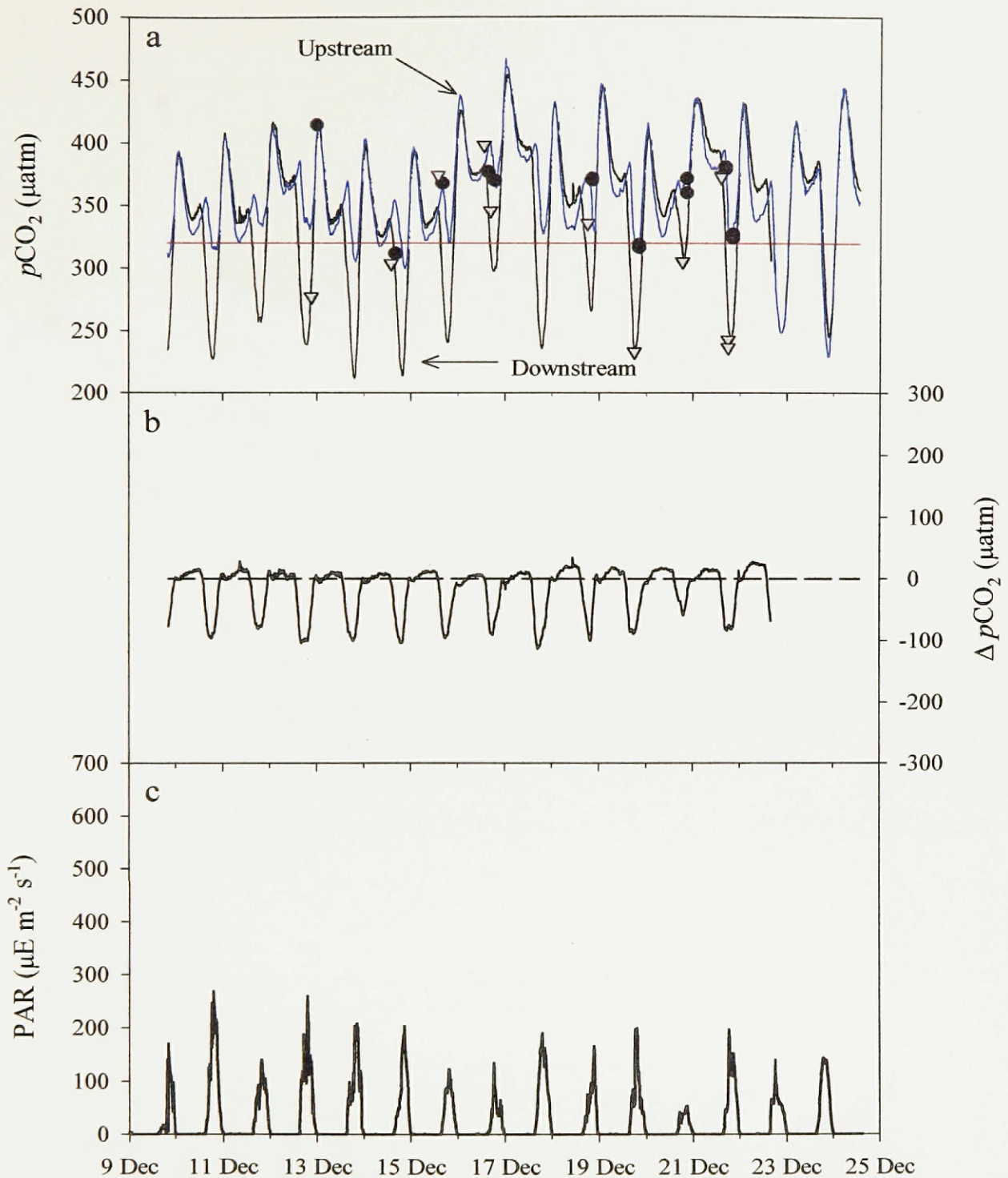


**Figure 8:** Measured  $p\text{CO}_2$  in the Clark Fork River during December 1999 (GMT). Up and downstream data are represented in plot a by blue and black curves, respectively. The red curve represents a local estimate of atmospheric saturation. Up and downstream calculated  $p\text{CO}_2$ 's are circles and triangles respectively. Downstream data is shifted back 2.5 h to account for travel time, so that up and downstream data represent the same water. The more interpretable  $\Delta p\text{CO}_2$  curve (b) reveals a decrease inversely correlated with PAR, but with little change at night. Reduced PAR (c) (compared to September data) is a significant factor in December's smaller daytime change. Note SAMI- $\text{CO}_2$  agreement midway through Dec 22 when instruments were located beside each other.

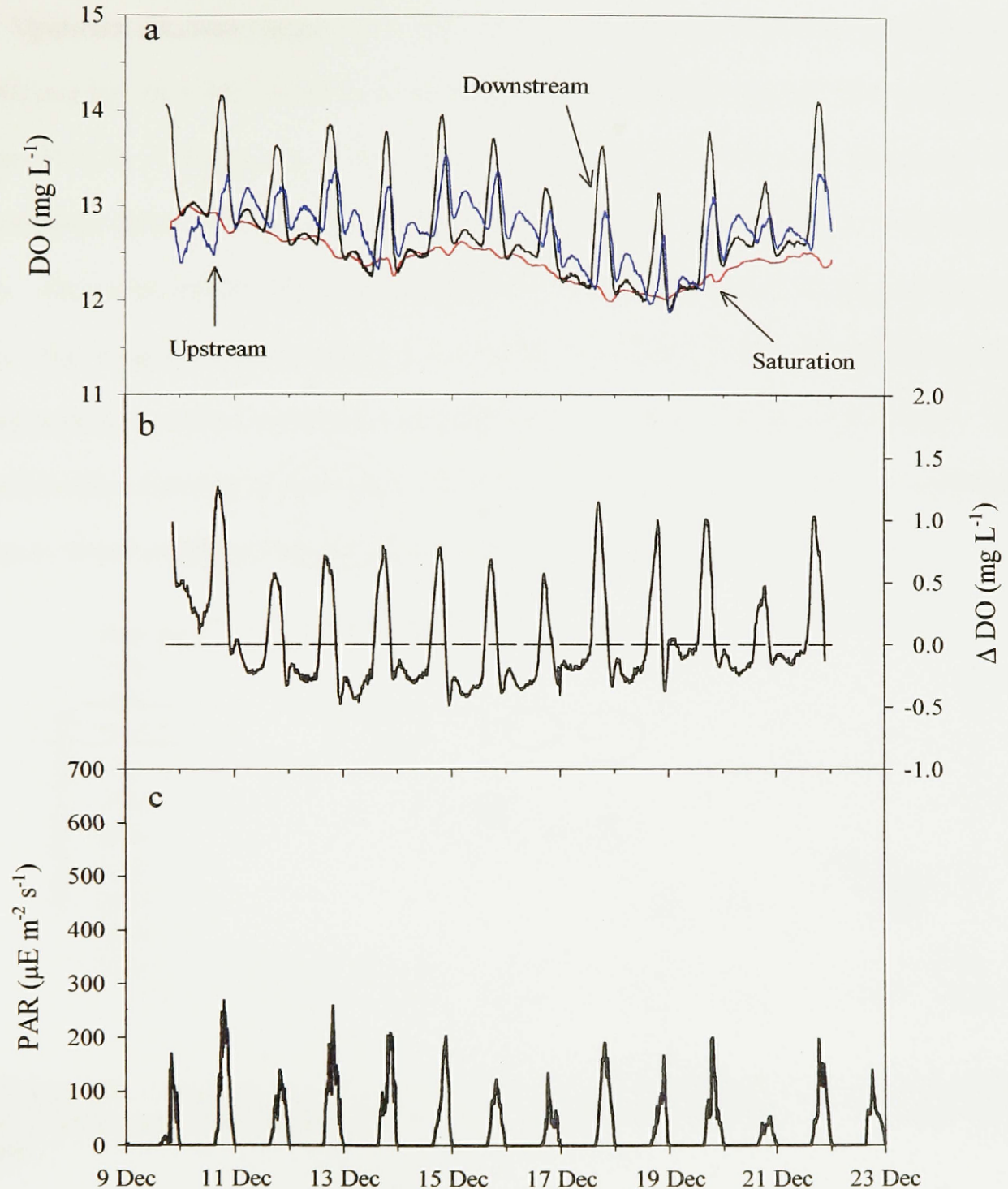


**Figure 9:** December *in situ* DO measurements in the Clark Fork River 1999 (GMT). In plot **a**, up and downstream data are represented by blue and black curves, respectively. Downstream data is shifted back 2.5 h for travel time. Note the reservoir's influence is still evident in the upstream DO cycles. The change in DO (**b**) correlates with PAR (**c**). Downstream DO saturation is represented by the red curve in plot **a**. Note scale difference in plots **a** and **b** compared to September.

### 4.3.3 Alkalinity

Upstream alkalinity ranged from 2622 to 2753  $\mu\text{eq kg}^{-1}$  with a mean concentration of 2660  $\mu\text{eq kg}^{-1}$  ( $n = 15$ ). Mean downstream alkalinity was 2662  $\mu\text{eq kg}^{-1}$  ( $n = 12$ ), ranging from 2619 to 2724  $\mu\text{eq kg}^{-1}$ . December alkalinities do not follow the same trend as in September; rather the data suggest that very little change occurs along the reach (Figure 10). The mean absolute difference between up and downstream is  $7 (\pm 8) \mu\text{eq kg}^{-1}$  ( $n = 12$ ). The long-term trend indicates a gradual decrease in both up and downstream concentrations, with a subsequent increase towards the end of the study period. This trend is also observed in December conductivity data (Figure 17). Reduced metabolism (due to winter conditions) and a shorter reach are believed to be important factors.

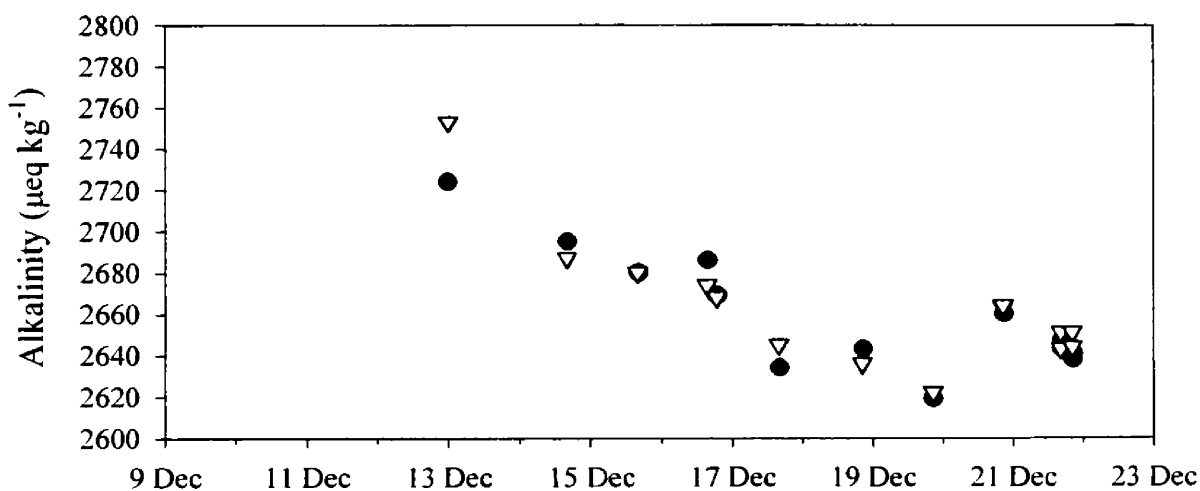


**Figure 10:** Alkalinity data for December 1999: Up and downstream data are represented by gray triangles and black circles, respectively. Error bars are included, but not visible on this scale.

### 4.3.4 pH

December spectrophotometric pH measurements are given in Table 4.2 and Figure 11. Sample perturbation by  $\text{Hg}^{2+}$  was discovered early in the December study, allowing

time to quantify the effect. A mean offset of  $0.1230 (\pm 0.0067)$  pH units ( $n = 7$ ) was determined by comparing spiked and unperturbed samples collected in December. The offset was subsequently applied to correct for this systematic error in December's pH data.

Upstream pH in December often exceeded downstream measurements, but agreement was much closer than in September (Figure 6). The mean absolute difference between up and downstream was  $0.059 (\pm 0.056)$  pH units ( $n = 10$ ). Differences in  $p\text{CO}_2$  are more likely to be the major source of pH disagreement, since alkalinities are similar between up and downstream locations (Figure 10). No long-term trends in pH data are apparent over the course of study (Figure 11).

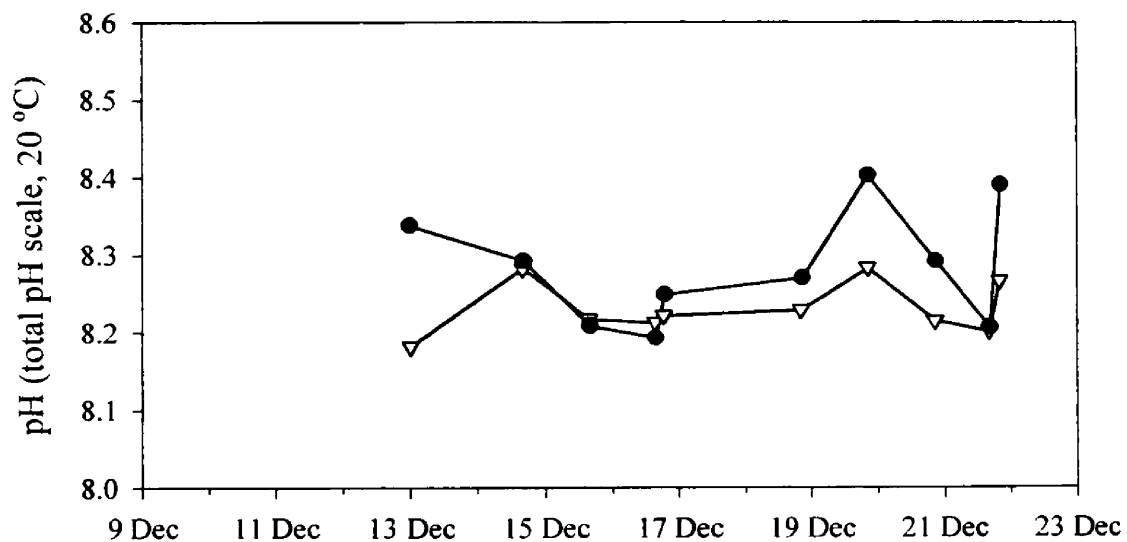


**Figure 11:** December spectrophotometric pH measurements, where up and downstream data are represented by gray triangles and black circles, respectively. Lines are presented for clarity only.

**Table 4.2:** Discrete alkalinity and spectrophotometric pH measurements in the Clark Fork River during December 1999. Samples marked with an (x) in the  $\text{Hg}^{2+}$  column were spiked to inhibit metabolism. Perturbed sample pH is offset using methods described in Section 4.3.4. Original pH is utilized for  $p\text{CO}_2$  calculations when  $\text{Hg}^{2+}$  is not a factor. Calculated and measured  $p\text{CO}_2$ 's are given for comparison.

Location	Date 1999 GMT	Year Day GMT	$\text{Hg}^{2+}$	pH	ALK $\mu\text{mol kg}^{-1}$	SAMI $p\text{CO}_2$ $\mu\text{atm}$	Calculated $p\text{CO}_2$ $\mu\text{atm}$	$\Delta$ $\mu\text{atm}$
Upstream	12/12	345.9965	x	8.1820	2753	404	414	10
	12/14	347.6701	x	8.2823	2687	344	312	-42
	12/15	348.6618	x	8.2172	2680	364	368	4
	12/16	349.6451	x	8.2129	2674	396	377	-19
	12/16	349.7792	x	8.2218	2668	371	370	-1
	12/18	351.8438	x	8.2288	2636	349	372	23
	12/19	352.8458	x	8.2830	2622	316	317	1
	12/20	353.8576	x	8.2149	2663	361	372	11
	12/21	354.6785	x	8.2013	2647	392	381	-11
	12/21	354.8396	x	8.2661	2644	330	324	-6
	12/18	351.8438		8.3529	2636	349	371	22
	12/19	352.8458		8.4033	2619	316	319	3
	12/20	353.8576		8.3503	2664	361	360	-1
	12/21	354.6785		8.3266	2651	392	379	-13
12/21	354.8396		8.3868	2651	330	327	-3	
Downstream	12/12	345.9875	x	8.3379	2724	274	277	3
	12/14	347.6806	x	8.2922	2695	339	304	-35
	12/15	348.6757	x	8.2082	2680	349	374	25
	12/16	349.6521	x	8.1930	2686	382	398	16
	12/16	349.7882	x	8.2486	2669	326	346	20
	12/18	351.8576	x	8.2701	2643	307	336	29
	12/19	352.8542	x	8.4025	2619	242	233	-9
	12/20	353.8701	x	8.2914	2660	319	305	-14
	12/21	354.6889	x	8.2062	2643	390	373	-17
	12/21	354.8486	x	8.3900	2638	272	237	-35
	12/21	354.6889		8.3279	2646	390	374	-15
12/21	354.8486		8.5034	2641	272	243	-29	



#### 4.4 *In situ* Chlorophyll-*a*

*In situ* suspended chlorophyll-*a* measurements ranged from 0.00 to 8.96  $\mu\text{g L}^{-1}$  during September and 2.01 to 11.54  $\mu\text{g L}^{-1}$  in December (Figure 12). The recurring diel pattern in both data sets shows a decrease in fluorescence during the photoperiod. The effect is not an instrumental artifact, but rather non-photochemical quenching of fluorescence primarily caused by increased irradiance [Kiefer and Reynolds, 1992; Marra, 1997]. Changes in chlorophyll-*a* per unit cell can also influence diel variability in fluorescence, but this effect is likely more significant over larger time intervals  $> 1$  day. The objectives for deploying the fluorometer were to quantify *in situ* biomass and observe any short or long-term trends. The effect of irradiance on fluorescence was not anticipated however, so to avoid the associated complications, fluorescence during the photoperiod was linearly interpolated between adjacent dark periods. Trends in chlorophyll-*a* were assumed to correlate with nighttime fluorescence. Following this adjustment, mean chlorophyll-*a* concentrations for September and December were 6.51 ( $\pm 0.76$ ) and 5.49 ( $\pm 1.18$ )  $\mu\text{g L}^{-1}$ , respectively ( $n = 690$  for each deployment). Mean chlorophyll-*a* concentrations were used in modeling photosynthesis for both September and December (see Section 5.1.2).

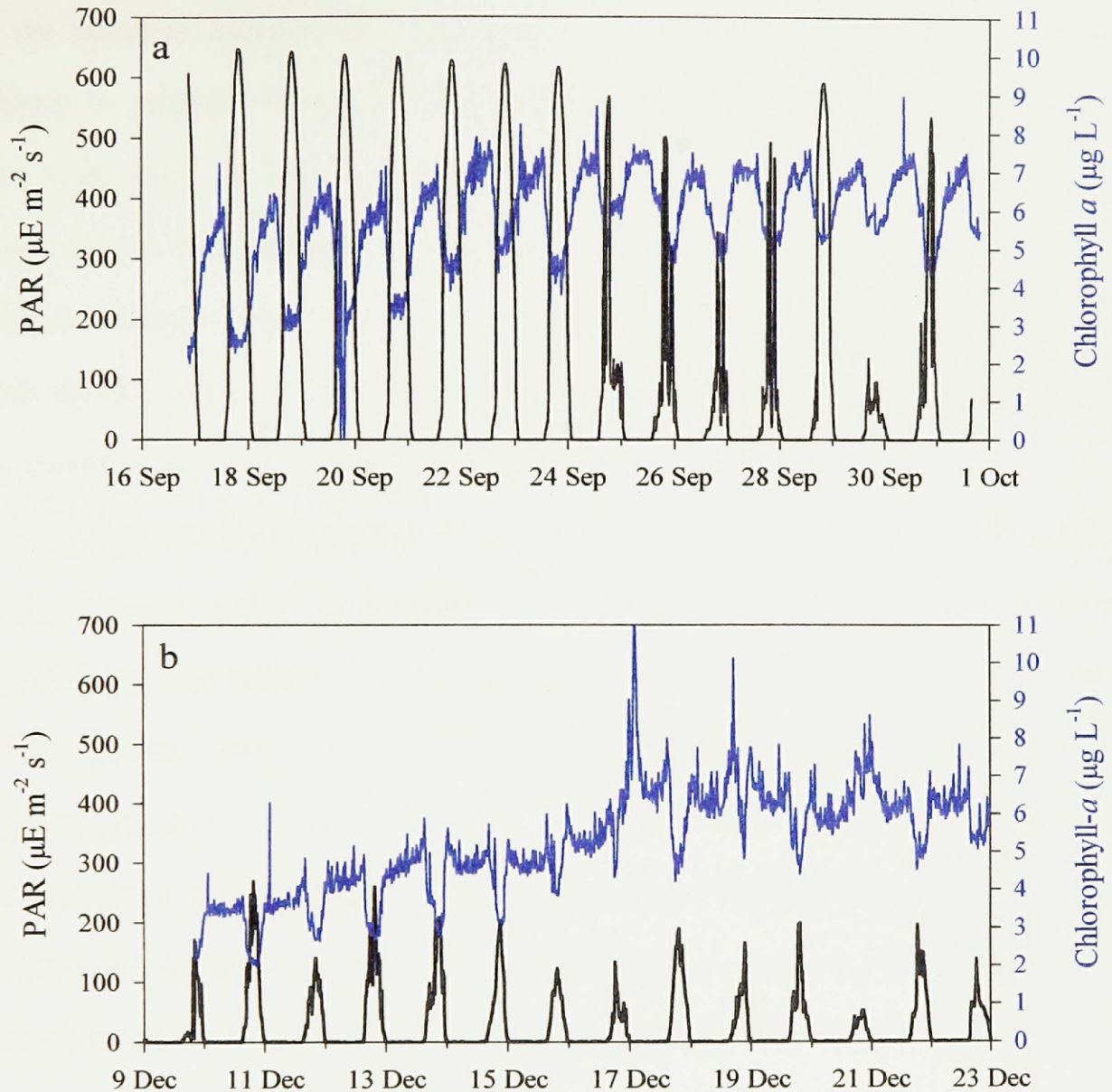


**Figure 12:** September (a) and December (b) *in situ* chlorophyll-*a* measurements (blue) plotted with PAR (black) (both monitored from downstream location). The plots reveal diel quenching of fluorescence. Note that decreased fluorescence during the photoperiod is apparently reversible on a short-time scale.

#### 4.5 Impoundment Effects

This section focuses upon an interesting impoundment effect observed in all upstream data. We observed that upstream variability in September is out of sync with

the diel PAR cycle. Examples of the effect are visible in expanded plots of Figures 13. At the upstream location, DO concentrations are highest in the middle of the night, contrary to expected variability. Metabolism is not the source of increasing DO since there is no light available for photosynthesis. Upstream DO concentrations are nearly always greater than saturation concentrations, so ingassing is not the source of the DO increase. There is also no known pattern in the Milltown Dam discharge that would cause the shift [*James Stilwell*, Montana Power Co., pers. comm.] We believe the effect was caused by the reservoir and is discussed in more detail below.

The odd inverse relationship is also apparent in December data, both in up and downstream data. Since the upstream station is much farther downstream from the dam than in September (Figure 1), the effect is less prominent. However, nighttime *humps* in DO data and the related *dips* in  $p\text{CO}_2$  data are evidence of the same upstream variability (Figures 8a and 9a).

The effect is believed to occur when river water upstream from the Milltown Dam reservoir meets the deeper slack water held behind the dam (see Figure 1). Biomass concentrations in the deeper reservoir waters are expected to be much lower than in the natural shallow waters. Periphyton are also not as prolific in the deeper water, with less available light at the river bottom. Chlorophyll-*a* measurements downstream indicate that suspended biomass is insignificant when compared to attached algae (see Section 5.1.2). The river chemistry in the reservoir is therefore believed to experience little change due to community metabolism during the residence time behind the dam. Similarly, the deeper water is less affected by diel changes in air temperature due to reduced mixing when compared to the turbulent, shallow water. Once the water returns

to its natural course, high local concentrations of periphyton once again begin utilizing the available nutrients (DO,  $p\text{CO}_2$ , etc), renewing the natural diel variability. In Figure 13a and b, upstream DO and  $p\text{CO}_2$  are out of sync with PAR (Figure 13c) by as much as 12 hours. Using estimates of the slack water volume [*James Stilwell*, MPC, pers. comm.] and USGS discharge, the residence time of water behind the dam is calculated to be approximately 10 hours. The close agreement between the apparent shift in the diel cycle and estimated residence time supports the conclusion that less productive reservoir water essentially suspends the metabolic diel gas cycle during residence behind the dam.

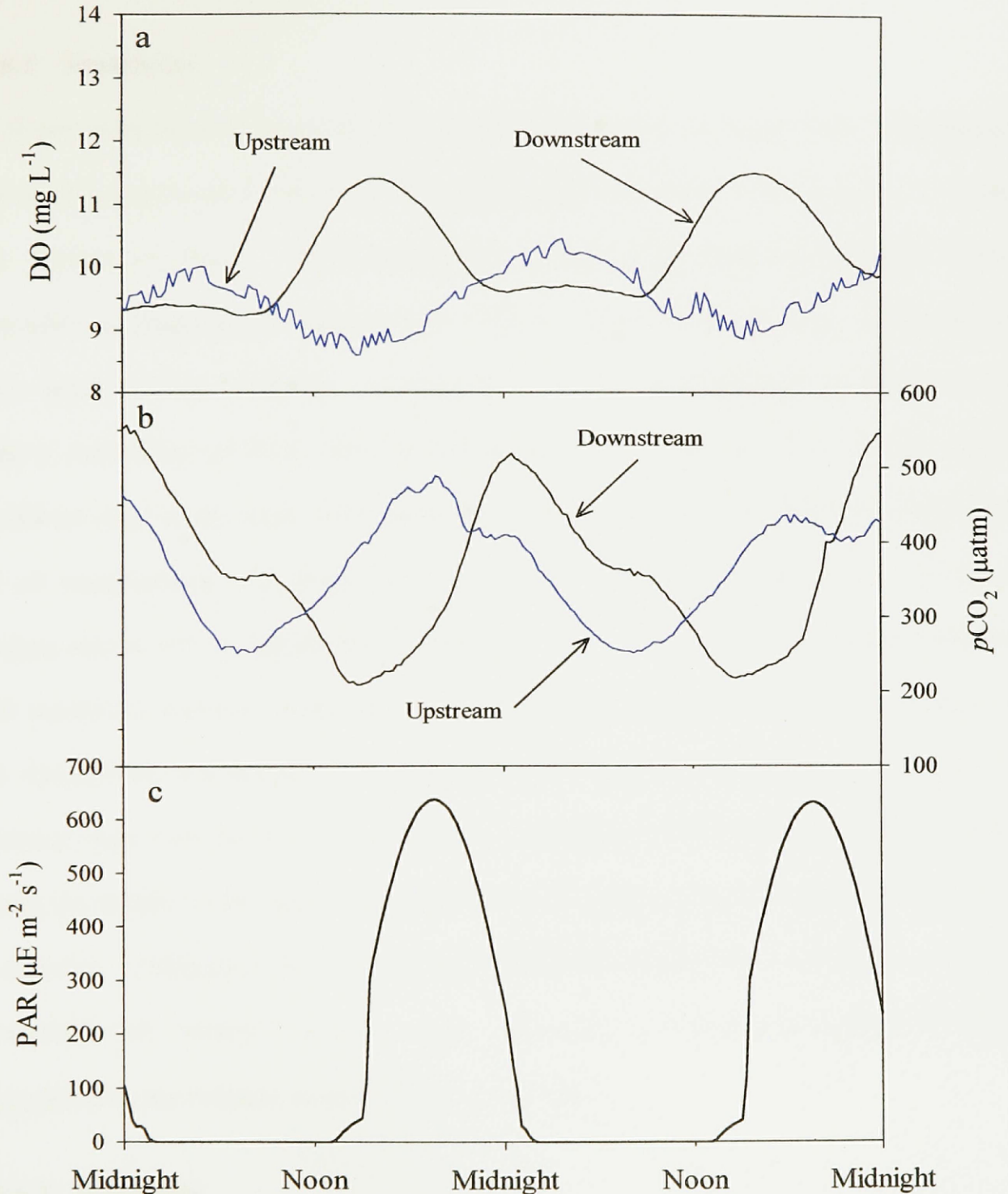


**Figure 13:** DO (a),  $p\text{CO}_2$  (b), and PAR (c) data in the Clark Fork River during September 1999 (GMT). Downstream data in both plots and PAR are shifted back 4.25 h to account for travel time. At any point in time, each curve is expected to represent the same section of water. Note that upstream DO is as much as 12 h out of sync with PAR, and hence the downstream curve.

## 4.6 Study Conditions

### 4.6.1 September

*In situ* temperature time-series for September are shown in Figure 14a. Temperature data on DO sondes and SAMI-CO<sub>2</sub> instruments agree to within better than 0.1 °C during both periods of study. The heating and cooling cycle was very dynamic during September as temperatures ranged from 7.38 to 15.76 °C (Figure 14a). Solar heating drove much of this variability, resulting in a strong diel signature as shown by the positive correlation of PAR with the temperature cycle (Figure 14c). Local weather conditions early in the study were marked by clear and sunny days, resulting in high PAR and air temperatures. On September 24 however, a cold front moved into the region bringing clouds but no significant precipitation. Lower air temperatures and diminished PAR resulted in a drastic reduction in river temperature. Over the course of the study, up and downstream temperature data differ both in magnitude and pattern. The reservoir residence time (see Section 4.5) results in maximum upstream temperatures occurring during the middle of the night, while downstream temperatures peak late in the afternoon as expected. Differences between up and downstream temperatures, however, reveal the anticipated diel variability (Figure 14b). The value of distributed sensors is further exemplified by the reduced complexity of the  $\Delta T$  plot.

### 4.6.2 December

In December, water temperatures ranged from 0.09 to 2.97 °C, with little (<1 °C) or no increases during the day (Figure 15a). Downstream data show a weak diel trend from solar heating, which is more apparent in the  $\Delta T$  plot (Figure 15b). However, the long-

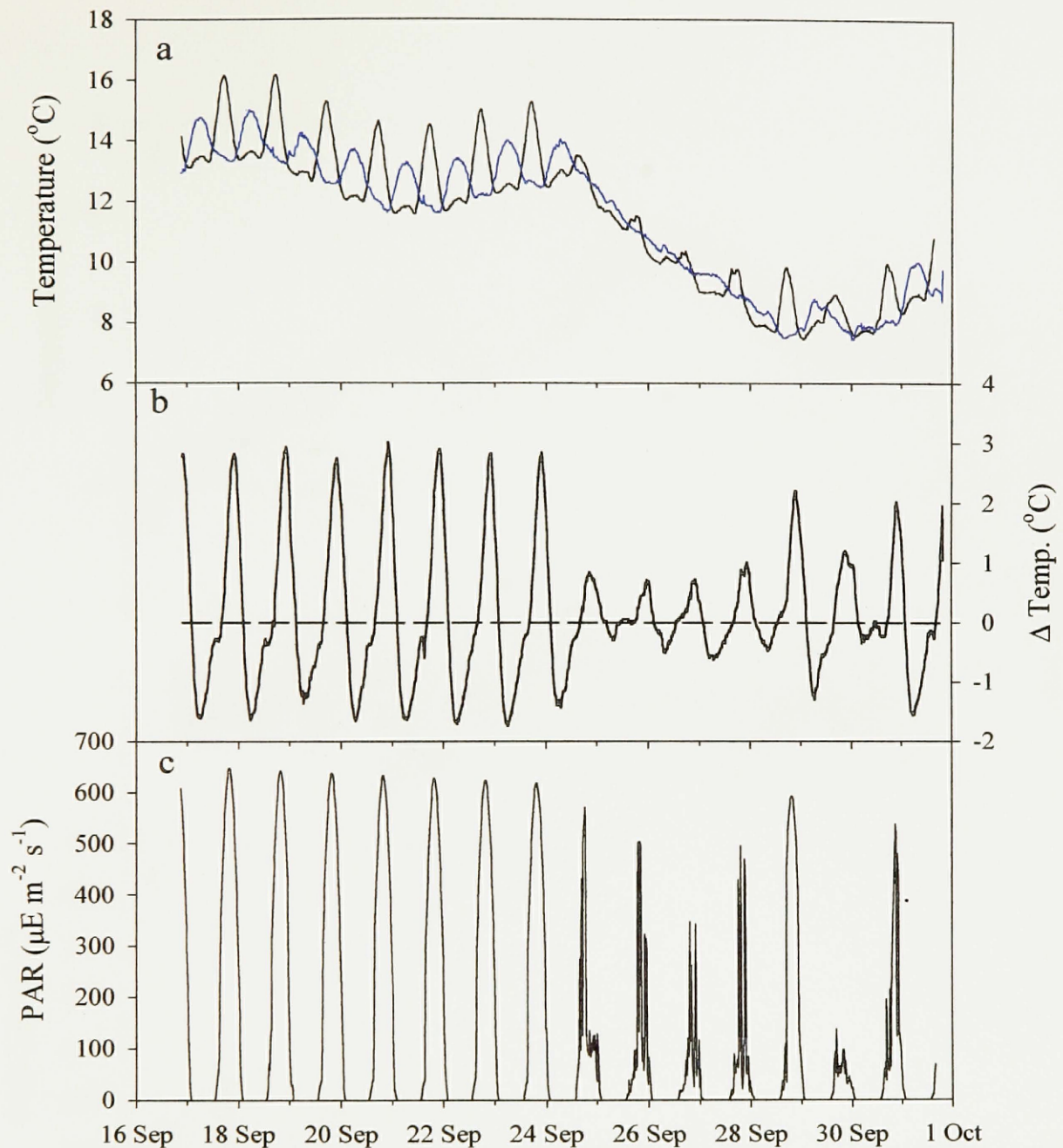


**Figure 14:** Temperature (a),  $\Delta T$  between up and downstream (b), and modeled PAR data (c) in the Clark Fork River during September 1999 (GMT). Up and downstream data are represented by blue and black curves, respectively. The downstream data is shifted 4.25 h to account for travel time. Note diel temperature cycle corresponds with PAR. The upstream diel temperature cycle in plot a reveals effects from the reservoir.

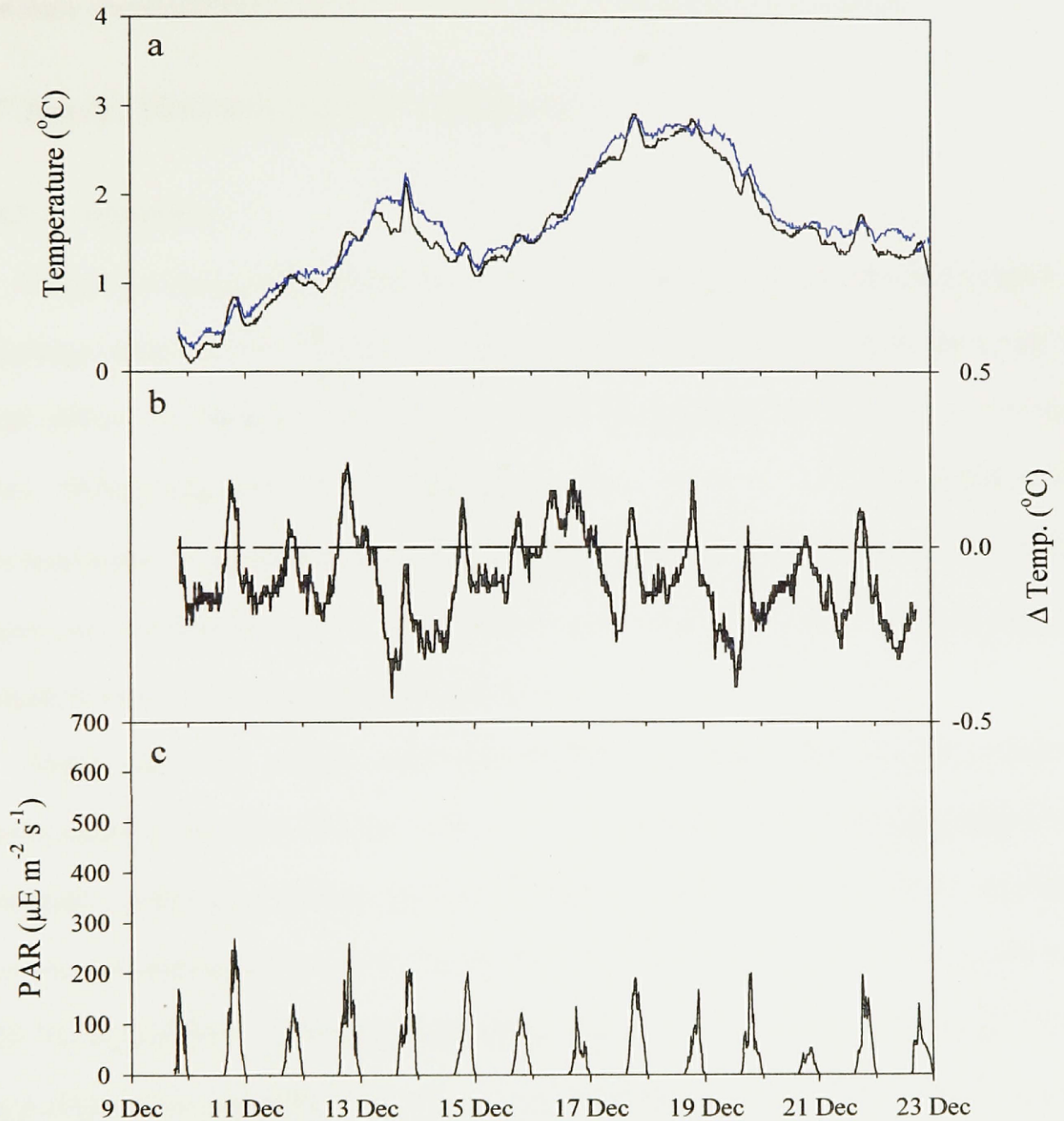


**Figure 15:** Temperature (a),  $\Delta T$  between up and downstream, (b) and measured PAR (c) data in the Clark Fork River during December 1999 (GMT). Up and downstream data are represented by blue and black curves, respectively. The downstream data is shifted 2.5 h to account for travel time. Note lower PAR compared to September (Figure 14).



term variability dominates. Characteristic cold and cloudy days caused the reduced variability. However, there was no significant precipitation during the period of study. The daily maximum PAR, shown in Figure 15c, is <40% that of September.

## 4.7 Depth, Discharge, and Conductivity

### 4.7.1 September

Discharge, depth, and conductivity time-series for September are shown in Figure 16. Discharge does not vary greatly during the study period and depth data show that the local effects of changing discharge are similar in magnitude for both sensors (Figure 16c). During September, mean discharge was  $36 (\pm 1.8) \text{ m}^3 \text{ s}^{-1}$  ( $n = 1383$ ) (Figure 16b). On September 21 an anomalous discharge spike occurred, which is also observed in both depth and conductivity plots. Validation of this event and other discharge spikes is critical to travel time estimates (see Section 4.1).

Since ionic  $\text{CO}_2$  species (and their cations) are likely the dominant source of conductance in the river [Wetzel, 1983],  $\text{CO}_2$  consumption during photosynthesis should decrease conductance during the day. Conductivity is also temperature dependent, however, increasing about 2-3%/ °C [Wetzel and Likens, 1991], so specific conductance (25 °C) is presented to eliminate temperature effects. A diel cycle in conductivity is seen as a result of its dependence on  $\text{CO}_2$ . A much stronger pattern is seen in the upstream data, perhaps influenced by better sensing conditions. The river was much more turbulent at the upstream location, leading to increased flushing of the conductivity sensor inlet on the YSI sonde.

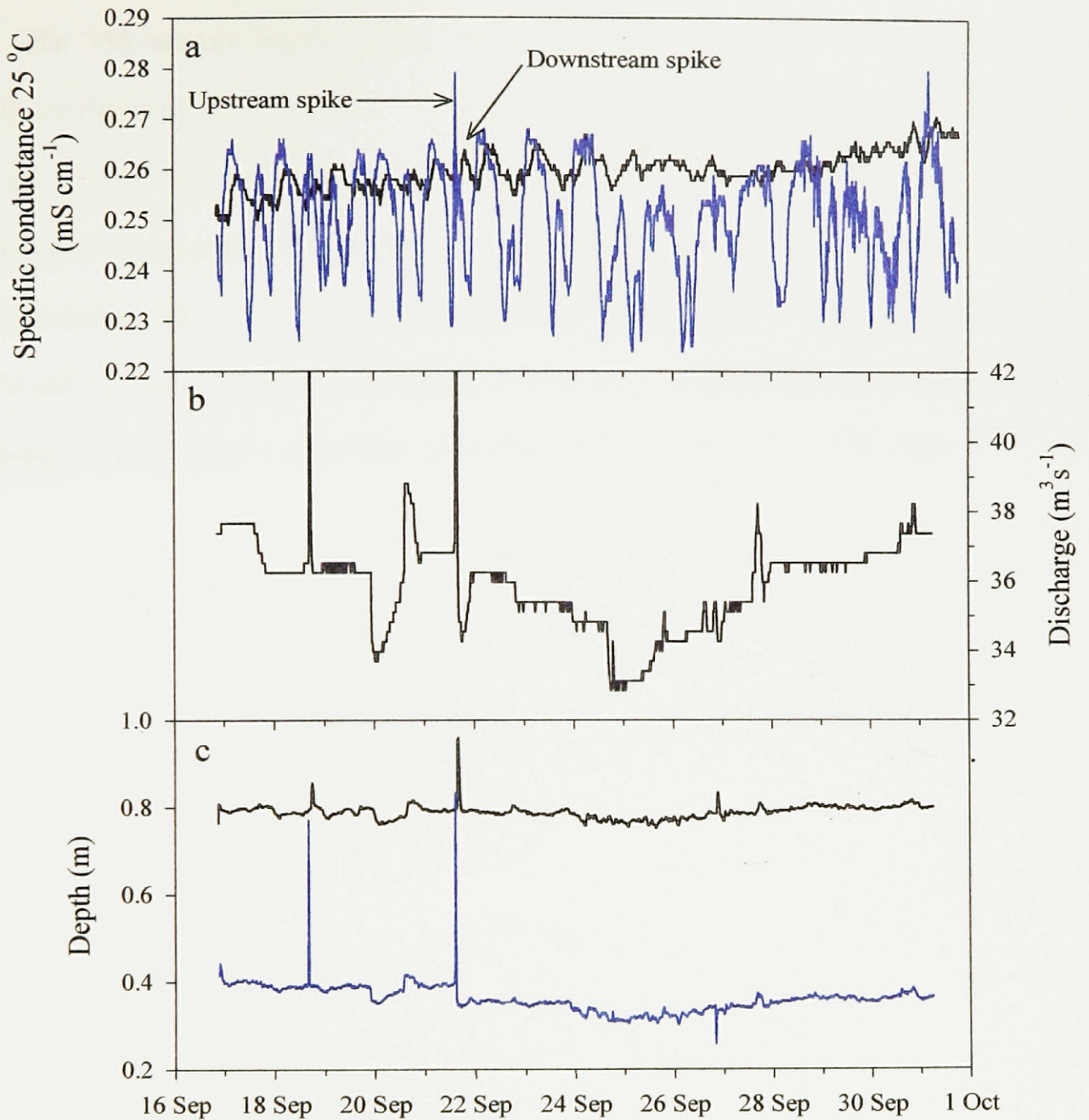


**Figure 16:** Specific conductance (a), discharge (b), and depth (c) data in the Clark Fork River during September 1999. Up and downstream data are represented by blue and black curves, respectively. The effects of distinctive discharge events are seen in all plots. The time axis is in GMT. Midnight GMT occurs at 6:00 pm MST, or right before dark.

### 4.7.2 December

The YSI sensors' batteries died on December 22, so analyses involving DO, depth, and conductivity do not extend beyond this date. Discharge over the 13-d time-series (Figure 17b) was  $40 (\pm 1.4) \text{ m}^3 \text{ s}^{-1}$  ( $n = 1295$ ), similar in magnitude and variability to that measured downstream in September (Figure 17b). A large discharge peak was observed on December 16, which is also seen in both depth and specific conductance data (Figures 17a and c). Conductivity does not show a pronounced pattern throughout the time-series, though a trend similar to that observed in September is apparent on some days.

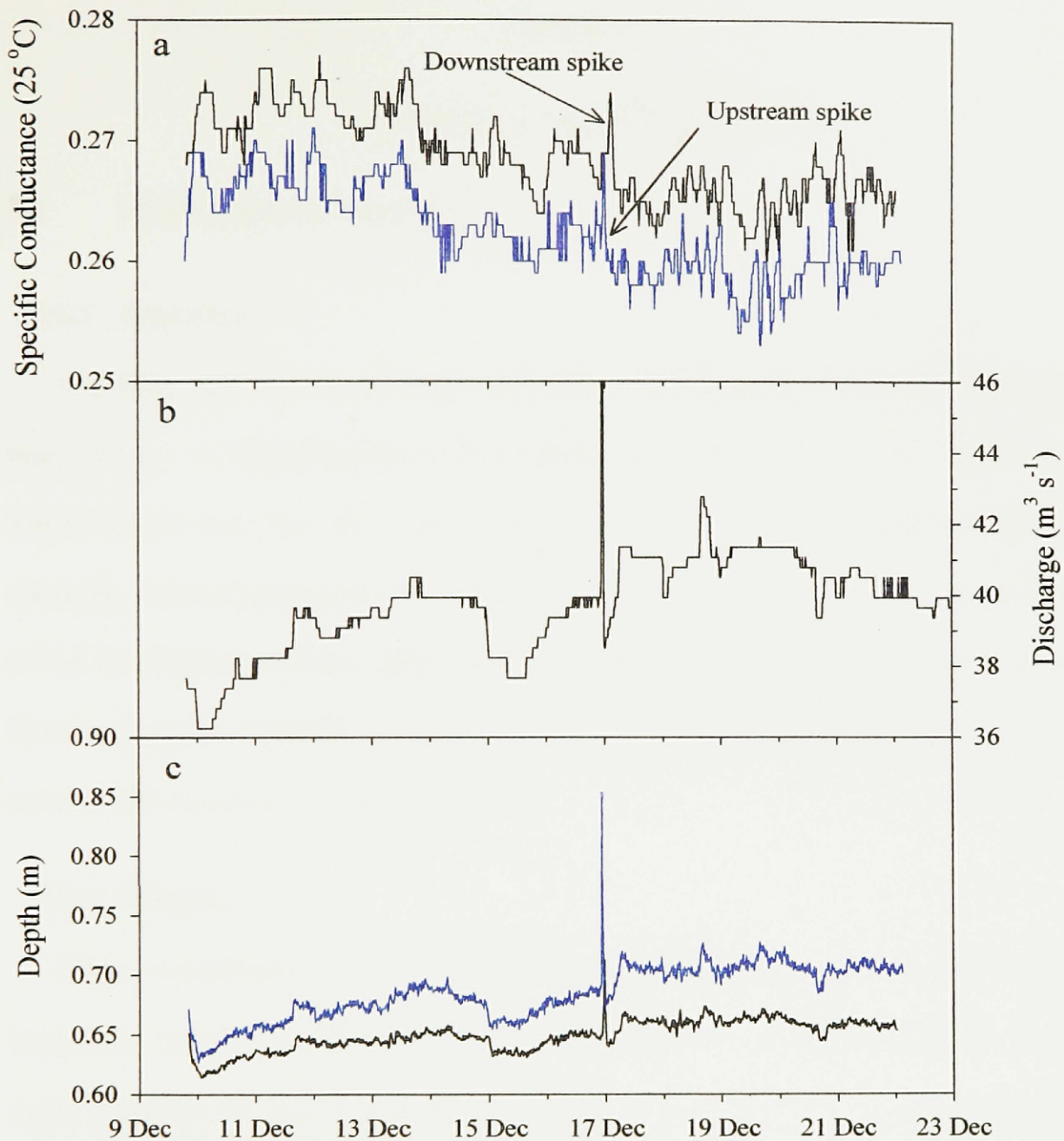


**Figure 17:** Specific conductance (a), discharge (b), and depth (c) data in the Clark Fork River during December 1999 (GMT). Up and downstream data are represented by blue and black curves, respectively. In plot a, note upstream and downstream conductivity spikes used for travel time determination.

## Chapter 5

### Modeling and Discussion

#### 5.1 Modeling parameters

##### 5.1.1 Overview

The following sections describe important modeling parameters and the rationale for their values. A compiled list of the parameters is also provided in Table 5.1. It is worthwhile to note that each time series can be modeled with exceptional agreement by changing various parameters as required. However, this subjective method does not reveal the model's efficacy when using available data. Parameter estimates determined from river data or published values are therefore employed whenever possible. Modeling assists in the evaluation of these estimates.

##### 5.1.2 Biomass

Mean concentrations of chlorophyll-*a* were 108 ( $\pm 4$ ) and 74 ( $\pm 2$ )  $\mu\text{g L}^{-1}$  for September and December, respectively. Chlorophyll-*a* concentrations were determined using Equation 18 and are assumed constant over the study reach. These values lie within a range of 25 to 250  $\mu\text{g L}^{-1}$  (assuming a mean river depth of 1 m) determined from recent *in situ* sampling of Clark Fork River periphyton [Vicki Watson, pers. comm.] Modeled periphyton (given as concentration), determined from *in situ* measurements of fluorescence, are relatively constant for each study period. Mean *in situ* chlorophyll-*a* measurements and other pertinent parameters (e.g. mean width, depth) are held constant, so differences in concentration depend upon changes in discharge (Section 3.2.2).

### 5.1.3 Photosynthetic efficiency and photoinhibition

The photosynthetic efficiency normalized for chlorophyll-*a*,  $\alpha$ , is a significant parameter in the photosynthesis model (Equation 16). Values of  $\alpha$  were estimated from

**Table 5.1:** Summary of important model parameters used in  $p\text{CO}_2$  and DO modeling.

<b>Photosynthesis</b>	<b>September</b>	<b>December</b>	<b>Source</b>
PQ	1.54	2.17	Field data
$P^B_s$ , mg C (mg Chl- <i>a</i> ) <sup>-1</sup> h <sup>-1</sup>	3	3	Modeling
$\alpha$ , $\mu\text{g C (mg Chl-}a)^{-1}(\mu\text{E m}^{-2}\text{s}^{-1})^{-1}$	15	15	Field data
$\beta$	0	0	Modeling
Chl- <i>a</i> , $\mu\text{g L}^{-1}$	108	74	Field data; modeling
<b>Respiration</b>			
RQ	0.85	0.85	<i>Wetzel and Likens (1983)</i>
$R_{20}$ , mol C L <sup>-1</sup> h <sup>-1</sup>	$5.6 \times 10^{-6}$	$5.6 \times 10^{-6}$	Field data
$\theta$	1.045	1.045	<i>Parkhill and Gulliver (1998)</i>
$\beta_R$	0	0	Modeling
<b>Gas Transfer</b>			
$K_{C(20)}$ , cm h <sup>-1</sup>	44	44	Field data
$K_{O(20)}$ , cm h <sup>-1</sup>	47	47	Field data

plots of DO flux against PAR and normalized for chlorophyll-*a* (Table 5.1). Assuming that photosynthesis is the dominant process in the early hours of the day, the initial slope, or  $\alpha$ , is determined using standard linear regression of data over ~2 h and fixing the intercept to zero. Respiratory processes and surface gas exchange are ignored for convenience. Since only a short time period was used, their contributions are assumed negligible. Only December downstream DO data were used for  $\alpha$  estimation. The travel time is long enough that changes in PAR over the reach make it difficult to determine

when the initial effects of photosynthesis are occurring.  $\Delta DO$  was calculated using sequential measurements, assuming a steady-state condition above the monitoring location. Regression estimates of  $\alpha$  (converted to rate of carbon flux) typically fell between 6 and 15  $\mu\text{g C (mg Chl-}a\text{)}^{-1} \text{ h}^{-1} (\mu\text{E m}^{-2} \text{ s}^{-1})^{-1}$ . The upper limit,  $\alpha = 15$ , was chosen for modeling both September and December community photosynthesis. This value lies within the range of 0.8-53.6 reported for other lotic systems [Jones and Adams, 1982; Carpenter, 1985; Jasper and Bothwell, 1986; Boston and Hill, 1991]. Higher  $\alpha$  represents a more efficient light collecting ability, but an established seasonal trend has not been shown with other studies [Jones and Adams, 1982; Jasper and Bothwell, 1986]. Variations in  $\alpha$  can reasonably be expected in response to shifts in the dominant species of periphyton throughout the seasons. However, more knowledge of local biology is required to quantify these differences.

Modeled photosynthesis allows for photoinhibition effects through the photoinhibition parameter,  $\beta (\mu\text{g C (mg Chl-}a\text{)}^{-1} \text{ h}^{-1} (\mu\text{E m}^{-2} \text{ s}^{-1})^{-1})$  (Equation 17). Photoinhibition did not appreciably increase the model's agreement with field data however, so its contribution was removed. This is not without precedent, as Hornberger et al. (1976) observed no photoinhibition in a stream study and found instead that photosynthesis increased linearly with light. Kirk (1994) also suggests that photoinhibition is less significant in attached plant communities because of adaptation to the light intensities available at their depth.

#### 5.1.4 Photosynthetic potential

The maximal rate of photosynthesis,  $P_s^B$  (Equation 17) for both seasons was fixed at 3  $\text{mg C (mg Chl-}a\text{)}^{-1} \text{ h}^{-1}$  (Table 5.1). This value lies in the middle of previously

mentioned literature values of  $0.11\text{-}5.49 \text{ mg C (mg Chl-}a\text{)}^{-1} \text{ h}^{-1}$ . Nighttime estimates of  $R_{20}$  and gas transfer velocities were used to constrain the photosynthetic rate during modeling of daytime data. It is reasonable to assume that a rapid and significant change in biomass during comparatively static conditions is unlikely, so  $P_s^B$  is held constant. Since  $P_s^B$  and  $\alpha$  are both constant, modeled variation in gas concentrations from photosynthesis is primarily regulated by irradiance.

### 5.1.5 Regression Analysis

**5.1.5a September:** As described in Section 3.1.2, estimates of gas transfer velocity and respiration are obtained through multiple linear regressions. A summary of the results is given in Table 4.3. Evidence of biofouling late in the study prevents the use of the full data set. For each nighttime period, 41 sets of  $p\text{CO}_2$  and temperature measurements were used. DIC was calculated from *in situ*  $p\text{CO}_2$  and mean alkalinity data determined from both monitoring locations. Atmospheric  $p\text{CO}_2$  was estimated from data obtained during similar days (based upon meteorological conditions) in September 2000. Analysis of nighttime  $\text{CO}_2$  data over 9 days in September yields a mean  $K_{C(20)} = 48 (\pm 24) \text{ cm h}^{-1}$  and a mean  $R_{20} = 5.6 \times 10^{-6} (\pm 2.1 \times 10^{-6}) \text{ mol CO}_2 \text{ L}^{-1} \text{ h}^{-1}$ .

Similar analyses were also performed using nightly DO concentration and temperature data, in combination with saturation estimates determined from Equation 4. The same number of nights and measurements per night were used as in the  $\text{CO}_2$  analysis. Multiple linear regressions yield a mean  $K_{O(20)} = 43 (\pm 4) \text{ cm h}^{-1}$  and a mean  $R_{20} = 0.18 (\pm 0.05) \text{ mg O}_2 \text{ L}^{-1} \text{ h}^{-1}$  consumed. The  $R_{20}$  estimated from DO corresponds to a  $R_{20} = 6.8$



$\times 10^{-6}$  ( $\pm 1.9 \times 10^{-6}$ ) mol CO<sub>2</sub> L<sup>-1</sup> h<sup>-1</sup> using a RQ = 0.85. If RQ is not used in conversion, CO<sub>2</sub> and O<sub>2</sub> analyses predict a RQ = 1.00.

**5.1.5b December:** Corresponding regression analyses were also performed using December CO<sub>2</sub>, O<sub>2</sub>, and temperature data. Estimates of K<sub>O</sub> and R<sub>20</sub> were made over 12 nights with 51 data sets per night. Regression results from CO<sub>2</sub> data yield a mean K<sub>C(20)</sub> = 11 ( $\pm 1$ ) cm h<sup>-1</sup> and a mean R<sub>20</sub> =  $1.22 \times 10^{-6}$  ( $\pm 6.5 \times 10^{-7}$ ) mol CO<sub>2</sub> L<sup>-1</sup> h<sup>-1</sup>.

DO analyses are similar to September regression results, generating a mean K<sub>O(20)</sub> = 50 ( $\pm 24$ ) cm h<sup>-1</sup> and a mean R<sub>20</sub> = 0.17 ( $\pm 0.25$ ) mg O<sub>2</sub> L<sup>-1</sup> h<sup>-1</sup> consumed. The respiration estimate is equivalent to R<sub>20</sub> =  $6.1 \times 10^{-6}$  ( $\pm 1.9 \times 10^{-6}$ ) mol CO<sub>2</sub> L<sup>-1</sup> h<sup>-1</sup> applying a RQ = 0.85. The R<sub>20</sub> estimated from CO<sub>2</sub> regression is much less than the rate predicted by O<sub>2</sub> data, resulting in a low RQ = 0.24.

**5.1.5c Regression error analysis:** Respiratory rates agree well between pCO<sub>2</sub> and DO regressions in September, and surface gas transfer estimates are also similar. December regression results using DO agree with September analyses, in both estimates of K<sub>O(20)</sub> and R<sub>20</sub>. December CO<sub>2</sub> data however, do not reveal comparable rates. Predictions of K<sub>C(20)</sub> are the lowest during the study by a factor of 4, while R<sub>20</sub> is an order of magnitude lower.

The apparent inconsistency in regression results is probably a result of invalid assumptions. Evidence of some unknown error is seen in the plots of studentized residuals against the response, though a statistical discussion is not presented here. Deviations in linearity by gas transfer and respiration will certainly introduce error. Inaccuracy in pCO<sub>2</sub> saturation estimates and closeness to *in situ* pCO<sub>2</sub> could contribute to gas transfer errors. R<sub>20</sub> is assumed constant throughout the night, yet contributions from

photorespiration could cause respiratory rates to degrade over night [Parkhill and Gulliver, 1998]. Applying a linear correction factor to DO data (to correct for drift) also introduces the possibility of systematic error. Regression accuracy depends upon normally distributed measurement error throughout the data set. Other significant riverine processes not considered in Equations 12 and 13 (e.g. calcite cycling) would also introduce error into the regression results.

### 5.1.6 Equation estimates of $K_C$ and $K_O$

Tsivoglou and Wallace's (1972) widely used equation (11) based upon changes in hydraulic energy results in an estimates of  $K_{O(20)} = 62 \text{ cm h}^{-1}$  and  $K_{C(20)} = 54 \text{ cm h}^{-1}$  for September. Using December's parameters, Equation 11 yields  $K_{O(20)} = 50 \text{ cm h}^{-1}$  and  $K_{C(20)} = 43 \text{ cm h}^{-1}$ .

The semiempirical relationship (Equation 12) provided by Melching and Flores (1999) yields a  $K_{O(20)} = 23 \text{ cm h}^{-1}$  for September, which corresponds to a  $K_{C(20)} = 22 \text{ cm h}^{-1}$  using Equation 15. The results are the same using hydraulic conditions (Equation 12) during December. Melching and Flores (1999) estimate error are anywhere between 44 and 78% for this equation.

The predictive Equations 11 and 12 yield dissimilar results for both  $O_2$  and  $CO_2$  gas transfer velocities. Regression estimates agree closer with the energy dissipation model, while hydraulic conditions indicate much lower gas transfer rates. Values of  $K_C$  and  $K_O$  used for modeling are discussed in Section 5.1.9.

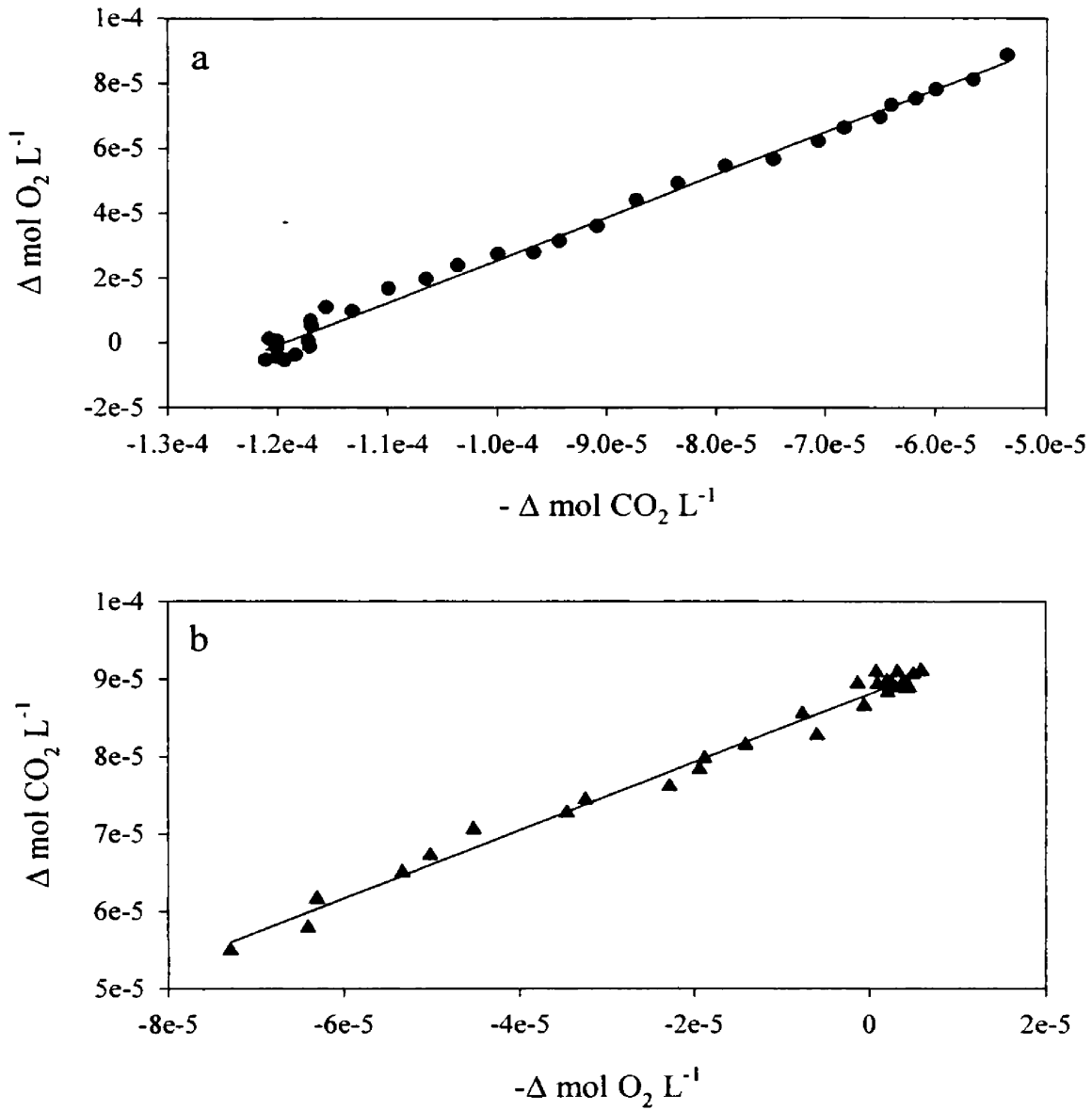


**Figure 18:** Representative plots used in the estimation of PQ and RQ during September and December 1999. September daytime data is used in plot **a**, yielding a slope and PQ = 1.52 ( $R^2 = 0.97$ ). Similarly, in plot **b** September nighttime data is used to determine RQ = 0.44 ( $R^2 = 0.99$ ). The grouping of data points occurs just before and after sunset in plots **a** and **b**, respectively.

### 5.1.7 PQ and RQ

Field measurements of  $p\text{CO}_2$ , DO, alkalinity, and temperature data were also used to estimate the local values of PQ and RQ. Prior to plotting the data, modeled gas flux as a result of gas transfer was subtracted from the total changes between up and downstream. The resulting slopes of the plots were taken as PQ. Contributions from respiration and other processes were assumed negligible for convenience. One plot for each is given in Figure 18 to show the linear relationship typically found. September field data produced a mean  $\text{PQ} = 1.54 (\pm 0.69)$  and a  $\text{RQ} = 0.47 (\pm 0.12)$  ( $n = 9$ ).

Mean values were also determined from December field measurements, resulting in a  $\text{PQ} = 2.17 (\pm 0.26)$  and  $\text{RQ} = 0.47 (\pm 0.17)$ . In contrast to September, December data did not produce linear relationships on each night. Only linear regressions revealing a visible linear trend ( $R^2 > 0.5$ ) were used in computing the mean, so 11 days and 6 nights were used.

During both deployments, PQ estimates are greater than the typical value of 1.2, most likely a combined result of inaccuracies in modeled DIC and surface gas transfer. The assumption that respiration and calcite cycling are negligible may also be a significant factor. RQ estimates agree between seasons, but are much lower than the literature value of 0.85. Literature values of RQ are typically not lower than 0.85 however, so the accepted value of 0.85 was used for converting between  $\text{CO}_2$  and  $\text{O}_2$  respiration rates. Inaccurate modeling assumptions and measurement error are possible sources of this discrepancy. Without additional knowledge on local biology however, no conclusions can be drawn. In general, PQ and RQ determination in natural aquatic systems is difficult.

**Table 5.2:** Results from multiple regression analyses for determining estimates of  $K_{C(20)}$ ,  $K_{O(20)}$ , and  $R_{20}$ . Estimates of  $R_{20}$  using DO data are converted to  $\text{mol L}^{-1} \text{h}^{-1}$  using a  $RQ = 0.85$  for comparison to  $\text{CO}_2$  regression results.

September 1999				
CO <sub>2</sub> Regression			O <sub>2</sub> Regression	
Day (GMT)	$K_{C(20)}$ (cm h <sup>-1</sup> )	$R_{20}$ (mol C L <sup>-1</sup> h <sup>-1</sup> )	$K_{O(20)}$ (cm h <sup>-1</sup> )	$R_{20}$ (mol C L <sup>-1</sup> h <sup>-1</sup> )
17	90	$1.03 \times 10^{-6}$	40	$3.99 \times 10^{-6}$
18	66	$3.16 \times 10^{-6}$	44	$5.64 \times 10^{-6}$
19	38	$3.61 \times 10^{-6}$	48	$4.69 \times 10^{-6}$
20	32	$4.34 \times 10^{-6}$	39	$6.70 \times 10^{-6}$
21	49	$5.48 \times 10^{-6}$	39	$8.21 \times 10^{-6}$
22	48	$5.65 \times 10^{-6}$	42	$9.04 \times 10^{-6}$
23	48	$6.19 \times 10^{-6}$	43	$8.36 \times 10^{-6}$
24	55	$6.45 \times 10^{-6}$	51	$8.68 \times 10^{-6}$
25	1.2	$5.36 \times 10^{-6}$	44	$5.60 \times 10^{-6}$
December 1999				
10	13	$1.38 \times 10^{-6}$	60	$3.16 \times 10^{-6}$
11	18	$1.53 \times 10^{-6}$	43	$7.02 \times 10^{-7}$
12	-15	$-3.56 \times 10^{-8}$	84	$4.68 \times 10^{-6}$
13	13	$5.93 \times 10^{-7}$	59	$4.89 \times 10^{-7}$
14	12	$7.04 \times 10^{-7}$	49	$-5.88 \times 10^{-7}$
15	15	$1.18 \times 10^{-6}$	53	$1.71 \times 10^{-6}$
16	12	$6.53 \times 10^{-7}$	5	$2.04 \times 10^{-5}$
17	7.2	$1.09 \times 10^{-6}$	13	$3.14 \times 10^{-5}$
18	21	$2.25 \times 10^{-6}$	38	$-1.70 \times 10^{-6}$
19	6.4	$1.37 \times 10^{-6}$	79	$2.16 \times 10^{-6}$
20	15	$1.75 \times 10^{-6}$	40	$3.05 \times 10^{-6}$
21	13	$2.12 \times 10^{-6}$	78	$7.35 \times 10^{-6}$

### 5.1.8 Respiration

Values of  $R_{20}$  (Equation 20) that agree best with the data vary for O<sub>2</sub> and  $p\text{CO}_2$ , as well as seasonally. However, in the interest of modeling consistency, one  $R_{20}$  was chosen

to represent all seasons (Table 5.1). Differences in community structure and function during seasons will almost certainly alter  $R_{20}$ , but lacking more specific knowledge on local species' seasonal metabolism, utilizing a constant  $R_{20}$  is appropriate. A  $R_{20} = 5.6 \times 10^{-6} \text{ mol CO}_2 \text{ L}^{-1} \text{ h}^{-1}$  was selected for modeling during both September and December. This rate was estimated from multiple regressions of nighttime data since respiration and gas transfer are assumed to be the only major processes contributing to gas variability. Variations with temperature are modeled using Equation 20, while respiration rates for DO are calculated using  $RQ = 0.85$  with  $R_{20}$  equal to that used for  $p\text{CO}_2$ .

Photorespiration was incorporated into modeling respiratory rates using Equation 20. The predicted fluxes in  $p\text{CO}_2$  and DO however, generally resulted in recurring inconsistencies when compared to field data. On a few individual days early in September, during maximum irradiance, modeled photorespiration did slightly increase agreement. The effect was minor however, and the photoinhibition parameter, or  $\beta_R$ , was eventually fixed at zero.

### 5.1.9 Gas transfer velocities

Values for  $K_C$  and  $K_O$ , in conjunction with  $R_{20}$ , were taken from the multiple regression results. Regression and equation estimates differed by as much as  $40 \text{ cm h}^{-1}$  with little consistency between methods. A mean  $K_{O(20)} = 47 \text{ cm h}^{-1}$  was chosen for modeling and from this estimate, using Equation 16,  $K_{C(20)} = 44 \text{ cm h}^{-1}$  (Table 5.1). Since surface gas transfer is primarily a physical process, seasonal differences in  $K_{C(20)}$  and  $K_{O(20)}$  are not expected to be significant. Since mean discharge is similar between study periods (Figures 16b and 17b), this is a reasonable assumption. These estimates were therefore utilized for modeling during both September and December.

## 5.2 Model Results

### 5.2.1 September

Modeled and field changes in  $p\text{CO}_2$  and DO are given in Figure 19. Although agreement is often quite good, it is apparent that metabolism and surface gas transfer cannot alone model changes in  $p\text{CO}_2$  at all times during September. Model predictions

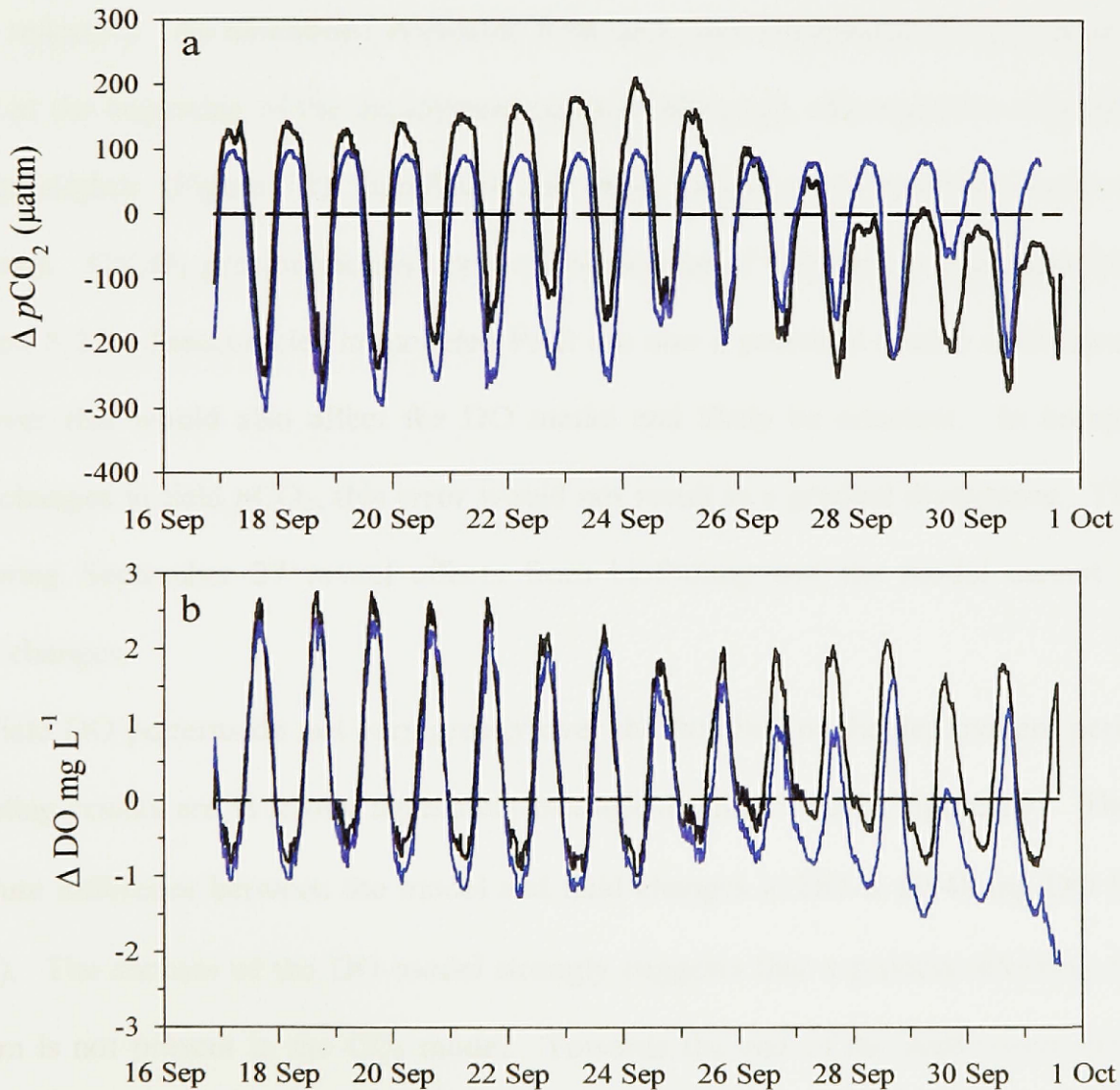


**Figure 19:** Modeled (blue) and *in situ* changes (black) in  $p\text{CO}_2$  (a) and DO (b) during September 1999 (UTC).

agree with field data for several days, but they do not match a gradual net increase over the time period. The mean absolute difference between the  $p\text{CO}_2$  curves is  $\pm 70 \mu\text{atm}$  ( $n = 1383$ ), a significant variation. Overall, modeled PAR (Section 3.2.2) works remarkably well in predicting community photosynthesis. Nightly increases as a result of respiration appear to remain relatively constant, however field  $p\text{CO}_2$  flux indicates a decrease in the net loss of  $p\text{CO}_2$ . Decreased photosynthesis or an additional source of  $\text{CO}_2$  can affect the same response. As mentioned, available PAR and river temperatures were similar for 1 week at the beginning of the deployment period. Although, chlorophyll-*a* concentrations change slightly (Figure 12), significant and rapid variations in metabolic rates are not expected.  $\text{CaCO}_3$  precipitation is one possible source of  $\text{CO}_2$  and is discussed further in Section 5.2.3. Inaccuracies in modeled PAR are also a potential source of disagreement, however this would also affect the DO model and likely be constant. In comparisons with changes in field  $p\text{CO}_2$ , this error would not result in a gradual divergence. The days following September 27 reveal effects from biofouling and the model cannot predict these changes.

Field DO patterns do not vary greatly over the first half of the deployment period and modeling results are in strong agreement through the first 9 days (Figure 19). The mean absolute difference between the model and field changes in DO is  $\pm 0.48 \text{ mg DO L}^{-1}$  ( $n = 1415$ ). The success of the DO model strongly suggests that a process affecting the  $\text{CO}_2$  system is not present in the  $\text{CO}_2$  model. Towards the end of the deployment period, as with  $p\text{CO}_2$ , DO field and model results deviate more significantly. At least part of this disagreement is suspected to be a result of instrument biofouling.



Plots revealing modeled contributions from gas transfer, photosynthesis, and respiration are given in Figure 20. Each plotted point represents the mean effect over the entire travel time. For instance, as a modeled section of water travels from up to downstream, contributions from each process are calculated at every time step and stored for computation of the mean. It is apparent from the plots in Figure 20 that contributions from gas exchange are more important to DO than  $p\text{CO}_2$ . Surface  $\text{O}_2$  gas exchange is a major component opposing photosynthetic production of  $\text{O}_2$  (Figure 20b). In contrast, daily respiratory production of  $\text{CO}_2$  is more significant (Figure 20a). During the night, DO losses from respiration and gas transfer are comparable, with gas transfer effects gradually decreasing until just before sunrise as DO nears saturation. On this scale, respiratory changes in both  $\text{O}_2$  and  $\text{CO}_2$  appear constant, suggesting that temperature has a minimal short-term effect on respiration.

In Figure 21a, modeled changes in  $K_C$  and  $K_O$  are shown for the September deployment. The effect of diel and long-term temperature fluctuation is clearly visible.

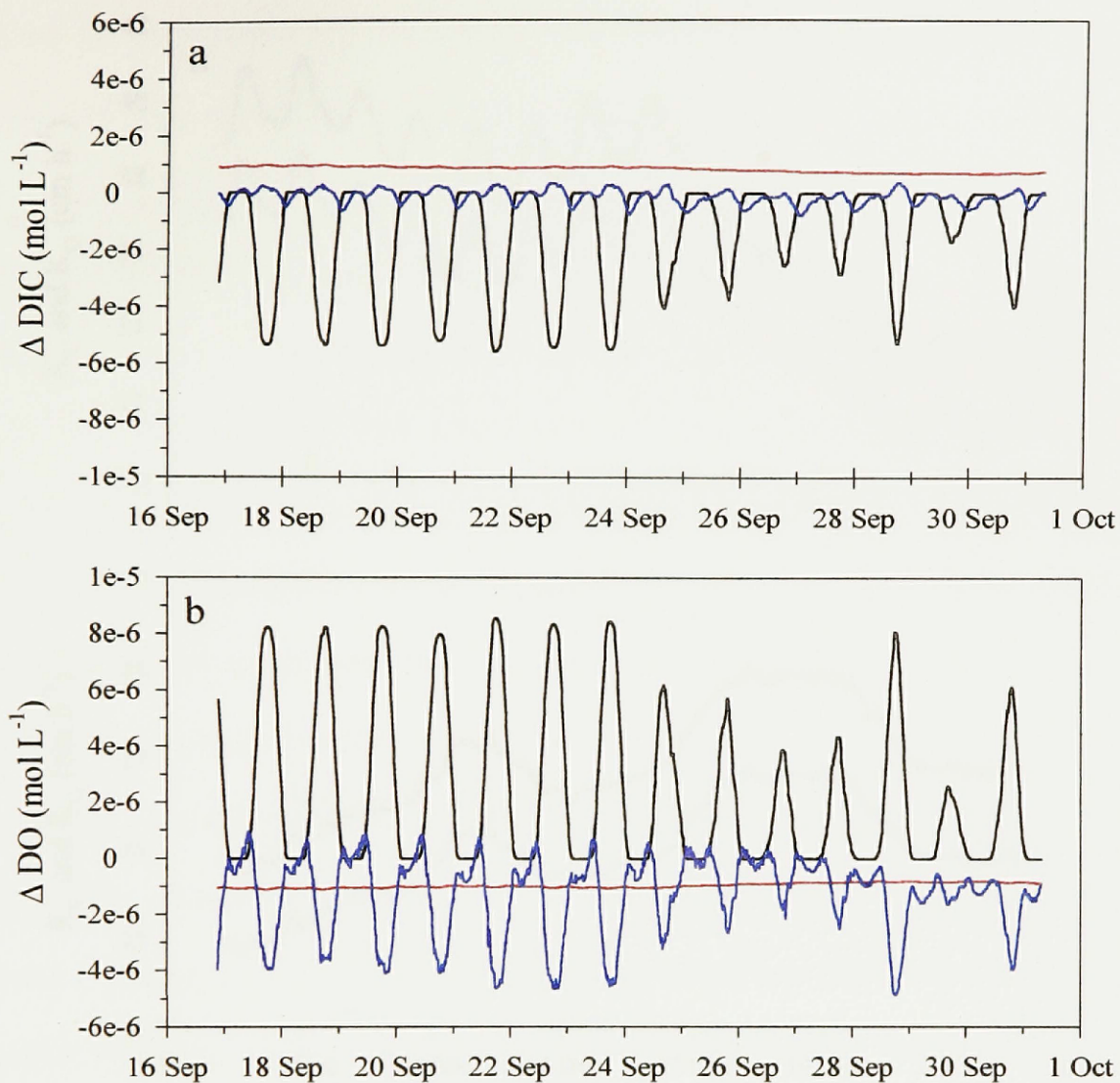


**Figure 20:** Modeled contributions from photosynthesis (black), respiration (red), and surface gas transfer (blue) during September 1999 (UTC). Molar effects on  $\text{CO}_2$  and  $\text{O}_2$  are shown in plots a and b, respectively.

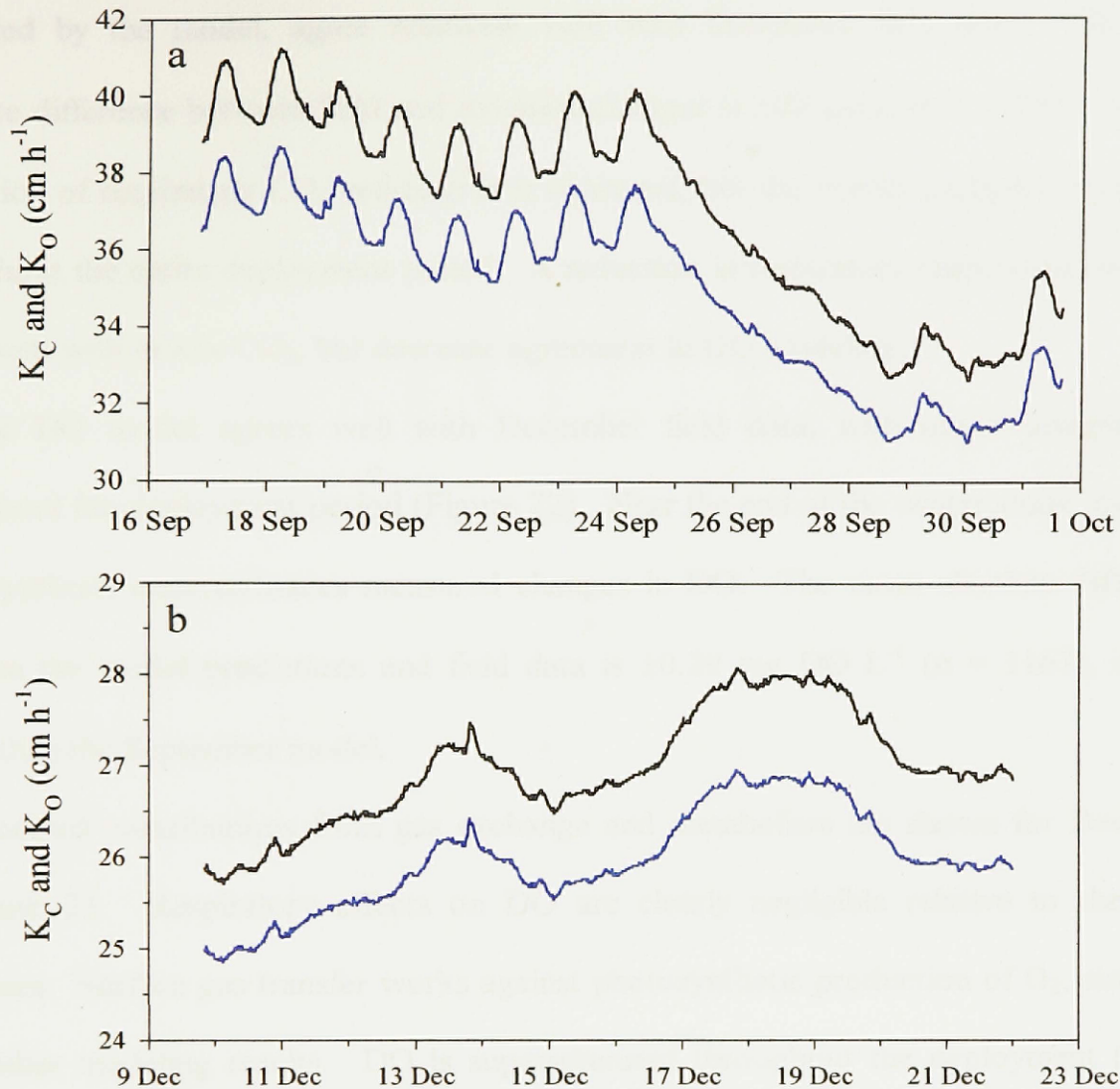


**Figure 21:** Modeled  $K_C$  (blue) and  $K_O$  (black) during September (a) and December (b) 1999 (UTC). Variability is controlled solely by temperature.

### 5.2.2 December

Modeled changes in  $p\text{CO}_2$  and DO are plotted with December field data in Figure 22. The seasonal differences between data in September and December are discussed in detail in Chapter 4, but briefly the winter temperatures and low PAR resulted in a substantial reduction in metabolic effects. Without varying either  $P_s^B$  or  $\alpha$  used in September, the model predicts the lower photosynthetic rates based solely on the decrease

in chlorophyll-*a* concentrations and irradiance in December. Changes in  $p\text{CO}_2$ , as predicted by the model, agree relatively well with December field data. The mean absolute difference between field and modeled changes is  $\pm 20 \mu\text{atm}$  ( $n = 1169$ ). An over prediction of respiratory  $\text{CO}_2$  production is observed, but the overall pattern is consistent throughout the entire deployment period. A reduction in respiratory rates would increase agreement with *in situ*  $\text{CO}_2$ , but decrease agreement in DO modeling.

The DO model agrees well with December field data, with minor disagreement throughout the deployment period (Figure 22). Near the end of the winter study, modeled photosynthesis underestimates measured changes in DO. The mean absolute difference between the model predictions and field data is  $\pm 0.29 \text{ mg DO L}^{-1}$  ( $n = 1167$ ), slightly better than the September model.

Modeled contributions from gas exchange and metabolism are shown for December in Figure 23. Respiratory effects on DO are clearly negligible relative to the other processes. Surface gas transfer works against photosynthetic production of  $\text{O}_2$ , similar to September modeling results. DO is supersaturated throughout the deployment (Figure 9a), so gas transfer is a sink for DO at all times. Figure 23a reveals that gas transfer is more significant in countering nightly production of  $\text{CO}_2$  than in September. In contrast to Figure 23b, respiration primarily opposes daytime consumption of  $\text{CO}_2$  rather than surface gas transfer.

The modeled fluctuation in  $K_C$  and  $K_O$  resulting from temperature changes is shown in Figure 21b. In contrast to the September model, long-term variation is more important than daily changes. Overall, December surface gas transfer velocities are smaller in

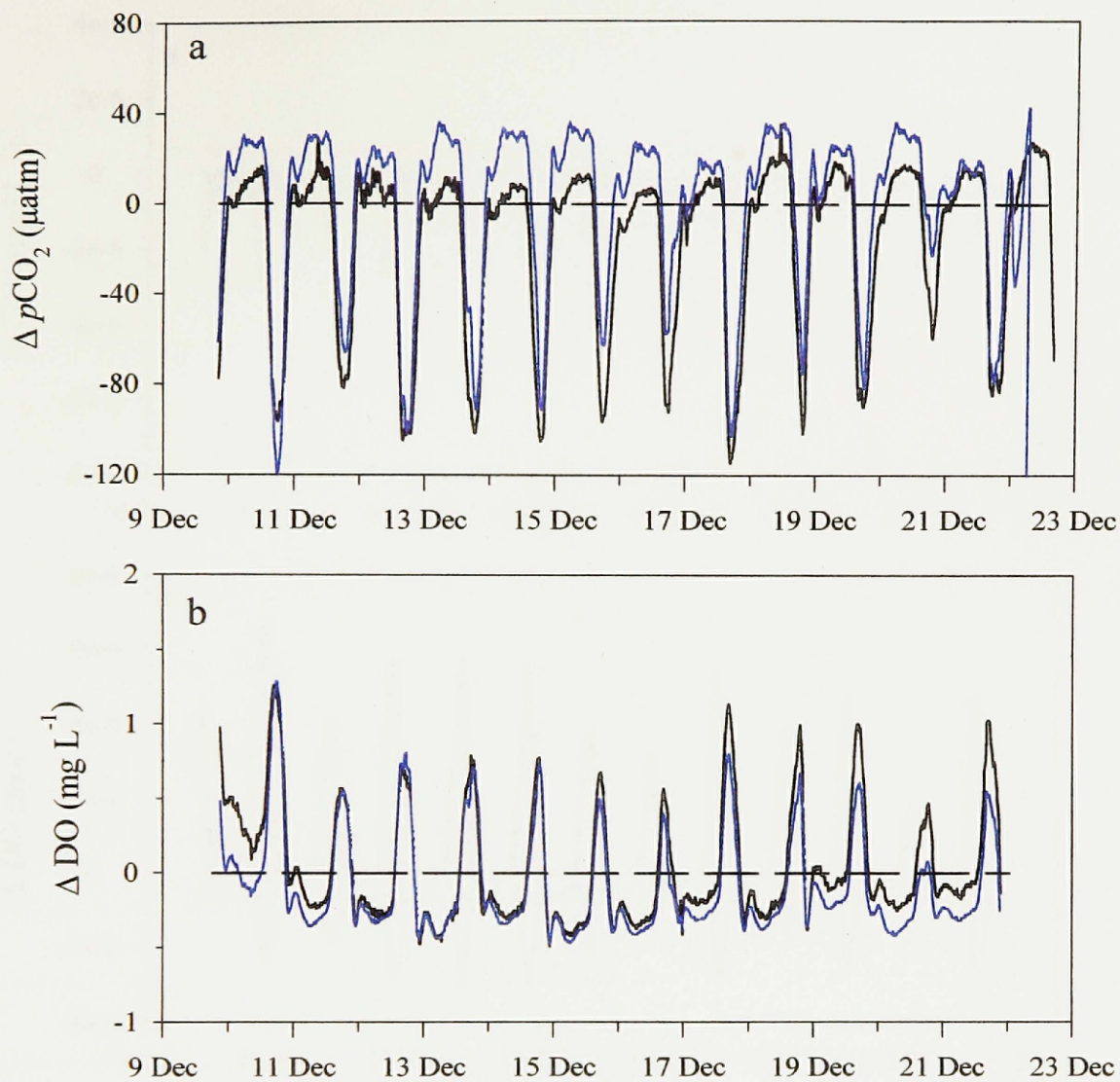


**Figure 22:** December modeled (blue) and *in situ* changes (black) in  $p\text{CO}_2$  and DO are shown in plots **a** and **b**, respectively.

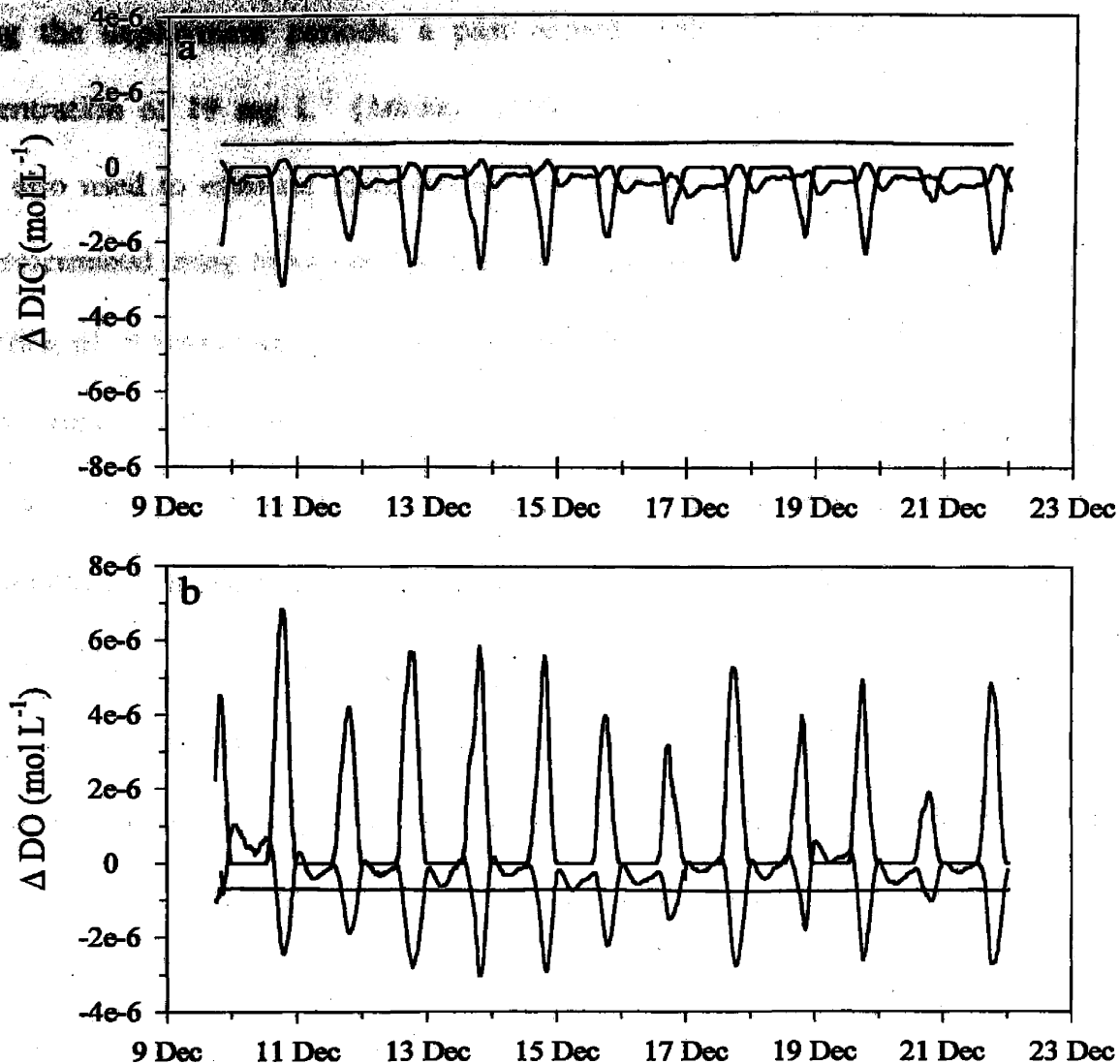


**Figure 23:** Modeled contributions from photosynthesis (black), respiration (red), and surface gas transfer (blue) in December 1999 (UTC). Molar changes in CO<sub>2</sub> and O<sub>2</sub> are shown in plots a and b, respectively.

contrast to September modeling. This is also observed when comparing the contribution plots between deployments.

### 5.2.3 Calcite cycling

Contributions from precipitation and dissolution of CaCO<sub>3</sub> to pCO<sub>2</sub> variability were not quantified during the study, so an examination of modeled  $\Omega$  yields the only insight.

$\Omega$  was determined using Equation 3. Although  $\text{Ca}^{2+}$  concentration was not monitored during the deployment periods, a past record (1997) of major ions yielded a mean concentration of  $19 \text{ mg L}^{-1}$  [Mickey, 1998]. Other reported major ion concentrations were also used to estimate ionic strength for calculation of activity coefficients.  $[\text{CO}_3^{2-}]$  was determined using *in situ*  $p\text{CO}_2$  data and constants and equations in Table 3.2. During modeling of downstream gas concentrations,  $\Omega$  was output to a file. The results of the model indicate that at all times during both deployment periods the river was supersaturated in calcite ( $\Omega > 1$ ) (Figure 24). Although this does not verify  $\text{CaCO}_3$  precipitation, it is highly thermodynamically favorable in September, as  $\Omega$  increased to  $> 4$ . Interestingly, downstream *in situ*  $p\text{CO}_2$  data increase over several days during the period when  $\Omega$  reaches its greatest value (Figure 3a). Precipitation, and the subsequent release of  $\text{CO}_2$ , is a possible source of this pattern. Lacking more evidence during this period (e.g.  $\text{Ca}^{2+}$  measurements), there can be no conclusion regarding the process's affect on river  $p\text{CO}_2$ .

Formation of  $\text{CaCO}_3$  during December is also favorable, though to a lesser degree. For instance,  $\Omega < 3$  during its highest value (Figure 24b). Effects from calcite cycling are not observed in December's  $p\text{CO}_2$  time-series because of the dominant metabolic pattern.

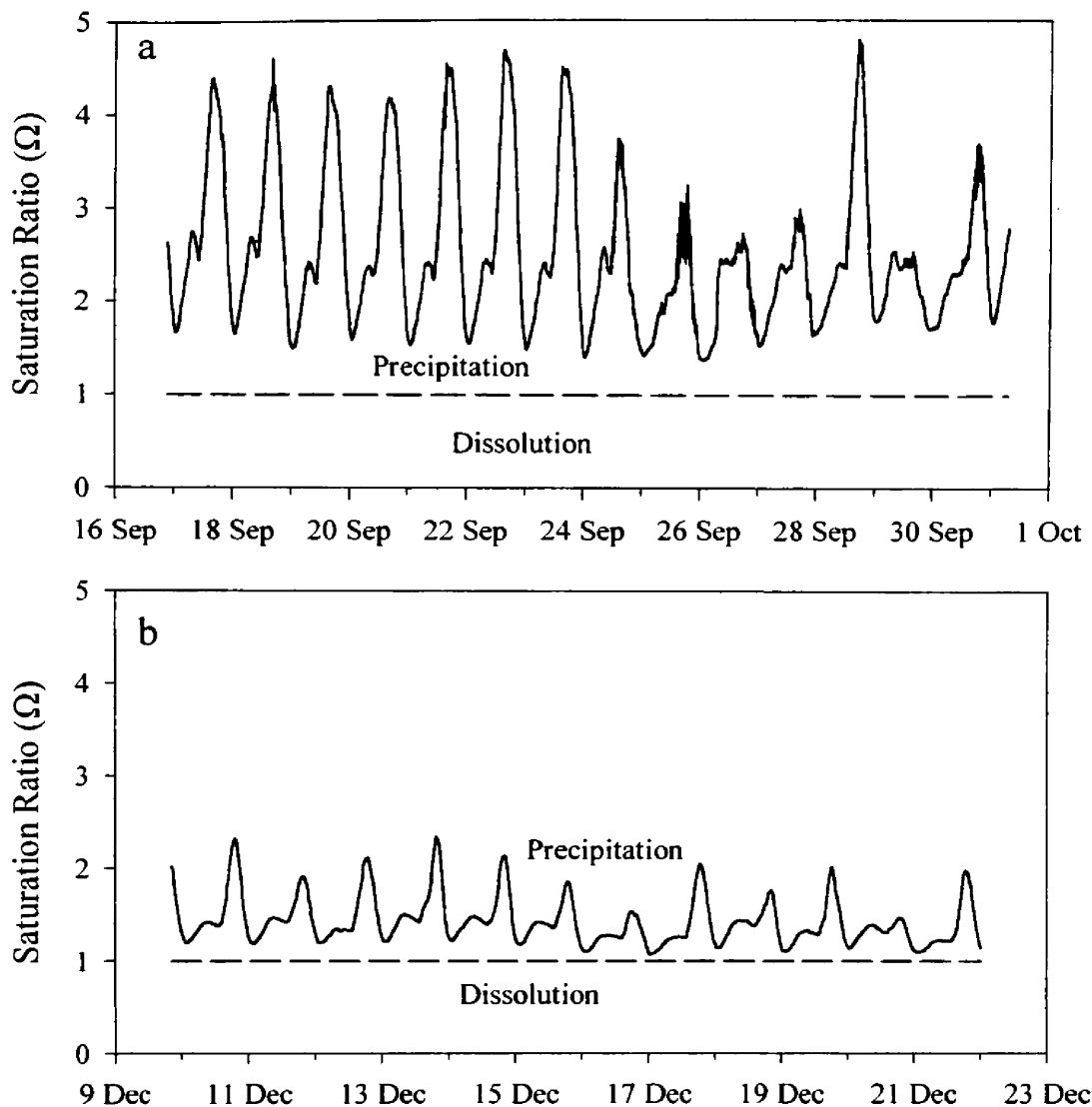


**Figure 24:** Modeled calcite saturation ratio during September (a) and December (b) 1999. The dashed line at  $\Omega = 1$  represents the partition between thermodynamic conditions favoring precipitation and dissolution of  $\text{CaCO}_3$ .

#### 5.2.4 Evaluating travel error

Accurate travel time is imperative in the analysis of river data monitored at two locations. Since gas flux accuracy depends upon precise travel time, any rates determined from gas flux are similarly affected. As a result of relatively constant discharge during each study, the travel time was assumed to remain constant throughout



each deployment. A sensitivity analysis was performed in order to determine the effect of travel time error. The difference in  $p\text{CO}_2$  and DO flux between different travel times was examined. For instance, a 0.75 h error (~15%) in travel time yields a maximum absolute deviation of  $1.47 \text{ mg L}^{-1} \Delta\text{DO}$  between a travel time of 2.25 and 3 h. The same error in travel time yields a maximum difference of  $194 \text{ } \mu\text{atm}$  in  $\Delta p\text{CO}_2$  ( $n = 2836$ ). The maximum differences occur in the daylight periods when photosynthesis is the dominant process. This suggests that errors in metabolic and physical rates based upon daytime data will be more significant if travel time is inaccurate. Resolving a unique travel time everyday will achieve the greatest accuracy. If an average travel time is used for modeling long-term variability, uncertainty can result in significant errors in gas flux.

### 5.2.5 Longitudinal dispersion

The modeling assumption that longitudinal mixing is negligible has also been made by other researchers using the Odum method [e.g. *Kelly et al.* 1974b; *Simonsen and Harremoës*, 1978; *Gausch et al.*, 1998]. Differences in the hydraulic parameters of each study reach (especially length) make it difficult to assess the validity of this assumption. Day (1975) reports that effects from longitudinal dispersion are more significant with increasing reach length, suggesting that September data were likely more affected by dispersion than in December. September conductivity data cannot yield information on longitudinal effects because sensing conditions were not comparable (discussed in Section 4.6.1). Similar conductivity peaks in Figure 17a however, support the assumption that dispersion was negligible during December. Further investigation is needed to accurately determine the effects of longitudinal mixing on  $p\text{CO}_2$  and DO variability in the Clark Fork River.

### 5.3 Model evaluation summary

The  $p\text{CO}_2$  and DO models prove to be valuable tools in assessing the relative contributions from surface gas transfer and metabolism in the Clark Fork River during deployments in 1999. Modeling is unable to accurately reproduce field measurements using estimated parameters, however the overall patterns of short-term and long-term variability are reproduced effectively. At least some of the disagreement is a result of measurement difficulties, however more knowledge of river biology and geochemistry (e.g.  $\text{CaCO}_3$ ) would certainly enhance the model's efficacy. Likewise, more time-series of other important geochemical parameters (e.g. alkalinity) would increase the accuracy of the theoretical calculations.

## Chapter 6

### Conclusions

Time-series from *in situ* gas sensors have revealed the complex gas dynamics in a riverine environment. Analyses indicate that diel fluxes in  $p\text{CO}_2$  and DO are predominantly controlled by metabolism, with surface gas transfer exerting a significant effect during periods of supersaturation. Data analysis is simplified by using distributed *in situ* sensors since utilizing the difference between the two curves eliminates significant sources of variability upstream. The upstream diel pattern is shifted with respect to time, most likely as a result of the impoundment. Consequently, a single station analysis at this location would not yield accurate estimates of metabolic or physical rates. The Odum method's advantage is clearly illustrated by comparing the complexity of the absolute and difference time-series' (Figures 3, 4, 8 and 9). Furthermore, combining  $p\text{CO}_2$  and DO data is clearly an effective tool, both for evaluating data quality, and for checking internal consistency between gas exchange and biological rate determination. Theoretical modeling compliments interpretations of *in situ* data, as well as providing a basis for future predictions.

The SAMI- $\text{CO}_2$  proved to be an exceptional tool in the analysis of the dominant biogeochemical processes at work in the Clark Fork River. Its ability to monitor high-frequency *in situ*  $p\text{CO}_2$  variability makes it a valuable resource for monitoring the  $\text{CO}_2$  cycle. Much of the difficulty estimating biological and geochemical contributions to  $\text{CO}_2$  flux arises when discrete sampling or incomplete data are utilized for analysis. *In situ* monitoring is crucial to understanding lotic system metabolism, as removing or disturbing community flora and fauna can change their natural response to variable

conditions. Similarly, gas transfer or metabolic research conducted in experimental lotic systems may not accurately represent natural *in situ* processes. Data comparison between adjacent instruments revealed good precision and the instrument's stability surpasses that of pH electrodes often used to calculate  $p\text{CO}_2$ . The possible error associated with these methods can also result in erroneous predictions of metabolic rates. Much greater difficulty resolving the changes in  $p\text{CO}_2$  would be expected if pH were relied upon for determination. Since the carbonate system is so important in riverine systems, the SAMI- $\text{CO}_2$  has the potential to advance understanding of short-term biogeochemical interactions.

Despite limitations and simplifications, theoretical and empirical models are able to predict changes in  $p\text{CO}_2$  and DO over the reach quite well. Future studies with improved methodologies and models will continue to enhance our understanding of the processes that control biogenic gases in rivers.

## References

- Baehr, M.M., In situ chemical sensor measurements in a freshwater lake: An analysis of the short-term and seasonal effects of ice cover, ice out, and turnover on CO<sub>2</sub> and O<sub>2</sub>, *Ph.D. Dissertation*, University of Montana-Missoula, 2000.
- Ballester, M.V., Martinelli, L.A., Krusche, A.V., Victoria, R.L. et al., Effects of increasing organic matter loading on the dissolved CO<sub>2</sub> and respiration rates in the Piracicaba River Basin, Southeast Brazil, *Water Res.*, 33(9), 2119-2129, 1999.
- Boston, H.L. and Hill, W.R., Photosynthesis-light relations of stream periphyton communities, *Limnol. Oceanogr.*, 36(4), 644-656, 1991.
- Bott, T.L., Brock, J.T., Cushing, C.E., Gregory, S.V., King, D., and Petersen, R.C., A comparison of methods for measuring primary productivity and community respiration in streams, *Hydrobiologia*, 60(1), 3-12, 1978.
- Bowker, D.W., Anyam, R.W., and Antoine, S.E., The relationships between the suspended and periphytic algae of the River Ithon, Wales, U.K., *Limnologica*, 26, 73-82, 1996.
- Brick, C. M., and Moore, J.N., Diel variation of trace metals in the Upper Clark Fork River, Montana, *Environ. Sci. and Tech.*, 30(6), 1953-1960, 1996.
- Byrne, R.H., and Breland, J.A., High precision multiwavelength pH determinations in seawater using cresol red, *Deep-Sea Res.*, 36, 803-810, 1989.
- Carpenter, R.C., Relationships between primary production and irradiance in coral reef algal communities, *Limnol. Oceanogr.*, 30(4), 784-793, 1985.
- Carr, J.J., Development of an autonomous *in situ* instrument for precise and stable freshwater measurement, *M.S. Thesis*, The University of Montana-Missoula, 2000.
- Chu, C.R. and Jirka, G.H., Reaeration in combined wind/stream driven flows, *J. Environ. Eng.*, 124(2), 79-88, 1998.
- Cicerone, D.S., Stewart, A.J., and Roh, Y., Diel cycles in calcite production and dissolution in a eutrophic basin, *Environmental Toxicology and Chemistry*, 18(10), 2169-2177, 1999.
- Clark, J.F., Wanninkhof, R., Schlosser, P., and Simpson, H.J., Gas exchange rates in the tidal Hudson River using a dual tracer technique, *Tellus*, 46B, 274-285, 1994.

- Daniil, E.I. and Gulliver, J.S., Temperature dependence of liquid film coefficient for gas transfer, *J. Environ. Eng.*, 114(5), 1224-1229, 1988.
- Dawson, J.J.C., Hope, D., Cresser, M.S., and Billett, M.F., Downstream changes in free carbon dioxide in an upland catchment, *J. Environ. Qual.*, 24, 699-706, 1995.
- Day, T., Longitudinal dispersion in natural channels, *Water Resour. Res.*, 11(6), 909-918, 1975.
- DeGrandpre, M.D., Hammar, T.R., Smith, S.P. and Sayles, F.L., *In situ* measurements of seawater  $p\text{CO}_2$ . *Limnol. Oceanogr.*, 40, 969-975, 1995.
- DeGrandpre, M.D., Baehr, M.M, and Hammar, T.R., Calibration-free optical chemical sensors, *Anal. Chem.*, 71(6), 1152-1159, 1999.
- Edmond, J.M., High precision determination of titration of alkalinity and total carbon dioxide content of sea water by potentiometric titration, *Deep-Sea Res.*, 17, 737-750, 1970.
- Elsinger, R.J. and Moore, W.S., Gas exchange in the Pee Dee River based on  $^{222}\text{Rn}$  evasion, *Geophys. Res. Lett.*, 10(6), 443-446, 1983.
- French, C.R., DeGrandpre, M.D., Carr, J.J., Dougherty, E.M., Eidson, L.A.K., and Reynolds, J.C., Spectrophotometric pH measurements of freshwater, submitted to *Anal. Chim. Acta* December 2000.
- Genereux, D.P. and Hemond, H.F., Determination of gas exchange rate constants for a small stream on Walker Branch Watershed, Tennessee, *Water Resour. Res.*, 28(9), 2365-2374, 1992.
- Gestring, S.L., The interaction of the Clark Fork River and Hellgate Valley Aquifer near Milltown, Montana. *M.S. Thesis*, The University of Montana-Missoula, 1994.
- Granéli, W., Lindell, M., and Tranvik, L., Photo-oxidative production of dissolved inorganic carbon in lakes of different humic content, *Limnol. Oceanogr.* 41(4), 698-706, 1996.
- Greb, S.R. and Graczyk, D.J., Frequency-duration analysis of dissolved-oxygen concentrations in two southwestern Wisconsin streams, *Water Resour. Bull.*, 31(3), 431-438, 1995.
- Guasch, A.H., Armengol, J., Marti, E., and Sabater, S., Diurnal variation in dissolved oxygen and carbon dioxide in two low-order streams, *Water Res.*, 32(4), 1067-1074, 1998.

- Gulliver, J.S., Hibbs, D.E., and McDonald, J.P., Measurement of effective saturation concentration for gas transfer, *J. Hydr. Eng.*, 123(2), 86-97, 1997.
- Gulliver, J.S., and Stefan, H.G., Stream productivity analysis with DORM-III: Productivity of experimental streams, *Water Res.*, 18(12), 1589-1595, 1984.
- Harris, D.C., in *Quantitative Chemical Analysis*, 4<sup>th</sup> ed., W. H. Freeman and Co., New York, NY, 1995.
- Hartman, B. and Hammond, D.E., Gas exchange rates across the sediment-water and air-water interfaces in South San Francisco Bay, *J. Geophys. Res.*, 89(C3), 3593-3603, 1984.
- Hemond, H.F., Acid neutralizing capacity, alkalinity, and acid-base status of natural waters containing organic acids, *Environ. Sci. Technol.*, 24, 1486-1489, 1990.
- Hoffer-French, K.J., and Herman, J.S., Evaluations of hydrological and biological influences on CO<sub>2</sub> fluxes from a karst stream, *J. Hydrol.*, 108, 189-212.
- Hongve, D., Shortcomings of Gran titration procedures for determination of alkalinity and weak acids in humic water, *Wat. Res.*, 24(10), 1305-1308, 1990.
- Hornberger, G.M., Kelly, M.G., and Eller, R.M., The relationship between light and photosynthetic rate in a river community and implications for water quality modeling, *Water Resour. Res.*, 12(4), 723-730, 1976.
- Jasby, A.D. and Platt, T., Mathematical formulation of the relationship between photosynthesis and light for phytoplankton. *Limnol. Oceanogr.*, 21, 540-547, 1976.
- Jasper, S. and Bothwell, M.L., Photosynthetic characteristics of lotic periphyton. *Can. J. Fish. Aquat. Sci.*, 43, 1960-1969, 1986.
- Jones, C.R., and Adams, M.S., Seasonal variations in photosynthetic response of algae epiphytic on *Myriophyllum spicatum* L., *Aquat. Bot.*, 13, 317-330, 1982.
- Kelly, M.G., Church, M.R., and Hornberger, G.M., A solution of the inorganic carbon mass balance equation and its relation to algal growth rates, *Water Resour. Res.*, 10(3), 493-497, 1974a.
- Kelly, M.G., Hornberger, G.M., and Cosby B.J., Continuous automated measurement of rates of photosynthesis and respiration in an undisturbed river community, *Limnol. Oceanogr.*, 19(2), 305-312, 1974b.
- Kiefer, D.A., and Reynolds, R.A., Advances in understanding phytoplankton fluorescence and photosynthesis, in Falkowski, P.G. and Woodhead, A.D., (Ed.), *Primary Productivity and Biogeochemical Cycles in the Sea*, Plenum Press, New York, 155-174, 1992.

- Kirk, J. T. O., in *Light and Photosynthesis in Aquatic Systems*, 2<sup>nd</sup> ed., Cambridge University Press, New York, 284-289, 1994.
- Kling, G.W., Kipphut, G.W., Miller, M.C., Arctic lakes and streams as gas conduits to the atmosphere: Implications for tundra carbon budgets, *Science*, 251, 298-301, 1991.
- Lambing, J.H., Hornberger, M.I., Axtmann, E.V., and Pope, D.A., Water-quality, bed-sediment, and biological data (October 1992 through September 1993) and statistical summaries of water-quality data (March 1985 through September 1993) for streams in the Upper Clark Fork Basin, Montana, *U.S.G.S. Open-File Report*, 94-375, 1994.
- Lewis, E., and Wallace, D.R., Program developed for CO<sub>2</sub> system calculations, ORNL/CDIAC-105, Carbon Dioxide Information Analysis Center, Oak Ridge National Laboratory, U.S. DOE, Oak Ridge, TN, 1998.
- Marra, J., Analysis of diel variability in chlorophyll fluorescence, *J. Mar. Res.*, 55, 767-784, 1997.
- Marzolf, E.R., Mulholland, P.J., and Steinman, A.D., Improvements to the diurnal upstream-downstream dissolved oxygen change technique for determining whole-stream metabolism in small streams, *Can. J. Fish. Aquat. Sci.*, 51, 1591-1599, 1994.
- Melching, C.S. and Flores, H.E., Reaeration equations derived from U.S. Geological Survey database, *J. Environ. Eng.*, 125(5), 407-414, 1999.
- Mickey, J.W., The effects of discharge variation on dissolved element concentrations through Milltown Reservoir, Montana, *M.S. Thesis*, The University of Montana-Missoula, 1998.
- Millero, F.J., The thermodynamics of the carbonate system in seawater, *Geochim. Cosmochim. Acta*, 43, 1651-1661, 1979.
- Moog, D.B. and Jirka, G.H., Macroroughness effects on stream reaeration, *J. Environ. Eng.*, 124(2), 89-99, 1998a.
- Moog, D.B. and Jirka, G.H., Analysis of reaeration equations using mean multiplicative error, *J. Environ. Eng.*, 124(2), 101-111, 1998b.
- Neal, C., Harrow, M., and Williams, R.J., Dissolved carbon dioxide and oxygen in the River Thames, *Sci. Tot. Environ.*, 210/211, 205-217, 1998.
- Odum, H.T., Primary production in flowing waters, *Limnol. Oceanogr.*, 1, 102-117, 1956.
- Owens, M., Edwards, R.W., and Gibbs, J.W., Some reaeration studies in streams, *Int. J. Air Wat. Poll.*, 8, 469-486, 1964.



- Park, P.K., Gordon, L.I., Hager, S.W., and Cissell, M.C., Carbon dioxide partial pressure in the Columbia River, *Science*, 166, 867-868, 1969.
- Parkhill, K.L. and Gulliver, J.S., Application of photorespiration concepts to whole stream productivity, *Hydrobiologia*, 389, 7-19, 1998.
- Platt, T., Gallegos, C.L., and Harrison, W.G., Photoinhibition of photosynthesis in natural assemblages of marine phytoplankton. *J. Mar. Res.*, 38, 687-701, 1980.
- Raymond, P.A., Caraco, N.F., and Cole, J.J., Carbon dioxide concentration and atmospheric flux in the Hudson River, *Estuaries*, 20(2), 381-390, 1997.
- Simonsen, J.F. and Harremoës, P., Oxygen and pH fluctuations in rivers, *Water Res.*, 12, 477-489, 1978.
- Stumm, W. and Morgan, J.J., in *Aquatic chemistry*, 3<sup>rd</sup> ed., John Wiley and Sons, Inc., New York, NY, 1996.
- Thyssen, N. and Kelly, M.G., Water-air exchange of carbon dioxide and oxygen in a river: Measurement and comparison of rates, *Arch. Hydrobiol.*, 105(2), 219-228, 1985.
- Tsivoglou, E.C. and Wallace, J.R., Characterization of stream reaeration capacity, Report prepared for Office of Research and Monitoring U.S. EPA, WA, (Report No. EPA-R3-72-012), 1972.
- Wanninkhof, R., Mulholland, P.J., and Elwood, J.W., Gas exchange rates for a first-order stream determined with deliberate and natural tracers, *Water Resour. Res.*, 26(7), 1621-1630, 1990.
- Wanninkhof, R., Relationship between wind speed and gas exchange over the ocean, *J. Geophys. Res.*, 97(C5), 7373-7382, 1992.
- Weiss, R.F., Carbon dioxide in water and seawater: The solubility of a non-ideal gas, *Marine Chemistry*, 2, 203-215, 1974.
- Wellnitz, T. and Rinne, B., Photosynthetic response of stream periphyton to fluctuating light regimes, *J. Phycol.*, 35, 667-672, 1999.
- Wetzel, R.G. and Likens, G.E., in *Limnological Analyses*, 2<sup>nd</sup> ed., pp. 391, Springer-Verlag, New York, NY, 1991.
- Wetzel, R.G., in *Limnology*, 2<sup>nd</sup> ed., pp. 686-689, Saunders College Publishing, Fort Worth, TX, 1983.

Wright, J.C. and Mills, I.K., Productivity studies on the Madison River, Yellowstone National Park, *Limnol. Oceanogr.* 12, 568-577, 1967.

## Appendix 1

```
'@@@@@@@@@@@@@@@@@@@@@@@@@@@@@@@@@@@@@@@@@@@@@@@@@@@@@@@@@@@@@
'
'                               Riverine pCO2 model
'                               diffusion & metabolism
'                               River version 3.0
'                               Microsoft® QuickBASIC®
'                               jason reynolds
'                               last modified 3/01
'@@@@@@@@@@@@@@@@@@@@@@@@@@@@@@@@@@@@@@@@@@@@@@@@@@@@@@@@@@@@@
```

```
>>>>>>>this program models the effects of metabolism and surface gas transfer on
>>>>>>>pCO2 in a flowing section of water. the model is comprised of two tiers:
>>>>>>>a) one moving through the data measurement by measurement, and b) iterative
>>>>>>>modeling of the biological and physical effects over the travel reach
```

```
' >>SUBROUTINES>>
```

```
DECLARE SUB carbon (TNEW, PCO2NEW, ALKNEW, TCO2NEW)
DECLARE SUB diffusion (TNEW, PCO2NEW, ALKNEW, TCO2NEW)
DECLARE SUB gas (TNEW, ALKNEW, TCO2NEW, PCO2NEW, OMEGA)
```

```
' >>DIMENSION VARIABLES>>
```

```
DIM SHARED F AS DOUBLE, FPRIME AS DOUBLE
DIM SHARED dt AS SINGLE, d AS SINGLE, PCO2SAT AS SINGLE
DIM SHARED ALKUP AS SINGLE, ALKDN AS SINGLE
DIM SHARED X AS INTEGER, KL AS INTEGER
DIM SHARED PARTM AS INTEGER, a AS SINGLE, flow AS INTEGER
DIM SHARED PHOTOS$, MODEL$, dTCO2R, dTCO2P, dTCO2D
DIM SHARED ARRAY(1 TO 2000), ATMOS(1 TO 2000), number%, hellgate%
DIM SHARED SHIFTR, SHIFT, ARRAY2(1 TO 2000), sun%, NUMERATOR
REDIM SHARED DIFF(1 TO 2000), FLD(1 TO 2000)
DIM SHARED YD, CALCIUM, CO32, KSP
DIM SHARED BETA, BETA2
```

```
'@@@@@@@@@@@@@@@@@@@@@@@@@@@@@@@@@@@@@@@@@@@@@@@@@@@@@@@@@@@@@
```

```
'included for troubleshooting only; comment out for proper function
'CLOSE #1: CLOSE #2: STOP
```

```
'@@@@@@@@@@@@@@@@@@@@@@@@@@@@@@@@@@@@@@@@@@@@@@@@@@@@@@@@@@@@@
```

```
' >>ERROR TRAP<<
```

'note: will catch input past end of file error  
ON ERROR GOTO 999

'@@

' >>PARAMETERS AND FILE INFORMATION<<

'prints graphic

11 CLS

COLOR 3, 8: CLS

FOR M = 2 TO 78

LOCATE 1, M: PRINT CHR\$(18)

NEXT M

'>>>>>>>user screen information

LOCATE 3, 3: PRINT ".this model calculates the effects of metabolism, diffusion, &"

LOCATE 4, 4: PRINT "temperature fluctuation on river pCO2"

LOCATE 7, 3: PRINT ".input data file must be comma or space delimited & formatted  
as:"

COLOR 6, 8

LOCATE 9, 3: PRINT CHR\$(175); "year day(d), pCO2(up, atm), temp(up, ";  
CHR\$(248); "C), temp(down), alkalinity(up, mol/l)"

LOCATE 11, 3: PRINT CHR\$(175); "photosynthetic rates in mol C/h"

COLOR 10, 8

'>>>>>>>user input (filenames)

LOCATE 14, 3: INPUT ".enter field data filename (include path): (TESTALK.PRN) ",  
data\$

IF data\$ = "" THEN data\$ = "TESTALK.PRN"

LOCATE 15, 3: INPUT ".enter full syntax for photosynthetic rate file: ", PHOTOS\$

IF PHOTOS\$ = "" THEN PHOTOS\$ = "C:\QB45\PHOTO(S).PRN"

LOCATE 16, 3: INPUT ".enter full syntax for file with atmospheric pCO2: ", ATMOS\$

IF ATMOS\$ = "" THEN ATMOS\$ = "C:\QB45\ATMOS(s).PRN"

LOCATE 17, 3: INPUT ".enter full syntax for irradiance file: ", LIGHTS\$

IF LIGHTS\$ = "" THEN LIGHTS\$ = "C:\QB45\LIGHT.PRN"

LOCATE 18, 3: INPUT ".enter file containing downstream pCO2 data: ", feeld\$

```
IF feeld$ = "" THEN feeld$ = "FLDCO2S.PRN"
```

```
LOCATE 25, 1: PRINT "Press any key to continue"
```

```
'>>>>>>>waits for key press to continue
```

```
DO: LOOP UNTIL INKEY$ <> "": CLS
```

```
'>>>>>>>screen graphic
```

```
FOR M = 2 TO 79
```

```
    LOCATE 1, M: PRINT CHR$(18)
```

```
NEXT M
```

```
COLOR 11, 8
```

```
LOCATE 4, 5: PRINT ".enter the following to begin: "
```

```
COLOR 10, 8
```

```
'>>>>>>>user input (storage filename, travel time, rates, depth)
```

```
'>>>>>>>default values set for September modeling
```

```
LOCATE 7, 5: INPUT ".save results to what filename? (DOODOO.DAT) ", savename$
```

```
IF savename$ = "" THEN savename$ = "DOODOO.DAT"
```

```
LOCATE 8, 5: INPUT ".travel time in hours? (4.25) ", tt
```

```
IF tt = 0 THEN tt = 4.25
```

```
LOCATE 9, 5: INPUT ".how many iterations? (20) ", it
```

```
IF it = 0 THEN it = 20
```

```
COLOR 11, 8
```

```
LOCATE 11, 5: PRINT ".enter metabolic and diffusional rates @ 20"; CHR$(248); "C"
```

```
COLOR 10, 8
```

```
LOCATE 13, 5: INPUT ".respiration rate in mol C/l/h? {5.6e-6} ", R
```

```
LOCATE 14, 5: PRINT ".enter photorespiration constant, "; CHR$(225); ": (0 to omit) "
```

```
LOCATE 14, 57: INPUT "", BETA
```

```
LOCATE 15, 5: INPUT ".gas transfer velocity for CO2 in cm/h? (44) ", KL
```

```
IF KL = 0 THEN KL = 15
```

```
LOCATE 17, 5: INPUT ".river depth in cm? (100)", d
```

```
IF d = 0 THEN d = 100
```

```
'@@@@@@@@@@@@@@@@@@@@@@@@@@@@@@@@@@@@@@@@@@@@@@@@@@@@@@@@@@@@'
```

```
' <<PARAMETER FOR UPDATING METABOLIC AND DIFFUSIONAL  
DATA>>
```

```
'>>>>>>>this function calculates the "flow" parameter for determining the array  
'>>>>>>>location (of light and photosynthesis) as the section of water travels over  
'>>>>>>>the reach
```

```
dt = tt / it: flow = dt / .25
```

```
'>>>>>>> <RETURN> continues; other key press returns to start
```

```
LOCATE 25, 5: INPUT ".press return to continue or enter any key to restart ", G$  
IF G$ <> "" THEN  
GOTO 11  
END IF
```

```
'>>>>>>>filename for storage of separate rate contributions  
LOG$ = "CARBON.PRN"
```

```
CLS  
COLOR 7, 8
```

```
'@@@@@@@@@@@@@@@@@@@@@@@@@@@@@@@@@@@@@@@@@@@@@@@@@@@@@@@@@@@@'
```

```
' >>LOAD PHOTOSYNTHESIS ARRAY<<  
'>>>>>>>inputs photosynthetic rates into array for photosynthetic effects
```

```
OPEN PHOTO$ FOR INPUT AS #1  
FOR number% = 1 TO 2000  
    INPUT #1, ARRAY(number%)  
    IF EOF(1) THEN EXIT FOR  
NEXT number%  
CLOSE #1
```

```
'@@@@@@@@@@@@@@@@@@@@@@@@@@@@@@@@@@@@@@@@@@@@@@@@@@@@@@@@@@@@'
```

```
' >>LOAD ATMOSPHERIC pCO2 ARRAY<<  
'>>>>>>>inputs atmospheric pCO2 data into array for gas transfer calculations
```

```
OPEN ATMO$ FOR INPUT AS #1  
FOR hellgate% = 1 TO 2000  
    INPUT #1, ATMOS(hellgate%)  
    IF EOF(1) THEN EXIT FOR  
NEXT hellgate%
```

CLOSE #1

'@@'

' <<GET FIELD IRRADIANCE DATA>>  
'>>>>>>>inputs PAR data into array for use with photorespiration model

OPEN LIGHT\$ FOR INPUT AS #1  
FOR sun% = 1 TO 2000  
    INPUT #1, ARRAY2(sun%)  
    IF EOF(1) THEN EXIT FOR  
NEXT sun%  
CLOSE #1

'@@'

' <<GET DOWNSTREAM DATA>>  
'>>>>>>>inputs field downstream data for statistical evaluation of model

OPEN feeld\$ FOR INPUT AS #5  
FOR X = 1 TO 2000  
    INPUT #5, FLD(X)  
    IF EOF(5) THEN EXIT FOR  
NEXT X  
CLOSE #5

'@@'

' >>GET UPSTREAM FIELD DATA<<  
OPEN data\$ FOR INPUT AS #1

'>>>>>>>tier 1 modeling counter

SHIFTR0L = 1

'>>>>>>>tier 1 modeling begins here

DO  
INPUT #1, YD, PCO2UP, TUP, TDN  
INPUT #1, ALKUP

'>>>>>>>compute time and alkalinity steps  
TSTP = (TDN - TUP) / (it - 1): ' [not used] ALKSTP = (ALKDN - ALKUP) \* .000001 /  
(it - 1)

'>>>>>>>load initial values

'>>>>>>>converts pCO2 and ALK to proper units of microatm and microequ kg-1, respectively

TNEW = TUP: PCO2NEW = PCO2UP \* .000001; ALKNEW = ALKUP \* .000001

'@@@  
'@@@

' >>ITERATIVE MODEL<<

'>>>>>>>tier 2 begins here

'>>>>>>>tier 2 counter

SHIFT = 0

'>>>>>>>iterative loop

FOR w = 1 TO it

'>>>>>>>initial pCO2 to DIC calculation

IF w = 1 THEN CALL carbon(TNEW, PCO2NEW, ALKNEW, TCO2NEW)

'@@@

' >>METABOLISM<<

' <<photorespiration constants>>

'>>>>>>>>>this function averages the previous 4 h PAR intensities for use in

'>>>>>>>>>calculating photorespiration; BETA is photorespiration constant

IF SHIFTROL > 20 THEN

average% = SHIFTROL + SHIFT

Iave = 0

BETA2 = BETA

FOR U = 1 TO 20

Iave = Iave + ARRAY2(average%)

average% = average% - 1

NEXT U

Iave = Iave / 20

ELSE

BETA2 = 0

END IF



```
'@@@@@@@@@@@@@@@@@@@@@@@@@@@@@@@@@@@@@@@@@@@@@@@@@@@@@@@@@@@@
'      <<RESPIRATION>>
'>>>>>>modified Arrhenius coefficient for modeling temperature affects on respiration

THETA2 = 1.045

RT = (R + (BETA2 * Iave)) * (THETA2 ^ (TNEW - 20))

'@@@@@@@@@@@@@@@@@@@@@@@@@@@@@@@@@@@@@@@@@@@@@@@@@@@@@@@@@@@@
'      >>PHOTOSYNTHESIS<<

'>>>>>>>controls shifting of photosynthesis file

PT = ARRAY(SHIFTROL + SHIFT)

'>>>>>>>metabolic contributions to change in DIC

dTCO2R = RT * dt: dTCO2P = PT * dt
TCO2NEW = TCO2NEW + dTCO2R + dTCO2P

'@@@@@@@@@@@@@@@@@@@@@@@@@@@@@@@@@@@@@@@@@@@@@@@@@@@@@@@@@@@@
'      >>ALKALINITY CHANGE DUE TO METABOLISM<<
'      >>based upon Redfield stoichiometry<<

dALK = (dTCO2R * (-18 / 106)) + (dTCO2P * (18 / 106))
ALKNEW = ALKNEW + dALK

'@@@@@@@@@@@@@@@@@@@@@@@@@@@@@@@@@@@@@@@@@@@@@@@@@@@@@@@@@@@@
'      <<pCO2 TO DIC, GAS TRANSFER EFFECTS, AND DIC TO pCO2>>

CALL gas(TNEW, ALKNEW, TCO2NEW, PCO2NEW, OMEGA)
CALL carbon(TNEW, PCO2NEW, ALKNEW, TCO2NEW)
CALL diffusion(TNEW, PCO2NEW, ALKNEW, TCO2NEW)
CALL gas(TNEW, ALKNEW, TCO2NEW, PCO2NEW, OMEGA)

'@@@@@@@@@@@@@@@@@@@@@@@@@@@@@@@@@@@@@@@@@@@@@@@@@@@@@@@@@@@@
'      <<SAVE DOWNSTREAM, SATURATION RATIO, AND CONTRIBUTION
DATA>>

IF w = it THEN
OPEN savename$ FOR APPEND AS #2
```

```
WRITE #2, YD, PCO2NEW
CLOSE #2
```

```
OPEN "SALKY.PRN" FOR APPEND AS #69
WRITE #69, YD, ALKNEW, ALKUP
CLOSE #69
```

```
'      <<saturation ratio calculation info file>>
```

```
OPEN "OMEGA.PRN" FOR APPEND AS #77
PRINT #77, YD, OMEGA
CLOSE #77
END IF
OPEN LOG$ FOR APPEND AS #3
WRITE #3, YD, dTCO2P, dTCO2R, dTCO2D
CLOSE #3
```

```
'>>>>>>change temperature via temperature step [calculated by (tempdown-
tempup)/travel time]
```

```
TNEW = TNEW + TSTP
```

```
'@@@@@@@@@@@@@@@@@@@@@@@@@@@@@@@@@@@@@@@@@@@@@@@@@@@@@@@@@@@@
```

```
'      <<CONTROLS LONGITUDINAL CHANGE IN VARIABLES>>
```

```
SHIFT = SHIFT + flow
```

```
'>>>>>>graphic for modeling: blue screen during day; black during night
```

```
IF ARRAY2(SHIFTROL) > 0 THEN COLOR 10, 9: CLS
IF ARRAY2(SHIFTROL) = 0 THEN COLOR 8, 8: CLS
```

```
'>>>>>>next step in tier 2 model
'>>>>>>tier 2 loop
NEXT w
```

```
'@@@@@@@@@@@@@@@@@@@@@@@@@@@@@@@@@@@@@@@@@@@@@@@@@@@@@@@@@@@@
```

```
'      >>MEAN AND ABSOLUTE MEAN DIFFERENCE<<
```

```
'>>>>>>statistical calculation between field downstream data and model
```

```
DIFF(SHIFTROL) = (PCO2NEW * 1000000!) - FLD(SHIFTROL)
```

```
'>>>>>>steps tier 1 counter
```

SHIFTR0L = SHIFTR0L + 1

'>>>>>>tier 1 loop  
LOOP UNTIL EOF(1)

666 CLOSE #1

'@@'

'>>>>>>alerts user that modeling is finished

COLOR 14, 8: CLS : LOCATE 13, 29: PRINT ".modeling complete"

'>>>>>>more statistical calculations

SUMMY = 0: ADDITUP = 0

'>>>>>>sums differences and absolute differences

FOR Z = 1 TO (SHIFTR0L - 1)  
    SUMMY = DIFF(Z) + SUMMY  
    ADDITUP = ABS(DIFF(Z)) + ADDITUP  
NEXT Z

'>>>>>>computes mean difference

MEAN = SUMMY / (SHIFTR0L - 1)

'>>>>>>computes absolute mean difference

REALMEAN = ADDITUP / (SHIFTR0L - 1)

NUMERATOR = 0

'>>>>>>standard deviation from mean

FOR V = 1 TO (SHIFTR0L - 1)  
    NUMERATOR = ((DIFF(V) - MEAN) ^ 2) + NUMERATOR  
NEXT V

STD = SQR(NUMERATOR / (SHIFTR0L - 2))

'>>>>>>prints statistical information to screen

COLOR 15, 8



**SUB carbon (TNEW, PCO2NEW, ALKNEW, TCO2NEW)**

```
'@@@@@@@@@@@@@@@@@@@@@@@@@@@@@@@@@@@@@@@@@@@@@@@@@@@@@@@@@@@@'
```

```
' >>COMPUTES DIC FROM pCO2NEW AND ALKNEW @ TNEW USING  
NEWTON'S METHOD<<
```

```
'>>>>>>temperature
```

```
KELVIN = 273.15 + TNEW
```

```
'>>>>>>dissociation constant for water [Millero, 1979]
```

```
KW = 10 ^ ((-4470.99 / KELVIN) + 6.0875 - (.01706 * KELVIN))
```

```
'>>>>>>combined constant for CO2 gas dissolution and carbonic acid formation  
[Weiss, 1974]
```

```
K0 = EXP(-60.2409 + (93.4517 * (100 / KELVIN)) + (23.3585 * LOG(KELVIN / 100)))
```

```
'>>>>>>dissociation constant for carbonic acid [Millero, 1979]
```

```
K1 = 10 ^ (-((6320.81 / KELVIN) - 126.3405 + (19.568 * LOG(KELVIN))))
```

```
'>>>>>>dissociation constant for hydrogen carbonate [Millero, 1979]
```

```
K2 = 10 ^ (-((5143.69 / KELVIN) - 90.1833 + (14.613 * LOG(KELVIN))))
```

```
'>>>>>>first estimate for hydrogen in Newton's method
```

```
HNEW = ALKNEW
```

```
' <<ITTERATION ROUTINE>>
```

```
DO
```

```
h = HNEW
```

```
F = (-h ^ 3) + ((KW + K1 * K0 * PCO2NEW) * h) + (2 * K1 * K2 * K0 * PCO2NEW) -  
(ALKNEW * h ^ 2)
```

```
FPRIME = (-3 * h ^ 2) + (KW) + (K1 * K0 * PCO2NEW) - (2 * ALKNEW * h)
```

```
IF h <= 0 THEN
```

```
h = ALKNEW
```

```
ELSE
```

```
HNEW = h - (F / FPRIME)
```

END IF

LOOP UNTIL ABS(HNEW - h) < 1E-13

' <<NEW DIC>>

TCO2NEW = K0 \* PCO2NEW \* (1 + (K1 / HNEW) + (K1 \* K2 / (HNEW ^ 2)))

END SUB

**SUB diffusion (TNEW, PCO2NEW, ALKNEW, TCO2NEW)**

```
'@@@@@@@@@@@@@@@@@@@@@@@@@@@@@@@@@@@@@@@@@@@@@@@@@@@@@@@@@@@@'
```

```
' >>MODELS FOR GAS TRANSFER EFFECTS<<
```

```
'>>>>>>>temperature correction of KL using modified Arrhenius relationship
```

```
'K = KL * (1.0241 ^ (TNEW - 20)) [NOT USED]
```

```
'>>>>>>>temperature correction of KL using schmidt numbers (equivalent)
```

```
K = KL / (((600 / (1911.1 - (118.11 * TNEW) + (3.4527 * (TNEW ^ 2)) - (.04132 * (TNEW ^ 3)))) ^ (-.5))
```

```
'>>>>>>>temperature
```

```
KELVIN = TNEW + 273.15
```

```
'>>>>>>>see CARBON SUBPROGRAM FOR REFERENCE INFORMATION
```

```
K0 = EXP(-60.2409 + (93.4517 * (100 / KELVIN)) + (23.3585 * LOG(KELVIN / 100)))
```

```
'>>>>>>>computes water-atmospheric pCO2 gradient
```

```
PCO2DEF = (ATMOS(SHIFTROL) * .000001) - PCO2NEW
```

```
'>>>>>>>computes change from surface gas transfer
```

```
dTCO2D = K * (PCO2DEF) * K0 * dt / d
```

```
'>>>>>>>computes new DIC
```

```
TCO2NEW = TCO2NEW + dTCO2D
```

```
END SUB
```

## SUB gas (TNEW, ALKNEW, TCO2NEW, PCO2NEW, OMEGA)

'@@'

' >>COMPUTES pCO2 FROM DIC AND ALKNEW @ TNEW USING NEWTON'S METHOD<<

' >>note: accuracy of results depends greatly upon constants<<

' >>note: this model computes fugacity NOT pCO2, but the difference is assumed negligible

'>>>>>>temperature

KELVIN = 273.15 + TNEW

'>>>>>>see CARBON SUBPROGRAM for reference information

KW = 10 ^ ((-4470.99 / KELVIN) + 6.0875 - (.01706 \* KELVIN))

K0 = EXP(-60.2409 + (93.4517 \* (100 / KELVIN)) + (23.3585 \* LOG(KELVIN / 100)))

K1 = 10 ^ (-((6320.81 / KELVIN) - 126.3405 + (19.568 \* LOG(KELVIN))))

K2 = 10 ^ (-((5143.69 / KELVIN) - 90.1833 + (14.613 \* LOG(KELVIN))))

'>>>>>>inital estimate for hydrogen ion concentration

HNEW = TCO2NEW

' <<ITERATION ROUTINE>>

DO

h = HNEW

F = h ^ 4 + ((ALKNEW + K1) \* h ^ 3) + (((K1 \* ALKNEW) - KW - (K1 \* TCO2NEW) + (K1 \* K2)) \* h ^ 2) + (((K1 \* K2 \* ALKNEW) - (2 \* K1 \* K2 \* TCO2NEW) - (K1 \* KW)) \* HNEW) - (K1 \* KW \* K2)

FPRIME = (4 \* h ^ 3) + (3 \* (ALKNEW + K1) \* h ^ 2) + (2 \* ((K1 \* ALKNEW) - KW - (K1 \* TCO2NEW) + (K1 \* K2)) \* h) + ((K1 \* K2 \* ALKNEW) - (2 \* K1 \* K2 \* TCO2NEW) - (K1 \* KW))

IF h <= 0 THEN

h = TCO2NEW

ELSE

HNEW = h - (F / FPRIME)

END IF

LOOP UNTIL ABS(HNEW - h) < 1E-17

' <<NEW pCO2>>

'>>>>>>calculates new pCO2



$$\text{HCO}_3 = \text{TCO}_2\text{NEW} * \text{K}_1 * \text{HNEW} / (\text{HNEW}^2 + \text{K}_1 * \text{HNEW} + \text{K}_1 * \text{K}_2)$$

$$\text{H}_2\text{CO}_3 = \text{HNEW} * \text{HCO}_3 / \text{K}_1$$

$$\text{PCO}_2\text{NEW} = \text{H}_2\text{CO}_3 / \text{K}_0$$

' <<CALCITE PRECIP INFO>>

'>>>>>>calculates saturation ration

$$\text{CO}_3 = \text{K}_2 * \text{HCO}_3 / \text{HNEW}$$

$$\text{CALCIUM} = .000475\#$$

'>>>>>>KSP: calcite solubility, [Stumm and Morgan, 1996]

$$\text{KSP} = 10^{(-171.9065 - (.077993 * \text{KELVIN}) + (2839.319 / \text{KELVIN}) + ((71.595 * \text{LOG}(\text{KELVIN}) / \text{LOG}(10))))}$$

'>>>>>>activity coefficients = 0.7; extended Debye-Huckel

$$\text{OMEGA} = (\text{CALCIUM} * (.7) * \text{CO}_3 * (.7) / \text{KSP})$$

**END SUB**

## Appendix 2

```
'@@@@@@@@@@@@@@@@@@@@@@@@@@@@@@@@@@@@@@@@@@@@@@@@@@@@@@@@@@@@
'
'           Riverine DO model
'           diffusion & metabolism
'           RiverDO version 3.0
'           Microsoft® QuickBASIC®
'           jason reynolds
'           last modified 3/01
'@@@@@@@@@@@@@@@@@@@@@@@@@@@@@@@@@@@@@@@@@@@@@@@@@@@@@@@@@@@@

'>>>>>>>this program models the effects of metabolism and surface gas transfer on
'>>>>>>>DO in a flowing section of water. the model is comprised of two tiers:
'>>>>>>>a) one moving through the data measurement by measurement, and b) iterative
'>>>>>>>modeling of the biological and physical effects over the travel reach

'           >>SUBROUTINES<<

DECLARE SUB diffusion (TNEW, DONE W)

'           >>DIMENSION VARIABLES<<

DIM SHARED dt AS SINGLE, D AS SINGLE, DOSAT AS SINGLE
DIM SHARED X AS INTEGER, KL AS INTEGER, SHIFTRL AS INTEGER, param
AS INTEGER
DIM SHARED PARTM AS INTEGER, SHIFT AS INTEGER
DIM SHARED PHOTO$, MODELP, dDOD, itTIME, A
DIM SHARED ARRAY(1 TO 2000), ARRAY2(1 TO 2000)
DIM SHARED number%, sun%, Iave, BETA, BETA2
DIM SHARED R
REDIM SHARED DIFF(1 TO 2000), FLD(1 TO 2000)

'>>>>>>>used for troubleshooting only; comment out

'CLOSE #1: STOP

'           >>ERROR TRAP<<
'>>>>>>>will catch input past end of file error

ON ERROR GOTO 999

'@@@@@@@@@@@@@@@@@@@@@@@@@@@@@@@@@@@@@@@@@@@@@@@@@@@@@@@@@@@@

'           >>PARAMETERS AND FILE INFORMATION<<
'>>>>>>>print graphics
```

```
11 CLS
COLOR 10, 8: CLS
```

```
FOR M = 2 TO 79
    LOCATE 1, M: PRINT CHR$(18)
NEXT M
COLOR 11, 8
```

```
'>>>>>>>print user information
```

```
LOCATE 3, 3: PRINT ".this model calculates the effects of metabolism, diffusion, and
temperature"
```

```
LOCATE 4, 4: PRINT "fluctuation on river DO using upstream field measurements as
initial values"
COLOR 10, 8
```

```
LOCATE 7, 3: PRINT ".input data file must be comma or space delimited & formatted
as:"
```

```
LOCATE 9, 3: PRINT CHR$(175); "year day, DO(upstream, mg/L), temp(up, ";
CHR$(248); "C), temp(down)"; CHR$(16); " field data file"
```

```
LOCATE 11, 3: PRINT CHR$(175); "photosynthetic rates (mg DO/L/h)"; CHR$(16); "
net production file"
```

```
LOCATE 13, 3: PRINT CHR$(175); "irradiance, ("; CHR$(230); "E/m"; CHR$(253);
"/s"; CHR$(16); " PAR file"
COLOR 7, 8
```

```
'>>>>>>>user input (filenames)
```

```
LOCATE 15, 3: INPUT ".enter field data filename (include path): (DO(S).PRN) ", data$
IF data$ = "" THEN data$ = "DO(S).prn"
```

```
LOCATE 16, 3: INPUT ".enter full syntax for photosynthetic rate file: ", PHOTOS$
```

```
LOCATE 17, 3: INPUT ".enter full syntax for field irradiance file: ", LIGHTS$
```

```
LOCATE 18, 3: INPUT ".enter full syntax for downstream DO data: (DNDO(S).PRN) ",
feild$
```

```
'@@@@@@@@@@@@@@@@@@@@@@@@@@@@@@@@@@@@@@@@@@@@@@@@@@@@@@@@@@@@@@@@@@@@@@@@@
```

```
' <<DEFAULT VALUES>>
```

'>>>>>>defaults for September modeling

```
IF feeld$ = "" THEN feeld$ = "DNDO(S).PRN"
IF PHOTOS$ = "" THEN PHOTOS$ = "DOPHOTO.PRN"
IF LIGHT$ = "" THEN LIGHT$ = "LIGHT(S).PRN"
```

COLOR 10, 8

'>>>>>>key press continues

```
LOCATE 25, 1: PRINT "Press any key to continue"
DO: LOOP UNTIL INKEY$ <> "": CLS
```

'>>>>>>screen graphic

```
FOR M = 2 TO 79
    LOCATE 1, M: PRINT CHR$(18)
NEXT M
COLOR 2, 8
```

'>>>>>>user input (filenames, travel time, constants, depth)

```
LOCATE 4, 5: PRINT ".enter the following to begin: "
COLOR 10, 8
```

```
LOCATE 7, 5: INPUT ".save results to what filename? (WAMPUM.DAT) ", savename$
    IF savename$ = "" THEN savename$ = "WAMPUM.DAT"
```

```
LOCATE 9, 5: INPUT ".travel time in hours? (4.25) ", tt
    IF tt = 0 THEN tt = 4.25
```

```
LOCATE 10, 5: INPUT ".how many iterations? (20) ", it
    IF it = 0 THEN it = 20
COLOR 13, 8
```

```
LOCATE 12, 5: PRINT ".enter metabolic and diffusional rates @ 20"; CHR$(248); "C"
COLOR 2, 8
```

```
LOCATE 14, 5: INPUT ".respiration rate in mg DO/L/h {-0.084}? ", R
```

```
LOCATE 15, 5: PRINT ".enter value for photorespiration constant, "; CHR$(225); " (0
to omit) "
```

```
LOCATE 15, 64: INPUT "", BETA
```

```
LOCATE 16, 5: INPUT ".gas transfer velocity for O2 in cm/h? {47} ", KL
```





```

'      <<OBTAIN DOWNSTREAM DATA (SHIFTED FOR TRAVEL TIME)>>

OPEN feeld$ FOR INPUT AS #5

FOR X = 1 TO 2000
  INPUT #5, FLD(X)
  IF EOF(5) THEN EXIT FOR
NEXT X

CLOSE #5

'@@@@@@@@@@@@@@@@@@@@@@@@@@@@@@@@@@@@@@@@@@@@@@@@@@@@@@@@@@@@
'@@@@@@@@@@@@@@@@@@@@@@@@@@@@@@@@@@@@@@@@@@@@@@@@@@@@@@@@@@@@

'      >>MODEL (tier 2)<<
'>>>>>>>start iterative modeling

itTIME = YD

FOR W = 1 TO it

'@@@@@@@@@@@@@@@@@@@@@@@@@@@@@@@@@@@@@@@@@@@@@@@@@@@@@@@@@@@@

'      <<PHOTORESPIRATION CONSTANTS>>
'>>>>>>>BETA determines maximum photorespiration
'>>>>>>>computes 4 h light average in determining photorespiratory effect

  IF SHIFTROL > 20 THEN
    average% = SHIFTROL + SHIFT
    Iave = 0
    BETA2 = BETA
    FOR U = 1 TO 20
      Iave = Iave + ARRAY2(average%)
      average% = average% - 1
    NEXT U
    Iave = Iave / 20
  ELSE
    BETA2 = 0
  END IF

'@@@@@@@@@@@@@@@@@@@@@@@@@@@@@@@@@@@@@@@@@@@@@@@@@@@@@@@@@@@@

'      <<RESPIRATION>>
'>>>>>>>modified Arrhenius coefficient

```

THETA2 = 1.045

RT = (R + (BETA2 \* Iave)) \* (THETA2 ^ (TNEW - 20))

'>>>>>>controls shift of photosynthesis as H2O travels downstream

PT = ARRAY(SHIFTROL + SHIFT)

'>>>>>>metabolic effects

dDOR = RT \* dt

dDOP = PT \* dt

DONEW = DONEW + dDOR + dDOP

'@@'

' >>GAS TRANSFER<<

CALL diffusion(TNEW, DONEW)

'@@'

' <<SAVE DATA>>

IF W = it THEN

OPEN savename\$ FOR APPEND AS #2

WRITE #2, YD, DONEW

CLOSE #2

END IF

itTIME = itTIME + (dt \* 60 / 1440)

OPEN change\$ FOR APPEND AS #3

WRITE #3, YD, itTIME, dDOR, dDOP, dDOD

CLOSE #3

'>>>>>>next iteration (tier 2)

TNEW = TNEW + TSTP

SHIFT = SHIFT + param

NEXT W

'@@'

' >>MEAN AND ABSOLUTE MEAN DIFFERENCE<<



'>>>>>>computes difference between field measurements and model

DIFF(SHIFTROL) = (DNEW) - FLD(SHIFTROL)

'@@'

'>>>>>>next upstream field data point

SHIFTROL = SHIFTROL + 1

'>>>>>>loops to next tier 1 step

LOOP UNTIL EOF(1)

666 CLOSE #1

'@@'

' >>STATISTICS<<

SUMMY = 0: ADDITUP = 0

'>>>>>>adds real and absolute differences

FOR Z = 1 TO (SHIFTROL - 1)

    SUMMY = DIFF(Z) + SUMMY

    ADDITUP = ABS(DIFF(Z)) + ADDITUP

NEXT Z

'>>>>>>computes mean difference

MEAN = SUMMY / (SHIFTROL - 1)

'>>>>>>computes absolute difference

REALMEAN = ADDITUP / (SHIFTROL - 1)

'>>>>>>standard deviation about mean

NUMERATOR = 0

FOR V = 1 TO (SHIFTROL - 1)

    NUMERATOR = ((DIFF(V) - MEAN) ^ 2) + NUMERATOR

NEXT V

STD = SQR(NUMERATOR / (SHIFTROL - 2))

COLOR 15, 8

```
'@@@@@@@@@@@@@@@@@@@@@@@@@@@@@@@@@@@@@@@@@@@@@@@@@@@@@@@@@@@@'
```

```
'>>>>>>>alerts user that modeling is finished
```

```
COLOR 14, 10: CLS : LOCATE 13, 29: PRINT ".modeling complete"
COLOR 0, 10
```

```
'>>>>>>>prints statistics to screen
```

```
LOCATE 15, 29: PRINT ".mean difference: ", MEAN
LOCATE 16, 26: PRINT ".standard deviation: ", STD
LOCATE 17, 31: PRINT ".absolute mean:", CHR$(241); REALMEAN
```

```
'>>>>>>>continue with modeling or end
```

```
LOCATE 25, 1: INPUT "Press return to restart or enter any key to end ", STOP$
IF STOP$ = "" THEN GOTO 11
CLS
END
```

```
'@@@@@@@@@@@@@@@@@@@@@@@@@@@@@@@@@@@@@@@@@@@@@@@@@@@@@@@@@@@@'
```

```
' >>ERROR TRAP PATHS<<
```

```
999
```

```
IF ERR = 62 THEN RESUME 666
PRINT ""
PRINT "quickbasic error code: "; ERR
ERROR ERR
```

**SUB diffusion (TNEW, DONEW)**

```
'@@@@@@@@@@@@@@@@@@@@@@@@@@@@@@@@@@@@@@@@@@@@@@@@@@@@@@@@@@@@'
```

```
' >>MODELS FOR GAS TRANSFER EFFECTS<<
```

```
'>>>>>>temperature correction of KL using modified Arrhenius relationship
```

```
'K = KL * (1.0241 ^ (TNEW - 20)) [NOT USED]
```

```
'>>>>>>temperature correction of KL using schmidt numbers (equivalent)
```

```
K = KL / ((530 / (1800.6 - (120.1 * TNEW) + (3.7818 * (TNEW ^ 2)) - (.047608 * (TNEW ^ 3)))) ^ (-.5))
```

```
'>>>>>>temperature
```

```
kelvin = TNEW + 273.15
```

```
'>>>>>>DO saturation (empirical model from: Wetzel, R.G. and Likens, G.E., in
```

```
'>>>>>>Limnological Analyses, 2nd ed., pp. 391, Springer-Verlag, New York, NY, 1991.
```

```
DOSAT = .89 * (EXP(7.7117 - (1.31403 * (LOG(TNEW + 45.93))))))
```

```
'>>>>>>computes gradient between air and water
```

```
DODEF = DOSAT - DONEW
```

```
'>>>>>>computes change due to gas transfer
```

```
dDOD = K * (DODEF) * dt / D
```

```
'>>>>>>computes new DO
```

```
DONEW = DONEW + dDOD
```

```
END SUB
```